ANALYSIS AND SYNTHESIS OF SISO H_∞ CONTROLLERS

Thesis
Submitted To

Graduate Engineering & Research
School of Engineering

UNIVERSITY OF DAYTON

In Partial Fulfillment of the Requirements for

The Degree

Master of Science in Electrical Engineering

by

Emilio Kourany Hammerschlag

UNIVERSITY OF DAYTON

Dayton, Ohio

May, 1993

ANALYSIS AND SYNTHESIS OF SISO H_∞ CONTROLLERS

APPROVED BY:

Malcolm W. Daniels, Ph.D.
Committee Chairman

Dana B. Rogers Ph.D.
Committee Member

Richard J. Kee D.E., P.E.
Committee Member

Franklin Eastep, Ph.D.
Interim Associate Dean/Director
Graduate Engineering and Reasearch
School of Engineering

Joseph Lestingi, D.E., P.E.
Dean
School of Engineering

ABSTRACT

ANALYSIS AND SYNTHESIS OF SISO H_∞ CONTROLLERS

Name: Kourany, Emilio
University of Dayton, 1993

Advisor: Dr. Malcolm W. Daniels

Classical feedback control theories are traditionally concerned with issues like stability and performance, however, they typically fail to address issues such as robustness and plant perturbation. This thesis is concerned with the robust stability and the robust performance of single-input single-output plants. The basic issue under analysis is how to realize the benefits of the usual feedback control structure in the presence of model uncertainty. This is accomplished by seeking feedback controllers providing robust stability and performance by minimizing weighted sensitivity functions of a linear system represented by its transfer function. A characterization of models for plants with unstructured uncertainty is introduced. Specifications and measures of stability and performance for robust controllers and the necessary and sufficient conditions to test the robust stability and the robust performance conditions of a control design are explored. A parametrization of feedback controllers that guarantee closed loop stability for both stable and unstable plants is shown and a systematic procedure for synthesizing robust controllers, known in the literature as H_∞ controllers, is presented. These systematic algorithms are based on the theory of interpolation by analytic functions and the solution to the model matching problem. A case study of the inverted pendulum positioning system is developed to illustrate the concepts of robust analysis and the H_∞ design algorithms. The H_∞ controller is compared to a classic state variable feedback solution.

ACKNOWLEDGMENTS

Some credit is due to those whom in one way or another contributed to the completion of this thesis. I can not possibly thank my advisor enough for all of his support, his time and attention, his sincere and honest interest in my thesis project, and the unconditional friendly hand he has lent me throughout my education and my days at the University of Dayton. For everything, thanks Malc. In addition, I would like to thank Dr. Dana Rogers and Dr. Richard Kee for their participation as members of my graduating committee and their thoughtful comments and guidance. I am also thankful to Dr. Donald Moon for awarding me the teaching assistantship which made it financially possible for me to attend graduate school. Most of all I would also like to express my gratitude to all the members of the faculty for making my experience at U.D. a pleasant one and for their continued help and support.

Le dedico esta tesis a mi familia y a mi querida Tessie. Quiero darle gracias a todos de una forma particular, pues cada uno de ustedes contribuyó con esta obra. A mi padre Emilio, que en páz descanse, ya que esta tesis es fruto de todas tus enseñansas, buenos consejos y el cáracter que sembrastes en mi. A mi madre Stella, porque sin tus esfuerzos y tu sabia incistencia esta tesis no fuese una realidad. A mi hermano Johnny, gracias por tu ayuda y todo tu apoyo. Jamás olvidare todas las noches que pasamos juntos en el laboratorio de control y los buenos momemtos que compartimos en U.D. A mi hermana Jenny gracias por tener tanta fé y tanta confianza en mi. Y a mi novia Tessie, por todo el apoyo que me prestates, por tu pasiencia, comprensión, y por darme la fuerza emocional para seguir adelante.

TABLE OF CONTENTS

LIST OF FIGURES

LIST OF TABLES

CHAPTER I
AN INTRODUCTION

1.1 Control Objectives and Norms

The general objective in control system design has been well defined since the establishment of automatic control as an engineering discipline. The classical objective of a control system is to ensure that the output of a system will be stable and behave in a specified manner in response to some reference or command input. This objective is typically met in either one of two control problem formulations: (i) in a regulator problem and (ii) in a tracking problem. Figure 1.1 illustrates a basic feedback system also called a servomechanism. In the first case, the objective might be to keep the output of the system "small" or close to some equilibrium point. In the second case, the aim is to keep the tracking error "small" for some reference signal variation. In addition, other signals of the control structure might have a constraint of a physical nature, like the control signal u in figure 1.1, which must be taken into consideration when the controller is designed for a real system. But exactly how small must these signals be in order for the control objectives to be met?

The input signals to a system are only rarely fixed or known. In most cases the system designer is able to characterize to some degree the type of inputs that the system might be exposed to. Based on this characterization of input signals, the system designer

develops a set of test inputs. The system is then designed to perform satisfactorily to this set of test inputs such as an impulse, step or ramp inputs, or white Gaussian noise. Despite the multitude of possible input signals, a natural measurement of the size of the signal is expressed explicitly by its norm. A "small" signal then, is defined as a signal of bounded norm. Which norm is appropriate depends on the particular application. The notion of norms and their use in a control design context is not new in the control arena. Norms have been implicitly used in classical frequency domain methods to guarantee the stability of the feedback loop. For example, the familiar gain margin imposes a bound or constraint on the magnitude of the open loop system frequency response at a phase angle of π radians.

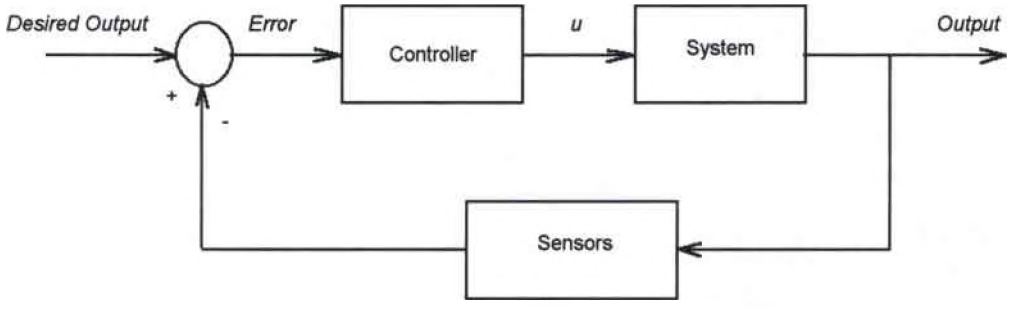

Figure 1.1 Single loop tracking feedback system

Consequently, the performance and stability objectives of a control system naturally lead to the introduction of norms. The performance specifications and the stability requirements may be expressed in terms of norm bounds on key signals and transfer functions of the system.

1.2 Norms of Signals and Systems

Generally speaking a norm expresses a quantifiable size typically of a mathematical function, vector, or signal. For instance, the most common norm is the Euclidean norm. This norm quantifies the length of a vector. There are two norms in particular that electrical engineers are well acquainted with. These are the 1- and 2- norms.

The **1-Norm** of a signal $x(t)$, is the integral of its absolute value. This norm is expressed mathematically in the form

$$\|x\|_1 = \int_{-\infty}^{\infty} |x(t)|dt \qquad \textbf{(1.1)}$$

The **2-Norm** of a signal $x(t)$ is related to the *rms* value of the signal and is mathematically defined by equation (1.2).

$$\|x\|_2 = \sqrt{\int_{-\infty}^{\infty} x^2(t)dt} \qquad \textbf{(1.2)}$$

Notice that this norm may be used to represent the normalized energy of a signal. Suppose that $i(t)$ is a current through a 1Ω resistor. Then the average power consumed by this resistor is given by $i^2(t)$ and its energy is equal to the square of its 2-norm.

A norm that is of significant importance in the design of robust controllers is the ∞-norm. The **∞-Norm** of $x(t)$, is the least upper bound of its absolute value and is denoted in closed form by

$$\|x\|_\infty = \sup_t |x(t)|. \qquad \textbf{(1.3)}$$

As an example, consider the equation $x(t) = \left(1 - e^{-t}\right)u(t)$, where $u(t)$ is a unit step function. The graphical representation of the function $x(t)$ is given in figure 1.2. Observe that $|x(t)|$ increases with time to a maximum value of one. It is clear from the figure that the minimum or least upper bound on $x(t)$ is then one. Nevertheless, there are an infinite number of upper bounds for this function. Thus, the infinity norm of $x(t)$ is, by definition, equal to one.

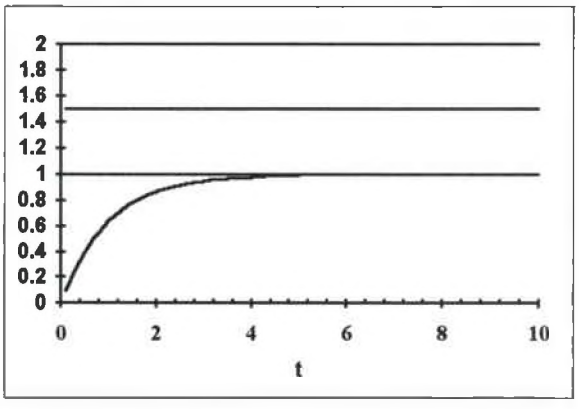

Figure 1.2 Plot of $x(t)$.

Linear system theory asserts that the impulse response of a causal, linear, and time invariant system, completely characterizes the system's dynamic response. This means that given the impulse response of the system, it is possible to predict the system's response to any input signal. The computational mechanism for obtaining the output response of an LTI system is the usual convolution integral as expressed in (1.4).

$$y(t) = \int_{-\infty}^{\infty} h(\lambda - t)u(\lambda)d\lambda \qquad \textbf{(1.4)}$$

where *u(t) is the system input*
y(t) is the system output
h(t) is the system impulse response

Thus, it is argued that the impulse response serves as a mathematical model of an LTI system. Since the impulse response of a system is merely a mathematical function, it is possible to compute a norm for this function. Consequently, norm measures for systems are computationally feasible. On the other hand, control engineers generally prefer to use the Laplace transform equivalent model for single input/single output systems (SISO) because it simplifies the mathematical procedures involved in system analysis and design. As a result of the benefits of the Laplace transform, the transform counterpart of the impulse response is used to mathematically model the system's dynamics. This transform counterpart is the transfer function of the system, $H(j\omega)$.

Two **system norms** will be introduced in this section: the **∞-norm** and the **2-norm**. The latter is easily derived from knowledge of the 2-norm of a signal and Parseval's theorem expressed by equation 1.5. Since the square root of the left hand side of equation 1.5 is the 2-norm of the impulse response function from 1.2, define the square root of the right hand side of 1.5 as the 2-norm of a system described by the transfer function $H(s)$. Equation 1.6 expresses the definition of the 2-norm of a system mathematically.

$$\int_{-\infty}^{\infty} h(t)^2 dt = \frac{1}{2\pi} \int_{-\infty}^{\infty} |H(j\omega)|^2 \, d\omega \qquad \textbf{(1.5)}$$

$$2-\textbf{norm} \qquad \|H(j\omega)\|_2 = \left[\frac{1}{2\pi}\int_{-\infty}^{\infty}|H(j\omega)|^2 d\omega\right]^{1/2} \qquad \textbf{(1.6)}$$

$$\infty-\textbf{norm:} \qquad \|H(j\omega)\|_\infty = \sup_{\omega}|H(j\omega)| \qquad \textbf{(1.7)}$$

The infinity norm of a system is by definition the least upper bound of the system's amplitude frequency response. This is mathematically denoted by (1.7). The ∞-norm has a convenient graphical interpretation both in the complex Nyquist plane and in the Bode magnitude response plot of the system. In the complex plane, the infinity norm of a transfer function equals the distance from the origin to the farthest point on the Nyquist plot. Equivalently, the infinity norm of a transfer function is the largest magnitude of the Bode plot or frequency response. The value of the ∞-norm may be computed either numerically or graphically. The analytic solution for the infinity norm of $H(j\omega)$ could be found in closed form by solving for the maxima of $H(j\omega)$. The graphical solution requires a search in the frequency range $\{\omega_N,\ldots,\omega_M\}$. An estimate for $\|H(j\omega)\|_\infty$ is obtained as,

$$\max_{N \le k \le M} |H(j\omega_k)| \qquad \textbf{(1.8)}$$

To illustrate the procedure, lets examine the Bode plot of the system expressed by 1.9. The infinity norm of this transfer function is determined from figure 1.3 and is equal to 4.8 (or 13.62 dB) at $\omega=1$ *rad/sec*. The corresponding Nyquist plot of figure 1.3b illustrates the same result. Note that the ∞-norm constraints $H(s)$ within a specified circular region of the complex plane of radius 4.8 and centered at the origin.

$$H(s) = \frac{1}{s^2 + 2\xi s + 1} \quad , \xi = .1 \tag{1.9}$$

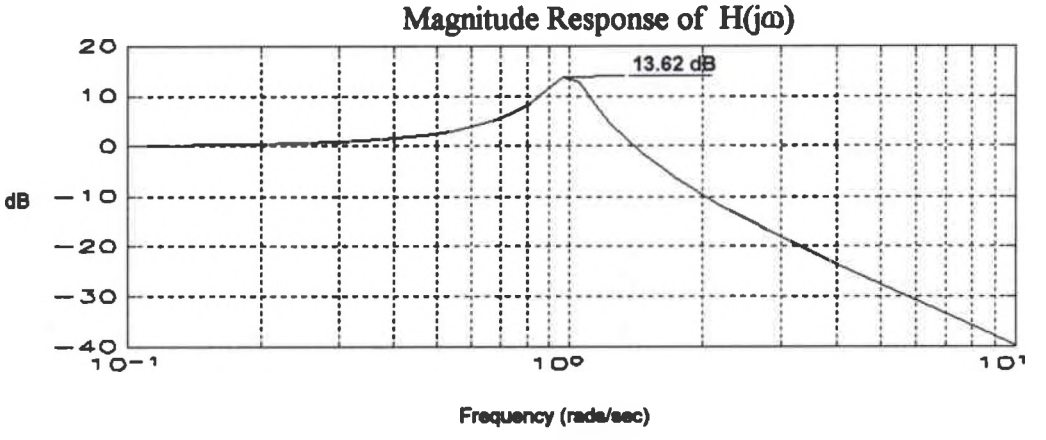

Figure 1.3 (*a*) Bode magnitude plot of $H(s)$

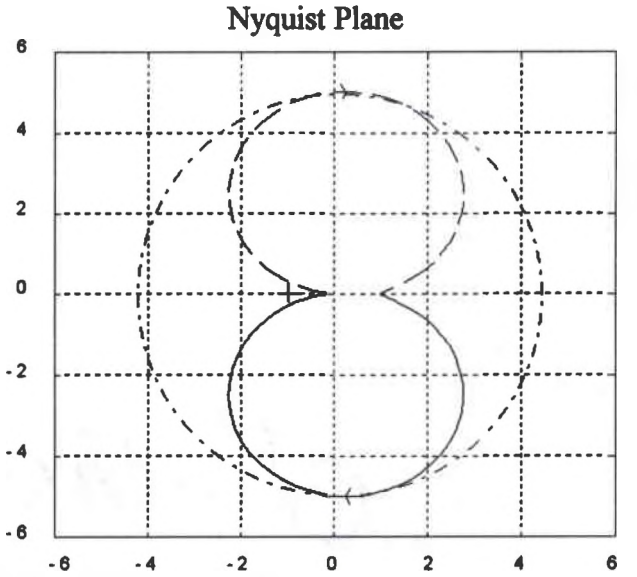

Solid and Dashed: Nyquist plot of H(s)
Dash-dot: Bound on H(s)

Figure 1.3 (*b*) Nyquist plot of $H(s)$

The utility of the infinity norm in the robust control context arises from certain mathematical properties which it possesses that make it desirable for modeling plant perturbations. Zames and Francis [8] argue that quadratic norms (e.g. 2-norm) are not well suited for plant perturbation studies. Their claim arises from the effects that plant perturbations place on the behavior of the closed loop system. Perturbed systems characteristically have closed loop transfer functions which are composed of the sensitivity term multiplied by a perturbation parameter which is a function of the plant's model. Zames and Francis [8] argue that because perturbation effects have this form, it is desirable to employ norms that are submultiplicative. This means that the norm of the product $||AB||$ of any two systems A, B, bears a simple relation to their separate norms i.e. $||AB|| \leq ||A|| \bullet ||B||$. The infinity norm of a system presented here has such multiplicative properties, whereas quadratic norms do not. It will be demonstrated in later chapters that the ∞-norm is of significant relevance and plays an important role in the solution of the robust control design problem.

1.3 Real Systems Versus Mathematical Models

It is necessary to make a distinction between a mathematical model of a system and the physical system it represents. Real or physical systems are those existing in the plant or field which the control engineer must successfully control. The mathematical model of a system is one which is obtained by application of the natural laws of physics and attempts to represent the dynamic behavior of the real physical system. Current feedback control design philosophies require a finite dimensional LTI model of the plant in order to devise controller for it. However, the practical reality is that linear processes do not often occur in nature. These mathematical models are inevitably contaminated with errors and

consequently there is no mathematical model that can precisely emulate a real physical system. Hence, a model should be considered only partially complete if it lacks some assessment of its errors. The control community has adopted the term *model uncertainties* to refer to these errors. Uncertainties usually infiltrate into the model via identification errors, unmodeled dynamics, linearization of the models for the purpose of controller design, and variation of plant parameters during plant operation. Models that are used to design controllers which do not incorporate these uncertainties are referred to as *nominal models*. Those models which, by some means, attempt to give a better, or closer to the real system, representation of the physical plant are called *perturbed models*.

1.4 The Unity Feedback System and Its Trade-offs

Morari and Doyle [7] used the Internal Model Control structure of figure 1.4 to explain the necessity of the feedback structure in automatic control design. In this case, G is the real physical plant to be controlled. The controller to be designed includes the parameter Q and the plant model P. Hence, the name internal model control. The feedback signal f is expressed as $f = (G - P)u + d$. Morari and Doyle [7] argued that if the model is exact (G=P) and there are no disturbances (d=0), then the model output y_m and the physical system output y_p are identical and the feedback signal f is zero. The point being made here is that if the open loop process is stable and all its inputs are known perfectly there is no need for feedback control. The feedback control structure is only necessary because of the uncertainties and disturbances inherent in natural processes. In fact, due to the lack of perfect models and exact knowledge of disturbances, classical and modern design methods rely heavily upon the feedback control structure.

Although the feedback structure has properties which make it desirable to handle disturbances and uncertainties, certain strict constraints must be satisfied to achieve suitable behavior in terms of disturbance rejection, noise immunity, and system stability and performance. Most classical and modern design methods completely ignore the uncertainties associated with the mathematical model of the plant.

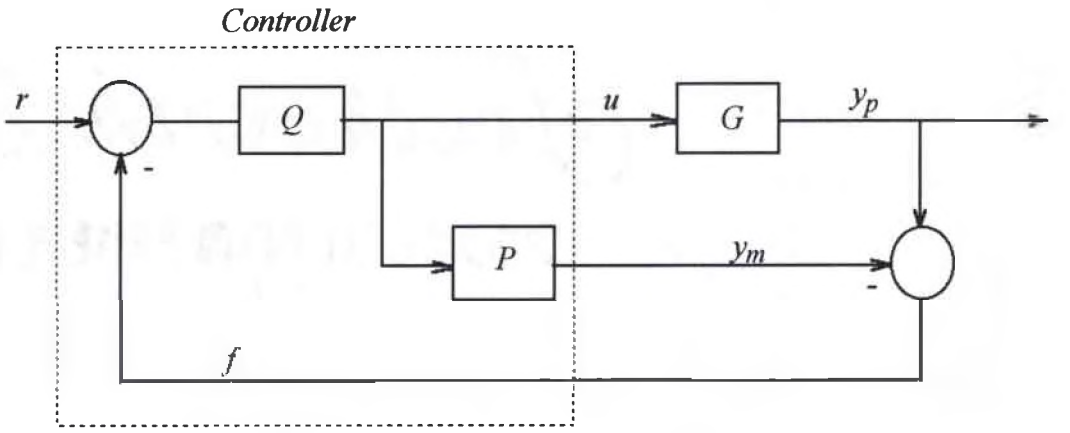

Figure 1.4 Internal Model Control (IMC) structure

As a result, typical phase lead / phase lag compensators and even some modern control design procedures fail to provide the system with stability and performance robustness to parameter variations and other types of perturbations. This and later sections of this thesis will explore some of the constraints mentioned above, particularly those involved with system robustness.

The diagram in figure 1.5 shows the standard unity feedback control configuration. This configuration has the following properties:

1. The input-output behavior is characterized by the closed loop transfer function from all the exogenous inputs (i.e. r, d, n) to the output. Note the occurrence of the same characteristic equation ($1+PC$) in each transfer function.

$$y = \frac{PC}{(1+PC)} r - \frac{PC}{(1+PC)} n + \frac{1}{(1+PC)} d \qquad \textbf{(1.10)}$$

2. The tracking error is equal to the difference between the output y and the command or reference signal r.

$$e \equiv r - y = \frac{1}{(1+PC)} r \qquad \textbf{(1.11)}$$

3. The sensitivity of the system (i.e. the transfer function from r to e) is

$$S = \frac{1}{(1+PC)} \qquad \textbf{(1.12)}$$

4. The complementary sensitivity (i.e. the transfer function from r to y) is denoted by

$$T = \frac{PC}{(1+PC)} \qquad \textbf{(1.13)}$$

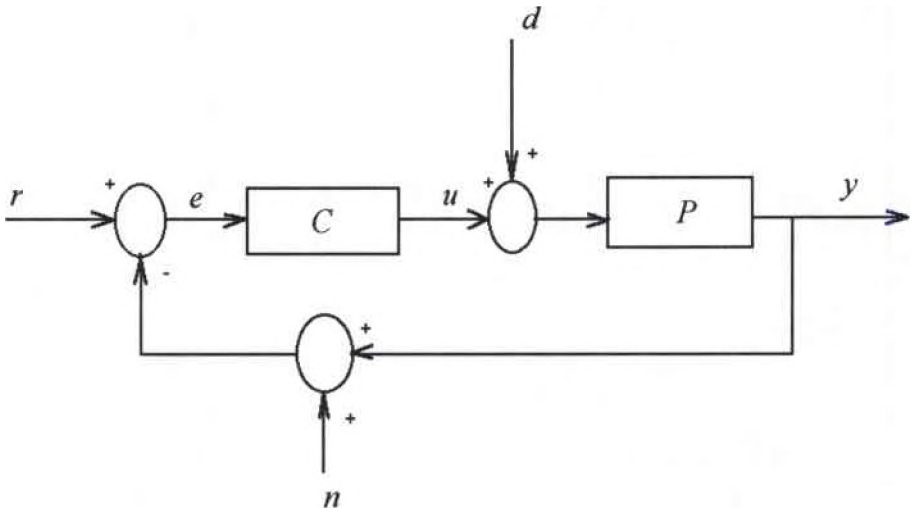

r: Reference signal — *e: Error signal*
u: Command signal — *y: Output signal*
n: Measurement noise — *d: Disturbance signal*
C: Controller — *P: Plant*

Figure 1.5 Elementary servo-control system

For SISO systems, the performance objective generally requires that the loop errors be small[1]. Assuming the system is stable, the second property suggests that loop errors in the presence of disturbances can be made small by making the sensitivity operator (i.e. $(1+PC)^{-1}$) small. In the light of classical feedback analysis, making the sensitivity operator small degenerates to reasonably reducing its magnitude, or conversely, making the open loop gain much larger than one (i.e. $PC >> 1$) over all frequencies where the disturbances are significant. Selecting the open loop transfer function gain as suggested, also appears to significantly improve the close loop tracking performance to reference signals, since $PC/(1+PC)$ approaches one as PC approaches infinity. It is these features that make the feedback structure appealing for control applications.

[1]Typically this loop error is taken as that defined by the second property.

Doyle and Stein [6] formulate the control performance objective for classical SISO systems in terms of explicit inequalities of the form:

$$W_x(j\omega) \leq |1 + P(j\omega)C(j\omega)|, \qquad \forall \omega \leq \omega_o \qquad \textbf{(1.14)},$$

where $W_x(j\omega)$ is a large positive function and ω_o specifies the active frequency range. Basically, condition 1.14 requires the magnitude of PC to be large at the frequencies where the disturbances might be significant. This type of specification guarantees good tracking accuracy. Also, it is evident from 1.10 that this condition also guarantees good disturbance rejection in the sense that y will be small for any appreciable d.

The preceding discussion can potentially mislead the reader into a deceptive conclusion. Namely, that feedback control design reduces to accomplishing high loop gains in the proper frequency range. Unfortunately, the feedback design problem is not quite so trivial. In most cases, loop gains cannot be made arbitrarily high over arbitrarily large frequency ranges. This inability to achieve good performance by selectively shaping the open loop transfer function typically arises as a result of the basic trade-offs involved with the feedback control structure. One of these trade-offs stems from the inability of the feedback control configuration to reduce the sensor noise error. This property is revealed in equation (1.10). Note that the transfer function from r to y is identical to the transfer function from n to y. Consequently, large loop gains over large frequency ranges reduce the system's sensitivity to disturbances while increasing the system's tracking accuracy both to the reference input and to measurement noise.

Some modern control theories provide a systematic solution for simultaneously achieving reasonable performance and reducing sensitivity to measurement noise. Among the most popular of these theories are the familiar LQG or linear quadratic Gaussian technique, and the Wiener-Hopf-Kalman frequency domain methods. In fact, Doyle and Stein [6] suggest that if the trade-offs between command/disturbance error reduction and sensor noise error reduction were the only constraints in feedback design the available modern theories would be more than sufficient. The problem however is this. Although finite dimensional LTI models may be used to design feedback controllers, these must be implemented and operate with real physical plants. This means that, while classical as well as modern design methodologies may be successful in achieving stable well behaved systems for a nominal plant model, this may only hold as long as the real physical plant does not stray too far from the nominal plant model. This introduces yet another constraint in the design of feedback controllers due to the inaccurate nature of the models. It turns out that these inaccuracies place strict limitations on the frequency range over which the open loop gains may be large.

1.5 Definitions and Classical Measures of Stability

In a typical control application a system's transfer function model, G is expressed as a rational function of complex variables with constant coefficients. In this case, G may have one of the following characteristics: It may be *proper* if $G(j\infty)$ is finite (i.e. the degree of the denominator $\geq$ degree of the numerator), it may be *strictly proper* if $G(j\infty) = 0$ (i.e degree of denominator > degree of numerator), *improper* if $G(j\infty) = \infty$ (i.e degree of numerator > degree of denominator), and *biproper* if G and G^{-1} are proper.

Given a bounded input $u(t)$, such that $\{|u(t)| \leq k : \forall t\}$, a system G is said to be *stable* if and only if the output, as given by (1.15), is bounded. This definition is common in undergraduate control textbooks and is well known as the bounded input/bounded output (BIBO) definition of stability.

$$|y(t)| \leq k \int_{-\infty}^{\infty} G(\tau)d\tau, \tag{1.15}$$

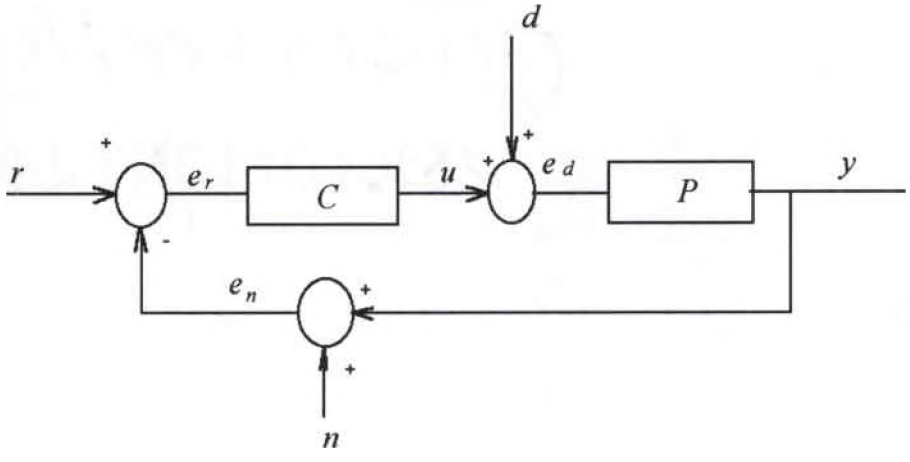

Figure 1.6 Basic feedback loop

Figure 1.6 shows the system loop errors in the basic feedback structure. These loop errors are defined by equation 1.16 in terms of the three exogenous inputs.

$$e_r = r - e_n$$
$$e_d = d + Ce_r$$
$$e_n = n + Pe_d$$

in matrix form
$$\begin{bmatrix} e_r \\ e_d \\ e_n \end{bmatrix} = \begin{bmatrix} 1 & 0 & 1 \\ -C & 1 & 0 \\ 0 & -P & 1 \end{bmatrix}^{-1} \cdot \begin{bmatrix} r \\ d \\ n \end{bmatrix} \quad \textbf{(1.16)}$$

In order to achieve reasonable results from the design algorithms that will be presented in this investigation, it is convenient to place certain constraints on the transfer functions of the components of the feedback structure shown in figure 1.6. The concept of system *well-posedness* has been used by Doyle, Francis and Tannenbaum [5] and others for defining the convenient properties for the transfer functions of the feedback components. In order to establish the meaning of *well-posedness* it suffices to look at the transfer functions from all the exogenous signals to the loop errors. A requirement for the system to be well-posed is that the 3x3 system matrix in (1.16) be invertible. In other words, the numerical value of the system characteristic equation $1 + PC$ must not equal zero at any frequency. This requires that $PC \neq -1$ or that $1 + PC$ not be strictly proper. Doyle, Francis, and Tannenbaum [5] have shown that the system is automatically well-posed if P is strictly proper and C is proper. These conditions will be assumed throughout the development of this work.

$$\begin{bmatrix} e_r \\ e_d \\ e_n \end{bmatrix} = \frac{1}{1+PC} \begin{bmatrix} 1 & -P & -1 \\ -C & 1 & -C \\ PC & P & 1 \end{bmatrix} \cdot \begin{bmatrix} r \\ d \\ n \end{bmatrix} \quad \textbf{(1.17)}$$

The solution of equation 1.16 is shown in equation 1.17. A system is said to be *internally stable* if and only if all nine transfer functions in (1.17) are BIBO stable. Consequently, internal stability guarantees bounded internal signals for all bounded exogenous signals. This definition provides further insight into the stability condition.

From classical control theory it is well known that a system is stable if the roots of its characteristic equation lie in the left hand s-plane (i.e. $Re\ s < 0$). In order to test internal stability of a system it is necessary to fulfill the following two conditions:

(a) *The transfer function 1 + PC has no zeros in Re $s \geq 0$.*

(b) *There is no pole-zero cancellation in Re $s \geq 0$ when the product PC is formed.*

Notice that the system may be internally unstable and still comply with condition (a). This case occurs when, in forming the term 1 + PC, unstable poles of C are canceled by the RHP zeros of P or vice versa. Therefore, condition (b) is critical to ensure internal stability. Nevertheless, as far as this paper is concerned the stability condition will be sufficiently satisfied in a bounded input-bounded output sense, meaning that a system will be considered stable if the output is bounded for any bounded excitation input. Therefore, condition (a) will be sufficient to test the stability of a system.

The robust design techniques which will be discussed in this thesis are known in the control literature as H infinity methods. Most of the analysis involved in the development of the H_∞ design technique considered in this work has been accomplished by concentrating on the complex mathematical nature of the problem. Hence, an additional or alternative definition of stability will be included which expresses the complex nature of the problem. First, let's define an analytic function. A complex function is said to be analytic at a point in some domain if the function is differentiable at every point in an absolute disk of radius x that encircles the point on that domain. For example, let the domain be the closed RHP and the function $G(s)$ be $G(s) = \frac{1}{s-1}$. Note that $G(s)$ is not differentiable at s = -1. Therefore, $G(s)$ is not analytic in the RHP. The alternative

definition of stability then is that a system or transfer function $G(s)$ is stable if it is analytic in the right half s-plane.

1.6 Organization

This thesis is composed of five chapters. Consecutively the chapters are an introduction, system analysis for robust design, synthesis of SISO H_∞ controllers, a case study: the inverted pendulum, and concluding remarks. The first chapter treats the preliminary concepts and definitions required to prepare the reader for the study of system robustness and the H_∞ design methods. The second chapter is devoted to the development of the tools necessary for the analysis of systems with model uncertainties. Also the robust stability and robust performance problems are defined in this chapter. In the third chapter design procedures are developed for achieving both robust stability and robust performance. In the fourth chapter the H_∞ design procedures introduced in chapter III are applied to the inverted pendulum problem as a case study. A comparison of the performance of the SISO feedback control structure with an H_∞ controller versus the traditional state variable feedback controller is also included. Finally, chapter five presents the conclusion of this investigation and a consideration of some future work.

CHAPTER II
SYSTEM ANALYSIS FOR ROBUST DESIGN

2.1 The Nominal Performance Condition

In quadratic design methods such as LQR/LQG the performance objective is formulated as the minimization a cost function. Morari and Doyle [7] argue that controllers designed on the basis of these theories have been shown to be prone to failure in environments subject to significant nonlinearity and/or dominated by uncertainties. Zames and Francis [8] also maintain that quadratic methods provide satisfactory performance only for a constrained disturbance spectrum, and therefore, are not dependable under large spectral variations. They suggest that in quadratic methods the integral-squared sensitivity is minimized for disturbances d or commands r having a single fixed power spectrum. While the assumption of fixed spectrum is reasonable for applications where the disturbance source is constant, for example 60 Hz noise, it is unrealistic for servomechanisms subject to broad band disturbances, or under command from a wide variety of signals. In practice, most servo-controllers are governed by a spectrum of disturbances and command signals, including pulses, steps, ramps, and narrow band signals of various frequencies. Design techniques that aim to increase the system's disturbance rejection to such signals have opted to group the spectrum of all disturbances into a uniquely described class. All signals pertaining to the class have stringent energy

constraints bounded by a weighting function $|F(j\omega)|^2$. Equation 2.1 gives a quantitative description of this class.

$$D = \left\{ \tilde{d}(s) = \frac{d(s)}{F(s)} \quad : \frac{1}{2\pi} \int_{-\infty}^{\infty} \frac{|d(j\omega)|^2}{|F(j\omega)|^2} d\omega = \left\| d(j\omega) F^{-1}(j\omega) \right\|_2^2 \leq 1 \right\} \qquad \textbf{(2.1)}$$

Figure 2.1 Basic system block diagram

The SISO H_∞ methods that will be presented in this thesis in effect minimize the maximum output energy for all disturbances in the class. To see this, consider fig. 2.1. Here the input signal x and the output signal y are related through the transfer function G. The *2-norm/2-norm system gain* is defined as the least upper bound (i.e. least maximum) on the 2-norm of the output given that the 2-norm of the input is bounded.

That is, $$sup\left\{ \|y\|_2 : \|x\|_2 \leq 1 \right\} \qquad \textbf{(2.2)}$$

It can be shown that the 2-norm/2-norm system gain of a system described by its transfer function G is given by the ∞-norm of G. By Parseval's theorem the 2-norm of a signal is directly related to the 2-norm of the signal's transform[1].

$$Then, \quad \|y\|_2^2 = \|\hat{y}\|_2^2 \qquad \textbf{(2.3 } \boldsymbol{a}\textbf{)}$$

[1]The hat notation in equation 2.3 refers to the Laplace transform of the signal.

$$= \frac{1}{2\pi} \int_{-\infty}^{\infty} |G(j\omega)|^2 \cdot |\hat{x}(j\omega)|^2 \, d\omega \qquad \textbf{(2.3 } b\textbf{)}$$

$$\leq \|G(j\omega)\|_\infty^2 \cdot \frac{1}{2\pi} \cdot \int_{-\infty}^{\infty} |\hat{x}(j\omega)|^2 d\omega \qquad \textbf{(2.3 } c\textbf{)}$$

$$\leq \|G(j\omega)\|_\infty^2 \cdot \|\hat{x}\|_2^2 \qquad \textbf{(2.3 } d\textbf{)}$$

$$\|y\|_2^2 \leq \|G(j\omega)\|_\infty^2 \cdot \|x\|_2^2 \qquad \textbf{(2.3 } e\textbf{)}$$

To show that $\|G(j\omega)\|_\infty$ is the least upper bound, let ω_o be a frequency such that $|G(j\omega)|$ is maximum, that is, $|G(j\omega_o)| = \|G(j\omega)\|_\infty$.

Additionally let $$|\hat{x}(j\omega)| = \begin{cases} c, & if \; |\omega - \omega_o| < \varepsilon \;\; or \; |\omega + \omega_o| < \varepsilon \\ 0, & otherwise \end{cases} \qquad \textbf{(2.4)}$$

where ε is a small positive number and c is a scalar such that x has unit 2-norm (i.e. $c = \sqrt{\pi/2\varepsilon}$).

Then substituting 2.4 into 2.3,

$$\|\hat{y}\|_2^2 = \frac{1}{2\pi} \int_{-\infty}^{\infty} |G(j\omega)|^2 |\hat{x}(j\omega)|^2 d\omega$$

$$= \frac{1}{2\pi} \int_{\omega_o - \varepsilon}^{\omega_o + \varepsilon} c^2 \, |G(j\omega)|^2 d\omega \qquad \textbf{(2.5)}$$

$$= \frac{c^2}{2\pi} \left[|G(j\omega)|^2 \right]_{\omega_o - \varepsilon}^{\omega_o + \varepsilon}$$

$$= \frac{1}{2\pi} \left[|G(-j\omega_o + \varepsilon)|^2 \pi + |G(j\omega_o + \varepsilon)|^2 \pi \right] \qquad \textbf{(2.6)}$$

$$= |G(j\omega_o)|^2 = \|G\|_\infty^2$$

Therefore, $\|y\|_2 = \|G\|_\infty \cdot \|x\|_2$ and the least upper bound on the output then is shown to be determined by the infinity norm of the transfer function G.

Suppose that the class of disturbances is slightly modified to

$$D = \left\{ d_{pf}(s) = W_1(s)d(s) \quad : \quad \|d_{pf}\|_2^2 \le 1 \right\} \qquad \textbf{(2.7)}$$

where the input disturbance is pre-filtered such that its energy is bounded to one as defined in the previous class. Figure 2.2 illustrates this arrangement in the unity feedback configuration. Note in this case that $W_1(s)(1 + PC(s))^{-1}$ is the transfer function from the disturbance signal d to the output signal y in figure 2.2. Due to its similarity to the sensitivity transfer function of 1.12 this transfer function is known in the robust control context as the *weighted sensitivity*. Also, note that letting G in 2.6 be the weighted sensitivity, its ∞-norm represents the maximum energy transfer from the disturbance d to the output y. This is expressed mathematically by equation 2.8.

$$\sup_{d \in D} \|y\|_2 = \left\| W_1(1 + PC)^{-1} \right\|_\infty = \|W_1 S\|_\infty \qquad \textbf{(2.8)}$$

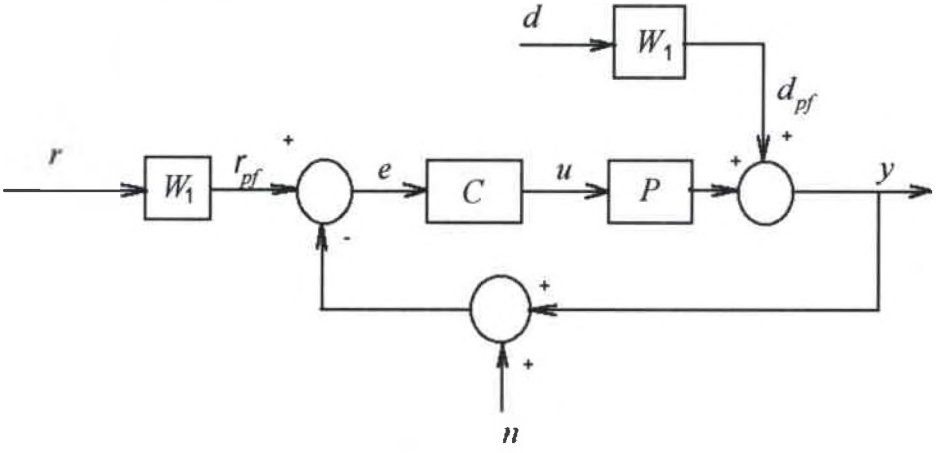

Figure 2.2 Unity feedback loop

Thus, minimizing the infinity norm of the weighted sensitivity minimizes the maximum output energy for all disturbances within the class D. It is not surprising to see that these same ideas apply equally to reference signals. Again, suppose that the class of reference signals is defined as the set

$$R = \left\{ r_{pf}(s) = W_1(s) \bullet r(s) \quad : \left\| r_{pf} \right\|_2^2 \le 1 \right\}, \tag{2.9}$$

where r_{pf} is a pre-filtered input so that its energy is again bounded to one. Recall that in this case the weighted sensitivity $W_1(s)(1 + PC)^{-1}$ is the transfer function from the reference input to the error signal shown in figure 2.2. By the same argument as before then, minimizing the weighted sensitivity minimizes the maximum error energy.

That is

$$\sup_{r \in R} \|e\|_2 = \left\| W_1(s)(1 + PC)^{-1} \right\|_\infty = \|W_1 S\|_\infty \tag{2.10}$$

Suppose now that the performance specification is expressed as a measure of the energy of the error. For instance, a common optimal specification requires that the error energy to either tracking or disturbance signals be less than one (i.e. $\| e \|_2 < 1, \ \forall r \in R$). This condition is satisfied provided that $\|W_1 S\|_\infty < 1$. Furthermore, suppose it is known apriori that good tracking accuracy, or alternatively, disturbance attenuation is achieved if the spectrum of $S(j\omega)$ lies underneath some predefined spectrum. This can be expressed in the form:

$$\|W_1 S\|_\infty < 1 \ \Leftrightarrow \ |S(j\omega)| < |W_1(j\omega)|^{-1}, \quad \forall \omega, \tag{2.11}$$

This condition will be denoted the *nominal performance condition*. If the condition is satisfied, the nominal feedback system is guaranteed to satisfy the predefined performance specification. The function $|W_1(j\omega)|^{-1}$ may be conceptually viewed as the desired attenuation factor. Since $W_1(j\omega)$ is a function of frequency the designer may specify different attenuation factors for different frequencies. The function $W_1(j\omega)$ will be referred to as the *performance weighting function* for the rest of this thesis.

The nominal performance condition has an interesting graphical interpretation which provides additional insight into the performance criteria. Let's examine 2.11 a little closer.

$$\begin{aligned} \|W_1 S\|_\infty < 1 \quad &\Leftrightarrow \quad \left|\frac{W_1(j\omega)}{1+L(j\omega)}\right| < 1, \quad \forall\omega \\ &\Leftrightarrow \quad |W_1(j\omega)| < |1+L(j\omega)|, \quad \forall\omega. \end{aligned} \tag{2.12}$$

where $L(j\omega) = P(j\omega)C(j\omega)$ is the loop transfer function. The last inequality in (2.12) indicates that at every frequency, the point $L(j\omega)$, located on the Nyquist plot of $PC(j\omega)$, lies outside the disk of center -1, and radius $|W_1(j\omega)|$. This is illustrated in figure 2.3. It is clear from the figure that the nominal performance specification will hold for all ω if every point on $L(j\omega)$ lies outside the corresponding disk.

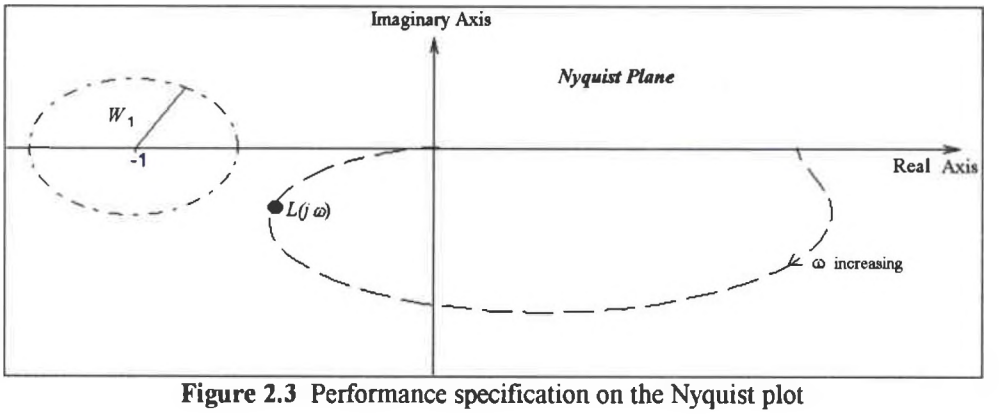

Figure 2.3 Performance specification on the Nyquist plot

What remains now is to show that SISO H_∞ design method minimizes the infinity norm of the weighted sensitivity. This will be demonstrated in a later section. However, it is interesting to note that whether the performance specification is posed by focusing on the response of the error to any of the exogenous signals, the performance criteria is reduced to placing a bound on the ∞-norm of the sensitivity transfer function S of the feedback system. To illustrate this, consider the transfer function from all exogenous inputs to the error *e*. For either *r* or *n* the transfer function is S, so the criteria is as previously determined. For *d*, however, the transfer function is *PS*. Hence, the performance criteria is still given by a weight on S of the form:

$$\|WPS\|_\infty = \|W_1 S\|_\infty \quad ; \quad where \quad W_1 = WP \tag{2.13}$$

2.2 Models of Uncertainty

2.2.1 Representations of Uncertainty

In this section, two popular schemes for representing uncertainty in linear models will be discussed. Although representations of uncertainty vary, depending on the particular errors associated with a system model, it seems reasonable to require that these representations at least incorporate two things: (i) convenient mathematical manipulation and (ii) knowledge of the physical mechanisms which cause differences between a plant and its corresponding model. The most basic technique employed is to model the plant as a member of a set P. For instance, parameter variation is one of the most usual sources of error. Since parameters generally vary within some boundaries, the typical approach is

to define the parameter as belonging to a specified membership set. For example, consider the plant model

$$P(s) = \frac{1}{s^2 + 2\xi s + 1}$$

This is the standard second order transfer function typical of an RLC circuit or a spring-mass damper setup. Suppose that it is known that ξ lies in some interval of values e.g. $[\xi_{min}, \xi_{max}]$. The plant P may be characterized as a member of the structured set

$$P = \left\{ P = \frac{1}{s^2 + 2\xi s + 1} \;:\; \xi_{min} \le \xi \le \xi_{max} \right\}.$$

These are highly parametrized formulations which are commonly referred to as *structured* uncertainty models. This type of uncertainty is frequently used to model the low frequency error components. There are, however, higher frequency errors which can not be adequately model by parametric formulations and the need exists for an alternative model which covers these latter cases. These alternative models are termed *unstructured* and represent high frequency dependent elements like actuator saturations, unmodeled dynamics, time delays, or low frequency plant disturbances. According to Doyle, Francis, and Tannenbaum [5], models incorporating unstructured uncertainties are more useful for two reasons. Firstly, all models should include some form of unstructured uncertainty since all models naturally lack accuracy, particularly at high frequency. Remember that a physical system, regardless of how linear it might be in a restricted frequency region, will cease to behave linearly as frequency increases. Secondly, the system analysis is greatly

simplified by assuming a specific type of unstructured uncertainty sometimes denoted *disk like uncertainty*. The H_∞ technique presented here will concentrate on this latter kind of uncertainty. Table 2.1 tabulates the most common of these latter kind of uncertainty.

Type	Unstructured Uncertainties
----------	$P_m = P/(1+\Delta W_2)$
----------	$P_m = P/(1+\Delta W_2 P)$
Additive	$P_m = P+\Delta W_2$
Multiplicative	$P_m = (1+\Delta W_2)P$

Table 2.1 Uncertainty Models

It is worth mentioning that unstructured representations of uncertainty are well suited to include plant model perturbations effects which are not at all uncertain. For example, it is customary to deliberately neglect known higher order dynamics in order to achieve a simpler nominal design model. In addition, some nonlinear systems can typically be accurately modeled. Nevertheless, due to a lack of effective nonlinear design techniques the model is linearized, as a small signal model, about a predetermined operating point in order to fit the problem to modern design procedures.

2.2.2 Unstructured Uncertainty Models

There are two major classifications of unstructured uncertainty models: *multiplicative* and *additive*. There names reveal their relationship to the nominal plant model, and both are readily illustrated graphically and explicitly stated mathematically.

(a) Multiplicative perturbations: Consider figure 2.4 which illustrates the multiplicative unstructured uncertainty model. Let the nominal plant transfer function be P and the perturbed plant transfer function be P_m. The multiplicative perturbation model is mathematically defined by (2.13) where the perturbed plant belongs to a set of transfer functions P_m described by Δ_m. Figure 2.4 provides a schematic representation of this uncertainty model.

$$P_m = \left\{ P_m(s) = P(s)(1 + \Delta_m(s) W_m(s)) \;:\; |\Delta_m(j\omega)| < |W_m(j\omega)|^{-1} \right\} \quad \textbf{(2.13)}$$

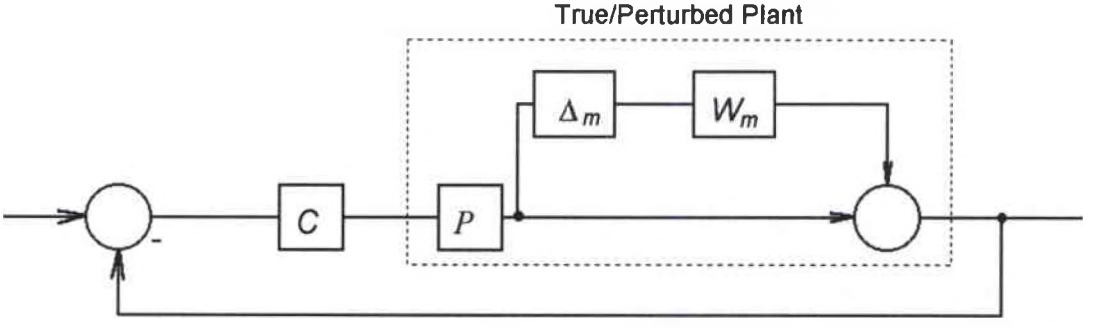

Figure 2.4 Multiplicative unstructured uncertainty model

In order to ensure that the model proves tractable for design synthesis the following requirements restrict 2.13: P and P_m have the same number of unstable poles, Δ_m is a variable transfer function satisfying $\|\Delta_m\|_\infty < 1$ and W_m is a fixed transfer function. Algebraic representation of 2.13 reveals some important features of this type of representation. Considering the first relationship in 2.14, the term $\Delta_m W_m$ completely describes the model uncertainty. The last inequality in 2.14 describes a disk like uncertainty in the complex plane. At each frequency the point P_m/P lies inside a disk of radius $|W_m|$ and center 1 and the ratio P_m/P may be considered the normalized plant

perturbation.

Note that $$\Delta_m W_m = \frac{P_m}{P} - 1$$

Hence if $$\|\Delta_m\|_\infty \leq 1,$$

Then $$|W_m(j\omega)| \geq \left| \frac{P_m(j\omega)}{P(j\omega)} - 1 \right|, \qquad \forall\omega \qquad \textbf{(2.14)}$$

It is pertinent to clarify at this time that this type of model might be quite conservative for some problems. Its conservativeness stems from the fact that in most cases W_m is not a constant, but a function of frequency and at times may constitute a generous approximation (see figure 2.8) to the true plant perturbation. The typical region of uncertainty is not exactly a disk, but rather an arbitrarily shaped geometric region, however, the benefit of assuming a disk like uncertainty is that the theoretical analysis is greatly simplified and the resulting systematic design process is remarkably practical. Finally, notice that this uncertainty model characterizes the set of perturbed plants by a nominal plant model and a weighting transfer function (W_m), described by the last equation in 2.14, which provides an uncertainty profile. It must be emphasized that the weighting transfer function must comply with the condition expressed by this inequality.

b) Additive perturbations: The additive uncertainty model, illustrated in figure 2.5, characterizes the set of perturbed plants P_a. Equation 2.15 expresses the additive perturbation model mathematically. The same conditions that restrict 2.13 are also applicable for equation 2.15. Algebraic reorganization of 2.15 reveals the characteristic nature of this type of representation. In a similar fashion to the multiplicative perturbation

case, the additive uncertainty is completely described by the term $\Delta_a W_a$. Also, the weighting function W_a is determined by the last inequality in 2.16 which relates it to the absolute model perturbation.

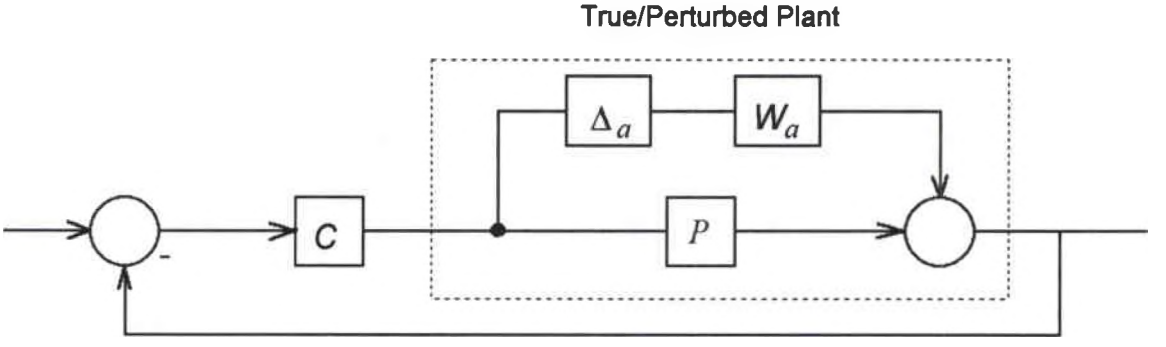

Figure 2.5 Additive unstructured uncertainty model

$$P_a = \left\{ P_a(s) = P(s) + \Delta_a(s) W_a(s) \;:\; |\Delta_a(j\omega)| < |W_a(j\omega)|^{-1} \right\} \qquad \textbf{(2.15)}$$

Note that, $\Delta_a W_a = P_a - P$,

hence if, $\|\Delta_a\|_\infty \leq 1$,

then, $|W_a(j\omega)| \geq |P_a - P|, \quad \forall\omega.$ **(2.16)**

c) Examples:

A few practical examples follow to demonstrate the computation of the uncertainty models described above. Consider the nominal plant transfer function $G(s)$ in 2.17. This is the typical model for a satellite with a single axis azimuth control problem (Franklin, Powell, Workman [1]). Suppose it is known that a better representation of the system is given by the higher order model $G_p(s)$ in 2.17, where the transfer function $G_p(s)$ would be the perturbed model. Equation 2.18 reveals the set of possible uncertainty profiles for

this system. The corresponding multiplicative and additive uncertainty models are determined from equation 2.14 and 2.16 and are shown graphically in figure 2.6.

$$G(s) = \frac{1}{s^2} \qquad \textbf{(2.17 } a\textbf{)}$$

$$G_p(s) = \frac{1}{s^2(s^2+2)} \qquad \textbf{(2.17 } b\textbf{)}$$

$$W_m(s) \geq \frac{s^2}{s^2(s^2+2)} - 1 \quad = \quad \frac{s^2+1}{s^2+2} \qquad \textbf{(2.18 } a\textbf{)}$$

$$W_a(s) \geq \frac{1}{s^2(s^2+2)} - \frac{1}{s^2} \quad = \quad \frac{s^2+1}{s^2(s^2+2)} \qquad \textbf{(2.18 } b\textbf{)}$$

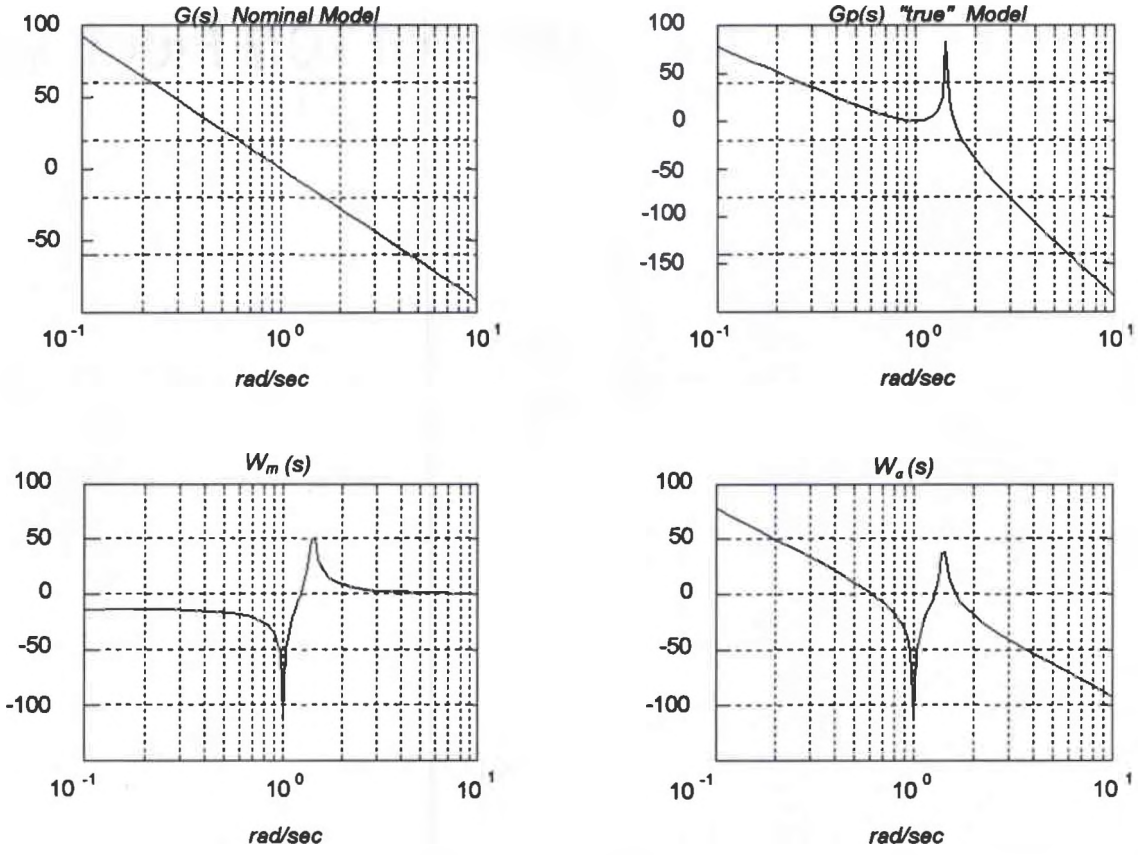

Figure 2.6 Modeling additive and multiplicative uncertainty

As a second example, consider the uncertainty associated with variable damping coefficients. The nominal, "true," and multiplicative weighting transfer functions are given in 2.19. The corresponding multiplicative weighting transfer function is shown graphically in figure 2.7.

$$P(s) = \frac{1}{s^2 + 2\xi_n s + 1} \qquad \xi_n = .4 \qquad \textbf{(2.19 } a\textbf{)}$$

$$P_m(s) = \frac{1}{s^2 + 2\xi s + 1} \qquad \xi \in (.1, .4) \qquad \textbf{(2.19 } b\textbf{)}$$

$$|W_m(j\omega)| \geq \left| \frac{P_m(j\omega)}{P(j\omega)} - 1 \right| \geq k \frac{(100s+1)(.05s+1)}{(s+1)^2} \qquad \textbf{(2.19 } c\textbf{)}$$

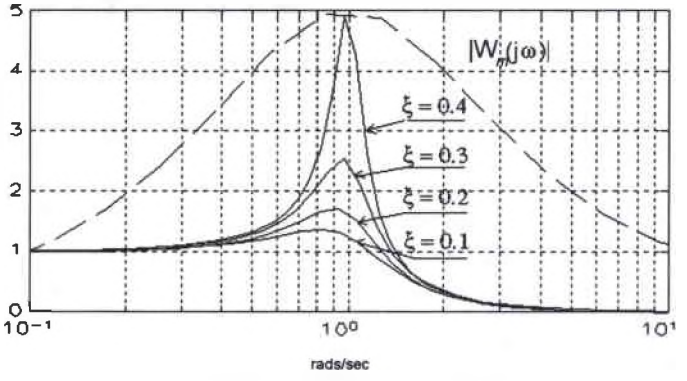

Figure 2.7 Damping uncertainty model

As a final example, consider the case of plants with transportation delay commonly encountered in chemical processes e.g. temperature control of fluids. Let $P(s)$ be the nominal plant and $P_m(s)$ be the perturbed plant. The multiplicative model in this case is expressed in 2.20.

$$P(s) = \frac{1}{s+1} \qquad \textbf{(2.20 } a\textbf{)}$$

$$P_m(s) = \frac{e^{-hs}}{s+1} \qquad :h \in [0,.2] \qquad \textbf{(2.20 } b\textbf{)}$$

$$|W_m(j\omega)| \geq \left|\frac{P_m(j\omega)}{P(j\omega)} - 1\right| \geq \left|e^{-hj\omega} - 1\right| \qquad ,\forall \omega, h \qquad \textbf{(2.20 } c\textbf{)}$$

2.3 Robustness and its Measures

The theory of control which aims to design controllers based on finite dimensional LTI models by incorporating the model uncertainties in the design process, is known in the literature as robust control theory. A controller is said to be robust with respect to some characteristic of the feedback system if it is able to maintain the characteristic for every plant of the perturbed set. The two most important characteristics of the feedback system are its stability and performance. Doyle, Kimura and Francis among other researchers in this field have developed measures to test the robustness of a system to these particular characteristics. These measures will be discussed in subsequent sections. The terminology *robust stability* and *robust performance* have gained wide acceptance among the control community to describe closed loop systems which meet stability and performance specifications even if the model does not accurately characterize the plant.

2.3.1 Classical Measures of Robust Stability

The classical measures of SISO stability are the *gain* and *phase* margins. The gain and phase margins follow directly from the Nyquist stability criterion [2], [3]. These margins essentially measure how close the Nyquist plot of a transfer function comes to encirclement of point (-1,0) or critical point on the Nyquist plane. Figure 2.9 provides a

graphical interpretation of these margins on the complex plane. The gain margin is then defined as the inverse of the distance from the origin to the point where the Nyquist plot intersects the real line and is a measure of how much the system gain may be increased before instability results. The phase margin equals the arc length, in radians, along the unit circle, from the Nyquist plot to the critical point. Consequently, if either is small the system is close to instability i.e close to encirclement of the critical point.

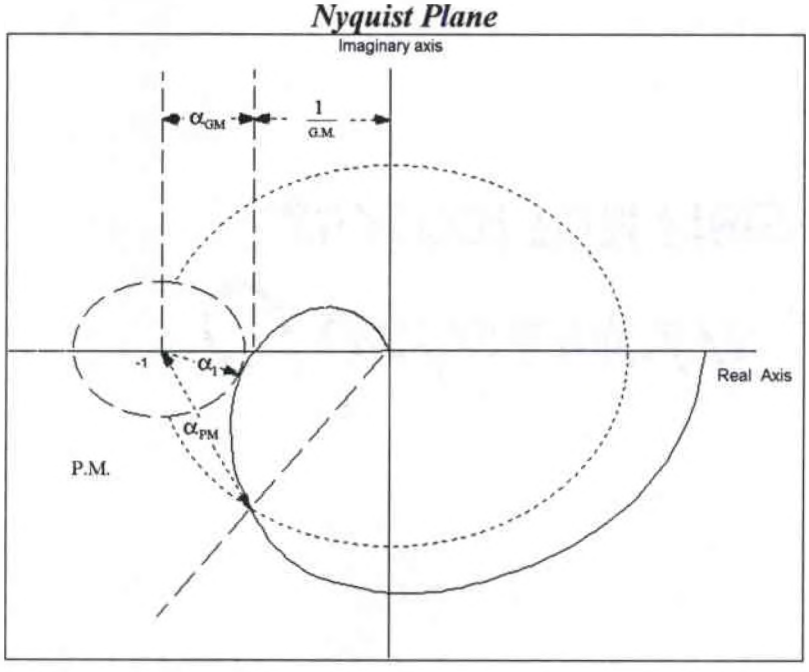

Figure 2.8 Phase and Gain margins on the Nyquist Plane

From figure 2.8 it is evident that these margins measure the distance from the critical point to the Nyquist plot in specific directions. The traditional or classical formulation of the control design problem incorporates performance and stability requirements into a single problem using the G.M. and P.M. definitions. The connection to the preceding discussion of the nominal performance condition provides an insightful connection to the H_∞ design problem. Recall equation 2.12 where $W_1(j\omega)$ provides a restriction on the open

loop plant transfer function. From figure 2.9 it is evident that $\|W_1(j\omega)\|_\infty$. bounds the G.M. and P.M. since $\alpha_1 < \alpha_{G.M.}$ and $\alpha_1 < \alpha_{P.M.}$.

As measures of robust stability, however, the gain and phase margins are somewhat inadequate because they do not convey information about the perturbation's effect on the stability of the system. In fact, they do not correlate the frequency dependent gains of a nominal system to the margins themselves. In order to improve their utility, these margins should measure the distance from the critical point to the Nyquist plot in all relevant directions. As a simple example consider the Nyquist plot in figure 2.9. This figure immediately reveals that gain and phase margins in this case completely fail to represent system robustness. While the phase margin is nearly 90 degrees and the gain margin is infinite, the system is still very close to instability. As a result, simultaneous small changes in gain and phase could cause instability. Thus, these margins do not provide insight into the stability of the system in the light of plant uncertainties, and therefore, the stability and performance of systems developed by design techniques based on these margins prove to be susceptible to plant perturbations.

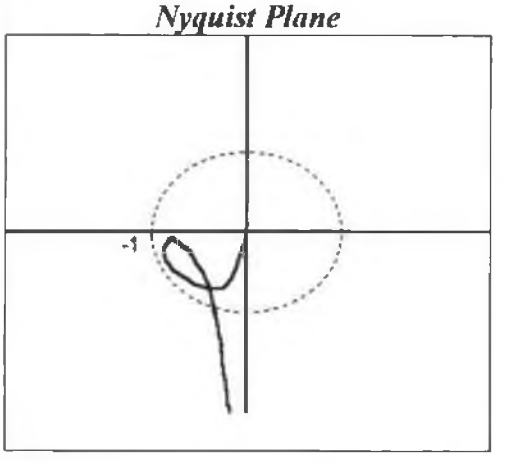

Figure 2.9 Robustness of Gain/Phase margins

2.3.2 Modern Robust Stability Analysis

Doyle and Francis were among the first to note the enticing relationship between the formulation of the stability problem of Nyquist and the infinity norm of the sensitivity transfer function. The following proof is developed in Doyle, Francis, and Tannenbaum [5] and is repeated here.

Let the smallest[2] distance from -1 to $L(j\omega)$ be denoted by d. Here $L(j\omega)$ is the Nyquist plot of the open loop transfer function. Then d is expressed by

$$d = \inf_{\omega} |-1 - L(j\omega)| = \inf_{\omega} |1 + L(j\omega)| \qquad \textbf{(2.21 } a\textbf{)}$$

$$d = \inf_{\omega} \left| \frac{1}{[1 + L(j\omega)]^{-1}} \right| = \left[\sup_{\omega} \frac{1}{|1 + L(j\omega)|} \right]^{-1} \qquad \textbf{(2.21 } b\textbf{)}$$

$$= \|S\|_{\infty}^{-1} \qquad \textbf{(2.21 } c\textbf{)}$$

Thus as $\|S\|_\infty$ becomes larger, d (i.e. the smallest distance) becomes smaller, the Nyquist plot comes closer to the critical point and the gain and phase margins decrease. Thus, the feedback system becomes nearly unstable and its performance degrades equivalently. It is comfortable to see that the later discussion heightens the findings of section 2.1, namely, the weighted sensitivity norm should be small for good performance. This norm then could serve as a measure of stability margin as well. However, it suffers partially from the same faults as the usual classical measures. While it indeed measures the smallest distance from the critical point to the Nyquist plot in all relevant directions, it fails to provide

---

[2] Here $\{ \inf_{\omega} \}$ refers to the minimum distance over all frequencies.

information about the plant perturbation effects. To remedy this lack of information, a better approach is to take the perturbed model itself into consideration. For instance, let the plant be perturbed to $P_p(j\omega)$ and $L_p(j\omega) = P_p(j\omega)C(j\omega)$ be the corresponding perturbed loop transfer function. Now, stability is guaranteed as long as the following inequality holds.

$$|Lp(j\omega) - L(j\omega)| < \|S\|_\infty^{-1}, \qquad \forall \omega$$

Figure 2.10 illustrates a graphical interpretation of this inequality in the Nyquist plane. Recall that $d = \|S\|_\infty^{-1}$ is the smallest distance from the critical point to the Nyquist plot of the loop transfer function. The left hand side of the above inequality is equivalent to the distance from the perturbed loop plot to the nominal loop plot at a given frequency. Since the point $L_p(j\omega)$ may lie anywhere around the point $L(j\omega)$, the distance between these two points is conservatively bounded to a disk around $L(j\omega)$ at every frequency ω. Consequently, as long as this disk does not encircle the critical point robust stability is preserved. This measure of stability is conservative in that it does not permit larger perturbations to occur at frequencies where $L(j\omega)$ is far from the critical point.

Modern Robust stability margins are obtained explicitly from the frequency dependent uncertainty models described in the previous section. Kimura [10] and Doyle, Francis and Tannenbaum [5] have developed such margins for the additive and multiplicative models respectively.

Consider again the multiplicative perturbation case for the plant set characterized in 2.22 with the unity feedback structure illustrated in figure 2.4. A controller C that

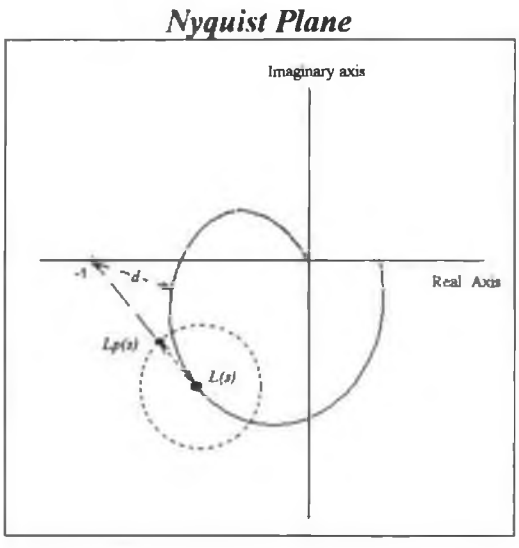

Figure 2.10 Robust stability margin

stabilizes the nominal plant P, will stabilize the entire family of perturbed plants if the positive number δ is small enough. If δ_{sup} is the least upper bound on δ such that C achieves stability for the entire family, then δ_{sup} is the stability margin for this uncertainty model.

$$P_m = \left\{ P_m = (1 + \Delta W_m) P \quad : \Delta \text{ is stable and } \|\Delta\|_\infty \leq \delta \right\} \qquad \textbf{(2.22)}$$

Doyle and Stein [6] developed a test for the robust stability criterion for multiplicative uncertainty models in the MIMO context. Later, Doyle, Francis, and Tannenbaum [5] presented an elaborated test for the SISO case. This test is summarized in theorem 1.

Theorem 1: *A controller C, in a closed loop feedback system as defined by figure 1.4, provides robust stability in the light of multiplicative uncertainties such that* $||\Delta_m||_\infty < 1$, *if and only if it achieves stability for the nominal plant and* $||W_m T||_\infty < 1$.

The proof of this theorem follows from the Nyquist stability criterion and can be found in Doyle and Stein [6]. The theorem can be used to find the stability margin $\|\delta\|_\infty$ mentioned above. Consider the case when $\delta > 1$, then it follows that, for the family of perturbed plants of equation 2.22,

$$\left\{P_m = (1+\Delta_1\delta W_m)P \quad : \quad \|\Delta_1\|_\infty \le 1\right\} \tag{2.23}$$

Where $\Delta_1 = \delta^{-1}\Delta$ and from theorem 1 then:

$$\delta_{sup} = sup\left\{\delta \quad : \quad \|\delta W_m T\|_\infty \le 1\right\} = \|W_m T\|_\infty^{-1} \tag{2.24}$$

Note that the smaller the size of $\|W_m T\|_\infty$, the greater will be the size of the smallest destabilizing multiplicative perturbation, and hence the greater will be the stability margin. The condition for robust stability defined by theorem 1 offers much insight into the stability robustness of a system when contemplated graphically in the Nyquist plane. The development of this graphical interpretation is as follows.

Given $$\|W_m T\|_\infty < 1$$

then,
$$\begin{aligned} \|W_m T\|_\infty < 1 &\Leftrightarrow \left|\frac{W_m(j\omega)L(j\omega)}{1+L(j\omega)}\right| < 1, \qquad \forall\omega \\ &\Leftrightarrow |W_m(j\omega)L(j\omega)| < |1+L(j\omega)|, \qquad \forall\omega \end{aligned} \tag{2.25}$$

Recall that the right hand side of the last inequality in 2.25 is the distance from the point (-1,0) to the Nyquist plot of $L(j\omega)$. Equation 2.25 then describes a disk of center $L(j\omega)$ and radius $|W_m L|$ at every frequency. Thus, at every frequency, much like in the case of figure 2.11, this disk must lie outside of the critical point so that stability is preserved. However, unlike the disk described by figure 2.11, the contour of this disk is shaped by

the multiplicative uncertainty profile function $W_m(j\omega)$. As a consequence, this margin is more relaxed than that previously defined due to the weighting function W_m.

Kimura [10] presented a similar test for the robust stability of additive perturbation models. Kimura defined a controller to be a *robust stabilizer* if it achieved robust stability for a set of perturbed plants. Kimura's test is restated in theorem 2.

> **Theorem 2:** *A controller C is said to be a robust stabilizer for a set of plants perturbed by additive uncertainties such that* $||\Delta_a||_\infty < 1$, *if and only if the closed loop system of figure 1.4 is stable for the nominal plant and* $\|W_a CS\|_\infty < 1, \quad \forall\omega$.

To close this section, table 2.2 summarizes the robust stability tests for the uncertainty models described in table 2.1.

Perturbation Model	Robust Stability Condition
$P/(1+\Delta W_2)$	$\|W_2 S\|_\infty < 1$
$P/(1+\Delta W_2 P)$	$\|W_2 PS\|_\infty < 1$
$P+\Delta W_a$	$\|W_a CS\|_\infty < 1$
$(1+\Delta W_m)P$	$\|W_m T\|_\infty < 1$

Table 2.2 Robust stability test for several perturbation models

2.3.3 Robust Performance

The idea behind the concept of robust performance is that the desired nominal performance, as specified by the designer, be achieved simultaneously with robust stability for a set of perturbed plants. It was demonstrated is section 2.1 that the nominal performance condition may be specified as an infinity norm bound on the weighted sensitivity of the system i.e. $\|W_1 S\|_\infty < 1$. In addition, theorem 1 established the robust stability condition for multiplicative uncertainties to be $\|W_m T\|_\infty < 1$. Clearly, the robust performance criteria requires both of these conditions to hold. More precisely, if a perturbed plant is modeled by a multiplicative uncertainty model, the sensitivity transfer function is perturbed to:

$$\begin{aligned} S_p &= \frac{1}{1+Lp} = \frac{1}{1+(1+\Delta W_m)L} \\ &= \frac{1}{(1+L)(1+\Delta W_m T)} = \frac{S}{1+\Delta W_m T} \end{aligned} \qquad \textbf{(2.26)}$$

Therefore, the weighted perturbed sensitivity is $W_1 S_p = \dfrac{W_1 S}{1+\Delta W_m T}$, and the robust performance condition will be satisfied if both the robust stability condition and the norm $\|W_1 S_p\|_\infty < 1$ are satisfied for all allowable perturbations. Theorem 3 provides a combined test for the robust performance condition. This is a difficult problem to solve. For a proof of this theorem see Doyle, Francis and Tannenbaum [5].

Theorem 3: A necessary and sufficient condition for robust performance is

$$\left\| |W_1 S| + |W_m T| \right\|_\infty < 1 \quad \text{(multiplicative perturbations)}$$

$$\left\| |W_1 S| + |W_a C S| \right\|_\infty < 1 \quad \text{(additive perturbations)}$$

2.4 Design Constraints

2.4.1 Algebraic Constraints on the Sensitivity and Complementary Sensitivity Functions

The condition for robust performance as expressed by theorem 3 places stringent constraints in the shape of the open loop frequency response of the nominal system. An elaborated mathematical proof of this fact can be found in Doyle, Francis, and Tannenbaum [5]. An intuitive analysis of the conditions for robust stability and nominal performance lead to the same conclusion and provides convenient graphical interpretation. Consider again equation 2.11 and add the robust stability condition of theorem 1. Noting the following relationships,

$$S = \frac{1}{1+L}, \quad T = \frac{L}{1+L}$$

If $|L(j\omega)| >> 1$ then $|S| \cong \frac{1}{|L|}$ and if $|L(j\omega)| << 1$ then $|T| \cong |L|$. Thus, if it is required from 2.11 that $|S| < |W_1|^{-1}$, then $\frac{1}{|S|} > |W_1|$ and consequently $|L| > |W_1|$ for all ω for which $|L(j\omega)| >> 1$. Similarly, requiring $\|W_m T\|_\infty < 1$ (from theorem 1), then $|T| < |W_m|^{-1}$ and consequently $|L| < |W_m|^{-1}$ for all ω for which $|L(j\omega)| << 1$.

The development above reveals the constraints imposed on the shape of open loop frequency response. Typically, the open loop transfer function has a low pass type frequency response, hence, the equations above require that the loop transfer function must be larger than $|W_1|$ at low frequencies and lower than $|W_m|^{-1}$ at high frequency. These constraints are graphically illustrated in figure 2.11

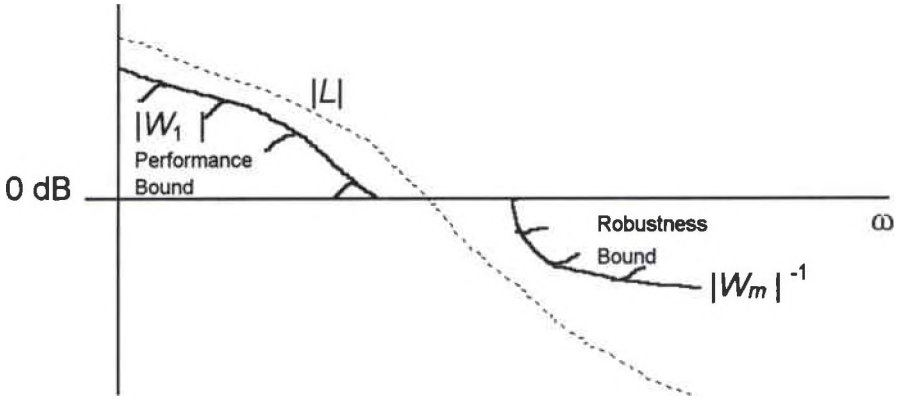

Figure 2.11 Loop shape constraints

The definition of the sensitivity and complementary sensitivity transfer function also places algebraic as well as interpolation restrictions on the design of a stabilizing controller. Note that the algebraic sum $S + T = 1$ must hold for all frequencies. This means that $|S(j\omega)|$ and $|T(j\omega)|$ can not both be less than 1/2 at the same frequency. On the other hand, the conditions shown below must hold for poles p and zeros z of the open loop transfer function.

$$S(p) = 0, \quad S(z) = 1,$$
$$T(p) = 1, \quad T(z) = 0.$$

2.4.2 Bounds on W_1 and W_m

Consider $\|W_1 S\|_\infty$ and suppose that the open loop transfer function has a zero at z in the RHP. Then, from the previous section, $\|W_1 S\|_\infty \geq |W_1(z)|$. This is a direct

consequence of the maximum modulus theorem. Thus, in order to satisfy the performance condition $\|W_1 S\|_\infty < 1$ the weighting function must satisfy $|W_1(z)| < 1$. That is to say, that the magnitude of the weight at the RHP zero of P or C must be less than 1. Similarly, assume that L has a pole at p. Then, $\|W_m T\|_\infty \geq |W_m(p)|$, therefore, a necessary condition for the robust stability criterion $\|W_m T\|_\infty < 1$ to hold is that the weight satisfy $|W_m(p)| < 1$. Furthermore, suppose that P has a zero z and a pole p in the RHP, and no other poles or zeros there. Also, suppose that C has neither poles nor zeros in the RHP. Then, both S and T can be factored into an all-pass and minimum phase terms like:

$$S = S_{mp} S_{ap} \quad and \quad T = T_{mp} T_{ap}$$

$$where\ S_{ap} = \frac{s-p}{s+p}, \quad and \quad T_{ap} = \frac{s-z}{s+z}$$

and S_{mp} and T_{mp} are the minimum phase transfer functions

From the preceding section it is true that $S(z) = 1$ and $T(p) = 1$. Therefore,

$$S_{mp}(z) = S_{ap}(z)^{-1} = \frac{z+p}{z-p}$$

$$T_{mp}(p) = T_{ap}(p)^{-1} = \frac{p+z}{p-z}$$

Finally, it follows that

$$1 > \|W_1 S\|_\infty = \|W_1 S_{mp}\|_\infty \geq |W_1(z) S_{mp}(z)| = \left| W_1(z) \frac{z+p}{z-p} \right|$$

$$1 > \|W_m T\|_\infty \geq \left| W_m(p) \frac{p+z}{p-z} \right|$$

The last inequality reveals that the closer the RHP pole and zero are to each other, the harder it becomes to achieve the desired performance or robust stabilization. As p approaches z the denominator in the right hand side of above inequalities decreases, making the ratio larger. This forces W_m or W_1 to be decreased at either p or z which ever may be the case. The weighting functions W_m or W_1, however, may be prohibited to be decreased at these frequencies by the requirements of 2.14 and the desired performance respectively.

2.5 The Robust Control Problem

In this chapter two prominent tests have been provided to assess both the nominal performance as well as the robust stability condition of the feedback control system as defined in figure 1.4. Furthermore, the robust performance condition, that is, guaranteed tracking in the face of plant uncertainty, is accomplished for multiplicative perturbations if both inequalities in 2.27 below are satisfied. A test for this condition was given in theorem 3.

$$\|W_m T\|_\infty < 1 \quad \text{and} \quad \left\| \frac{W_1 S}{1 + \Delta W_m T} \right\|_\infty < 1, \quad \forall \Delta \qquad \textbf{(2.27)}$$

Now that the necessary conditions for robustness given certain characteristics of the feedback system have been established. Lets summarize the objectives and design specifications of the robust control problem.

- **Robust Stability Problem:** Given the nominal plant P and the uncertainty description W_m, find a controller C, if one exists, that stabilizes all plants belonging to the perturbed set P_m.
- **Robust Performance Problem:** Given a class of plants described by P_m and a weighting upper bound function W_1 for the sensitivity S, find a robustly stabilizing controller C such that $\|W_1 S\|_\infty < 1 \qquad \forall \omega, and \forall P_m \in P_m$.

The design of robust controllers becomes a process of synthesizing a controller which complies with either the robust stability (i.e. theorem 1) or the robust performance (i.e. theorem 3) test as required by the designer and the particular control problem. Doyle and Kimura have both developed procedures for obtaining robust stabilizing controllers for multiplicative and additive perturbed sets respectively [6] [10]. Francis and Zames [9], on the other hand, have developed procedures for designing controllers that minimize the infinity norm of the weighted sensitivity. Despite considerable efforts among the robust control community, a systematic procedure to find a controller that satisfies the robust performance condition stated by theorem 3 has yet to be found.

CHAPTER III
SYNTHESIS OF SISO H_∞ CONTROLLERS

In this chapter a procedure will be developed to systematically synthesize a controller which complies with either the robust stability or the robust performance specifications discussed in the previous chapter. The design technique which will be used to address the robustness problem is referred to as "H_∞ control" in the control literature. The first section of this chapter defines the standard H_∞ control problem. Some preliminary mathematics required throughout the development of the design procedure are introduced in the second section. Finally, the design procedure for robust stabilization and robust performance are developed in the last two sections.

3.1 The Standard and Optimal SISO H_∞ Control Problem

3.1.1 The Generalized Problem

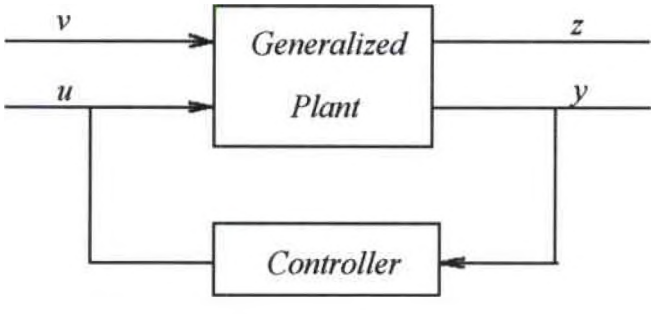

Figure 3.1 General control structure

Consider the generalized feedback structure of figure 3.1. The generalized plant consists of all of the fixed components of the system: the plant, actuators, sensors... The controller is the part to be designed. The signal vector *v* is composed of all the exogenous inputs while *u*, *y* and *z* contain all the controlled inputs, the sensor measurements, and the signals under control respectively. The tracking error, actuator and plant outputs are examples of signals that might be group under the generalized signal *z*.

Let T_{vz} represent the transfer function from *v* to *z*. The H_∞ design method aims to devise a controller which minimizes the infinity norm of T_{vz}. The generalized H_∞ design problem is summarized by the problem statement below.

> ***Problem 1:*** *Find a controller K(s), stabilizing the generalized plant, such that* $\|T_{vz}\|_\infty < \gamma$, *where* γ *is a small positive number less than or equal to 1.*

In addition, if the controller *K(s)* achieves the desired performance while minimizing the value of γ, the controller *K(s)* is considered optimal. If *K(s)* is an optimal controller then γ is denoted the optimum γ or γ_{opt}. Therefore, γ_{opt} may be defined as

$$\gamma_{opt} = inf \|T_{vz}\|_\infty \qquad \forall \quad stabilizing \quad K(s) \qquad \textbf{(3.1)}$$

3.1.2 The Mixed-Sensitivity Approach

For the SISO unity feedback structure specifically, the generalized diagram of figure 3.1 becomes figure 3.2 *a*. The diagram of figure 3.2 *b* is equivalent to that of figure 3.2 *a* although it exhibits a more familiar and usual feedback structure.

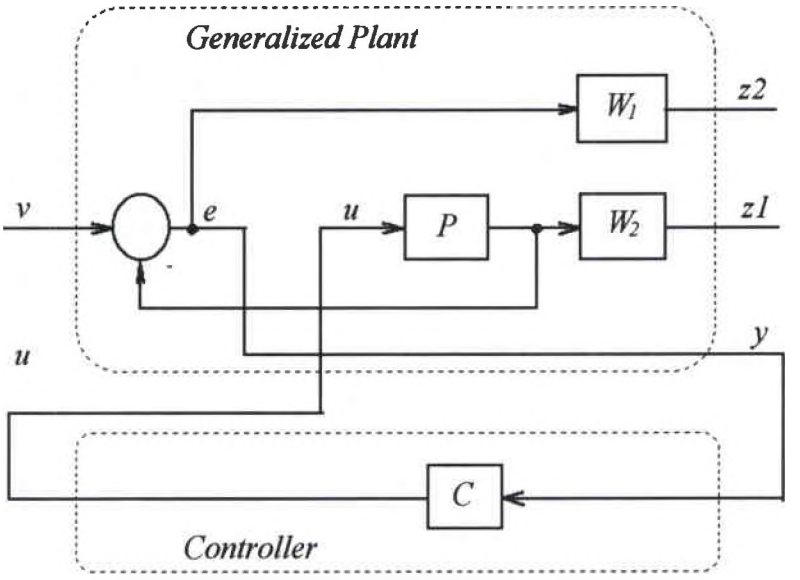

(*a*)

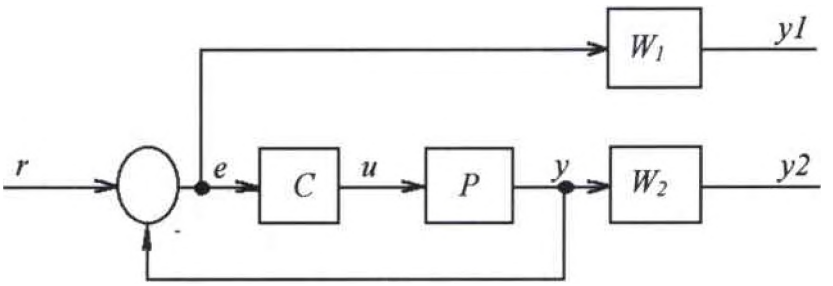

(*b*)

Figure 3.2 H_∞ control structure-mixed sensitivity approach

Note that for the structure presented in figure 3.2 *a*, the plant P has been augmented by W_1 and W_2, the performance weighting function and the uncertainty profile function respectively. For this structure the transfer function from v to z is represented by the vector function in 3.2.

$$T_{vz} \equiv \begin{bmatrix} W_1 S \\ W_2 T \end{bmatrix} \qquad \text{where} \quad z \equiv \begin{bmatrix} z_1 \\ z_2 \end{bmatrix} \qquad \textbf{(3.2)}$$

The infinity norm of this transfer function is sometimes known as the mixed sensitivity cost function because it penalizes both the sensitivity and the complementary sensitivity. The control signal u in figure 3.2 *b* is referred to as the ***robust stabilizing control law*** and is equal to $C(s)y(s)$. The standard H_∞ control problem may now be formulated for the system of figure 3.2. as follows:

> ***Problem 2:*** Given the desired performance level $\gamma > \gamma_{opt}$, find a the robust stabilizing control law $u(s) = C(s)y(s)$, *such that* $||T_{vz}||_\infty < \gamma$. If $\gamma = \gamma_{opt}$, the control law is said to be optimal.

Note that the definition of T_{vz} in equation 3.2 may be conveniently altered by the designer to achieve either or both of the objectives and design specifications described in section 2.4. That means that the statement of problem 2 may serve to satisfy either the *robust stability problem* or the *robust performance problem* separately simply by careful selection of the transfer function T_{vz}. For example, in a regulator case the designer might be solely interested in the robust stabilization of the system. In this case T_{vz} could be selected to be equal to W_2T with W_1 equal to zero. The counterpart of the former strategy is to select T_{vz} to be W_1S and let W_2 be zero. The latter selection, subject to the statement of problem 2, would yield the minimization of the nominal performance test as discussed in section 2.1.

Since the standard H_∞ control problem aims to make the ∞-norm of T_{vz} small it is also called in the literature the H_∞ *small-gain problem.* Moreover, the method for the design of a robust controller that will be presented in this chapter is occasionally referred to as the mixed sensitivity approach for finding the solution to problem 2, because it attempts to minimize the mixed sensitivity cost function.

3.2 Robust Control Synthesis and Related Mathematical Problems

The method of solution for the mixed sensitivity problem involves the use of a transformation which serves to synthesize all controllers which will make the closed loop system stable. This transformation is known as the *Q-parametrization* and is related to the works of Youla, Jabr, and Bongiorno [12]. Briefly speaking, the Q-parametrization formulates the controller transfer function in terms of a parameter Q. The controller can be obtained by proper design of Q and subsequent substitution into the controller formulation. The Q-parametrization has been used by Zames and Francis [8], Morari and Doyle [7], and Kimura [10] to characterize a class of stabilizing controllers in their theoretical investigations of system robustness. Given a parametrized set of stabilizing controllers, the robust stabilizer design problem is rearranged to fit the model matching problem which is solved by use of the Nevanlinna-Pick theory. The robust performance problem follows along similar lines with some additional adjustments.

The topics that follow are preliminary mathematical problems related to the synthesis of the robust controllers presented in this investigation. The discussion of these topics is necessary to understand the development of the systematic procedures that will be presented in the latter two sections.

3.2.1 The Q-Parametrization

The Q-parametrization was first introduced by Zames in [11] for open loop stable plants and later by Zames and Francis [8] for open loop unstable plants to characterize the family of all stabilizing controllers. The convenient feature of the Q-parametrization is that it guarantees closed loop stability. Recall the IMC structure of section 1.4 (pg. 9). It is argued in chapter I that the feedback control structure is only required because of disturbances and some uncertainty about the system. In fact, the feedback signal f as described in section 1.4 expresses the uncertainty about the process. Recall that when the plant model is exact and there are no disturbances the feedback signal disappears and the IMC structure becomes open loop. Under this open loop condition the criteria for stability of the nominal system follows trivially. Basically, for the system of figure 1.4 to be stable, under the condition that $f = 0$, both the plant G and the parameter Q must be stable.

An alternative representation of the block diagram of figure 1.4 is given by figure 3.3. Note that the block diagram of figure 3.3 has the form of the unity feedback structure. The mathematical manipulations which effect this transformation are omitted, but they have no effect on the response of the signals u and y to the inputs r and d. Indeed, the block diagrams of figures 1.4 and 3.3 are equivalent. The controller block of figure 3.3 may be replaced by a new block containing a compensator C. This compensator C is expressed by equation 3.3 in terms of the *stable* parameter Q and the plant model P,

$$C = \frac{Q}{1 - PQ}, \quad Q \in \Phi. \tag{3.3}$$

where the symbol φ represents the family of stable, proper and real rational transfer functions. This compensator description, known as the *Q-parametrization*, provides a simple parametrization of all stabilizing controllers for a stable plant G. The essential idea is that by using Q as a design variable instead of C, a potentially unstable design variable is replaced by a stable one and consequently closed loop stability is guaranteed. The advantage of this type of parametrization is truly of remarkable advantage, particularly for the case where the plant G is unstable.

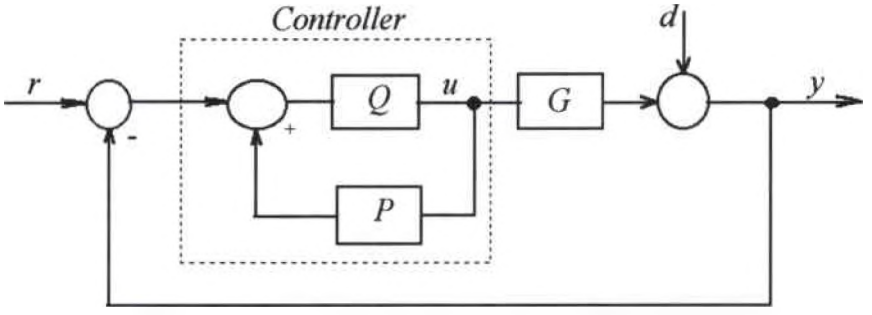

Figure 3.3 Alternate representation of the IMC structure

In order to extend the transformation of equation 3.3 to the case of unstable plants it is necessary to introduce the concept of a *coprime factorization*. Let P be a real rational transfer function. A representation of the form

$$P = \frac{N}{M}, \qquad N, M \in \varphi, \tag{3.4}$$

$$NX + MY = 1 \tag{3.5}$$

where N and M are coprime is called a coprime factorization of P over φ. Two functions N and M in φ are said to be coprime if there are two other functions X and Y also in φ

such that 3.5 is true. One consequence of the condition for coprimeness is that N and M have no common zeros in the closed RHP or at infinity. Consider equation 3.6 as an example. In this example, if $z = p$ then equation 3.5 does not hold when evaluated at $s = z$ or $s = p$, thus, N and M are not coprime.

$$N = \frac{(s-z)}{(s-1)} \qquad M = \frac{(s-p)}{(s-1)} \tag{3.6 a}$$

$$\text{if } z = p, \text{ then at } s = z: \quad 0 = \frac{(z-z)}{(z-1)} X(z) + \frac{(z-p)}{(z-1)} Y(z) \neq 1 \tag{3.6 b}$$

A procedure, based on Euclid's algorithm, for finding four transfer functions in φ satisfying equation 3.4 and 3.5 is provided below. Euclid's algorithm is outlined in appendix B.

An Algorithm to Find the Coprime Factorization of a Function G(s)

Given the transfer function G, the procedure is as follows:

i. If G is stable, set $N = G$, $M = 1$, $X = 0$, $Y = 1$ and stop.

ii. Transform $G(s)$ into $g(\lambda)$ under the mapping $s = (1-\lambda)/\lambda$. Let $n(\lambda)$ be equal to the numerator of $g(\lambda)$ and $m(\lambda)$ be the denominator of $g(\lambda)$.

iii. Use Euclid's algorithm with polynomials $n(\lambda)$ and $m(\lambda)$ to find polynomials $x(\lambda)$, $y(\lambda)$ such that $nx + my = 1$.

iv. Transform $n(\lambda)$, $m(\lambda)$, $x(\lambda)$, and $y(\lambda)$ to $N(s)$, $M(s)$, $X(s)$, and $Y(s)$ under the mapping $\lambda=1/(s+1)$.

Theorem 4 yields the controller parametrization for the general case.

Theorem 4: *Let $P = N/M$ be a coprime factorization over φ, where P may or may not be stable. Let X and Y be two functions in φ such that $NX + MY = 1$. Then the set of all controllers C for which the feedback system is stable equals:*

$$\left\{C = \frac{X + MQ}{Y - NQ}: \quad Q \in \varphi\right\}.$$

A proof of this theorem is available in Doyle, Francis and Tannenbaum [5]. Notice that the parametrization of equation 3.3 is a special case of the more general parametrization of theorem 4. For instance, when the plant is stable the parametrization of theorem 4 reduces to that of equation 3.3 under the following assignments:

$$N = P, \qquad M = 1, \qquad X = 0, \qquad Y = 1$$

$$\textit{then} \qquad C = \frac{X + MQ}{Y - NQ} = \frac{Q}{1 - PQ}.$$

3.2.2 Nevanlinna-Pick Theory

Nevanlinna-Pick or NP theory is concerned with an interpolation problem for a specified class of functions. The relevance of this theory to circuit and linear systems analysis has been reported in [13]. More importantly, in the context of this work, NP

theory plays a crucial part in the solution of the model matching problem. The SISO H_∞ problem is solved by manipulating its formulation to fit the model matching problem and it is necessary then to discuss the NP problem solution. The NP theory discussed here has been extracted both from Kimura [10] and Doyle, Francis and Tannenbaum [5]. It's use in the H_∞ problem is discussed in the next section of this thesis.

A function $u(s)$, analytic in the closed RHP and satisfying $|u(j\omega)| \leq 1$, $\forall\omega$, is called a *bounded real* (BR) function. If the equality condition is dropped then it is called a *strongly bounded real* (SBR) function. Note that a BR or SBR function has an ∞-norm bounded to 1. The NP interpolation problem may now be formulated.

Assume that the points $\{\alpha_1, ..., \alpha_n\}$ lie in the open complex RHP, and that the points $\{\beta_1, ..., \beta_n\}$ lie in some domain of the complex plane. The NP interpolation problem is to find a BR or SBR function $u(s)$ which satisfies the interpolation conditions,

$$u(\alpha_i) = \beta_i, \qquad i = 1,....., n \tag{3.7}$$

The additional constraints of stability and properness are added for algorithmic convenience.

The NP problem then is to find a stable and proper function $u(s)$ which has an infinity norm less than or equal to one, and whose graph passes through all points (α_i, β_i). The NP problem is said to be solvable if such a function $u(s)$ exists. If $u(s)$ is stable and proper and $u(\alpha_i) = \beta_i$, then the magnitude of $u(s)$ is $|\beta_i|$ at the point $s = \alpha_i$. According to the maximum modulus theorem [5] then its maximum magnitude is $\geq |\beta_i|$. This implies

that $\|u(s)\|_\infty \geq \beta_i$. One of the conditions of the problem is, however, that $\|u(s)\|_\infty \leq 1$. Therefore, an additional condition which guarantees solvability of the NP problem is that every member of the β data set must satisfy $|\beta_i| \leq 1$, $i = 1,....,n$.

An Hermitian[1] matrix exists, associated with the NP problem data called the *Pick matrix.* The ij^{th} element of the Pick matrix is

$$\frac{1-\beta_i\bar{\beta}_j}{\alpha_i+\bar{\alpha}_j} \quad \textit{where the hat denotes a complex conjugate}$$

The solvability condition of the NP problem is completely determined by the Pick matrix in 3.8 and has been established in Walsh [13]. It follows from Pick's theorem that the NP problem is solvable if and only if the Pick matrix is positive semidefinite for BR functions and positive definite for SBR functions.

$$\textit{Pick Matrix} = \begin{bmatrix} \frac{1-\beta_1\bar{\beta}_1}{\alpha_1+\bar{\alpha}_1} & \cdots & \frac{1-\beta_1\bar{\beta}_n}{\alpha_1+\bar{\alpha}_n} \\ \cdots & \cdots & \cdots \\ \frac{1-\beta_n\bar{\beta}_1}{\alpha_n+\bar{\alpha}_1} & \cdots & \frac{1-\beta_n\bar{\beta}_n}{\alpha_n+\bar{\alpha}_n} \end{bmatrix} \qquad \textbf{(3.8)}$$

A procedure for synthesizing such a function $u(s)$ which parametrizes all the solutions to the NP problem exists and is known as Nevanlinna's algorithm. Nevanlinna's algorithm is rather involved and therefore is omitted here, however, it is available in appendix B.

---

[1] Given a square complex matrix A, and its complex conjugate transpose A^*, a matrix is said to be *Hermitian* if $A = A^*$. The eigenvalues of a Hermitian matrix are real. In addition, A is positive definite or semidefinite if and only if its eigenvalues are > 0 or ≥ 0 respectively.

3.2.3 Model Matching Problem

Let $T_1(s)$ and $T_2(s) \in \varphi$. The model matching or approximation problem is to find a stable transfer function $Q(s)$ that minimizes the ∞-norm $(T_1\text{-}T_2Q)$. The term $(T_1\text{-}T_2Q)$ may be considered as an error transfer function under the following interpretation: T_1 is a model, T_2 is a plant, and Q is a cascade compensator to be designed so that the model matching error is minimized. The internal model control structure displayed in figures 1.4, and 3.3 is closely related to this interpretation.

Denoting the minimum model matching error by γ_{inf},

$$\gamma_{inf} = \inf_{Q\ stable} \|T_1 - T_2Q\|_\infty, \qquad \textbf{(3.9)}$$

where the design strategy is to make the definition of γ_{inf} as given by 3.9 fit the formulation of the standard H_∞ control problem as described by problem 2. The advantage of such a manipulation is that the solution of the model matching problem already exists. This strategy reveals a solution of 3.9 which indirectly leads to a systematic method of finding a control law that solves the robust stabilizing control problem and satisfies the conditions stated in problem 2. The term γ_{inf} in 3.9 refers to the minimum numerical value of gamma taken over the set of all stable solutions, Qs, of the model matching problem.

The subject of how to transform the H_∞ control problem into the model matching problem is discussed in the next section. This section is concerned with the solution of equation 3.9. Note that the trivial solution, of course, is the case when the error or

$\gamma_{inf} = 0$. Then $T_1 = T_2 Q$ and the unique solution Q is equal to $T_1 T_2^{-1}$ provided that the ratio is stable.

The solution to the model matching problem that will be discussed here may be found in Doyle, Francis and Tannenbaum [5]. γ_{inf} is the minimum gamma such that $\|T_1 - T_2 Q\|_\infty \leq \gamma$ for some stable Q. Let γ be a fixed positive number and consider the mapping of $Q \mapsto G$ given by 3.10. The inverse mapping specifies the solution to the model matching problem in terms of G and may be expressed by equation 3.11

$$G = \gamma^{-1} \cdot (T_1 - T_2 Q) \qquad \textbf{(3.10)}$$

$$Q = \frac{T_1 - \gamma \cdot G}{T_2} \qquad \textbf{(3.11)}$$

The solution of the model matching problem is found by constructing a function G, satisfying equation 3.9, such that the parameter Q is stable. Under the mapping of 3.10, G will be stable if Q is stable, but the converse is not true since T_1 and T_2 are members of the set φ. In order for Q in 3.11 to be stable, G must satisfy certain conditions.

Let $\{z_i: i = 1,\ldots,n\}$ be the zeros of T_2 in the open RHP. It is assumed for simplicity that T_2 has no zeros in the $j\omega$ axis. Given a stable Q, then G satisfies the following interpolation conditions:

$$G(z_i) = \gamma^{-1} \cdot T_1(z_i), \qquad i = 1,\ldots,n. \qquad \textbf{(3.12)}$$

Therefore, if G is stable and satisfies the condition in 3.12, then Q will be stable. Reformulating the definition of γ_{inf} subject to the mapping of the relationship in 3.10, γ_{inf} is the minimum gamma such that a function G exist, analytic in the RHP, satisfying the interpolation condition in 3.12 and $\|G\|_\infty \leq 1$. Note that the constraints imposed on G in order to find a stable Q fit the Nevanlinna-Pick problem description after minor adjustments. In this particular case, the NP problem data is given by 3.13.

$$\{\alpha_1, \ldots, \alpha_n\} \qquad \textit{where} \quad \alpha_i = z_i, \ \textit{the RHP zeros of} \ T_2$$
$$\{\gamma^{-1}\beta_1, \ldots, \gamma^{-1}\beta_n\} \qquad \beta_i = T_1(z_i) \qquad \textbf{(3.13)}$$

It can be readily shown that the Pick matrix associated with this data set equals $B - \gamma^{-2}D$, where the ij^{th} element of B and D are, respectively,

$$\frac{1}{\alpha_i + \overline{\alpha}_j}, \qquad \frac{\beta_i \overline{\beta}_j}{\alpha_i + \overline{\alpha}_j}.$$

It follows from Pick's theorem that γ_{inf} exists only if the Pick matrix $B - \gamma^{-2}D$ is positive semidefinite. An explicit way to compute γ_{inf} is given by lemma 1 below. Lemma 1 is a direct quote from Doyle, Francis, and Tannenbaum [5].

Lemma 1: *γ_{inf} equals the square root of the largest eigenvalue of the matrix $B^{-1/2}DB^{-1/2}$, where $B^{-1/2}$ is the inverse of the square root of the matrix B.*

The Model Matching Problem Solution Algorithm

A procedure for solving for γ_{inf}, and $Q(s)$ given T_1 and T_2 is outlined below:

i. Identify the zeros of T_2 in the open RHP.

ii. Find the β data set as indicated by 3.13 and form the related matrices B and D.

iii. Compute the optimum gamma as described by lemma 1 (use the Matlab program "gamopt.m" provided in appendix C) .

iv. Solve the NP problem as indicated in appendix B for the data set:

$$\begin{matrix} z_i & \cdots & z_n \\ \gamma_{inf}^{-1}\beta_i & \cdots & \gamma_{inf}^{-1}\beta_n \end{matrix}$$

and let the solution be denoted by the function G.

v. The solution to the model matching problem is given by $Q = \dfrac{T_1 - \gamma_{inf} G}{T_2}$.

For the particular case when T_2 has only one zero, s_o in RHP, the solution is given by 3.11 with $\gamma_{inf} G$ equal to $T_1(s_o)$. The proof is given in appendix B.

3.3 Optimal and Sub optimal Robust Stabilization

3.3.1 Robust Stability Margin Optimization

In this section a method for designing a controller which maximizes the robust stability margin will be addressed. In sections 2.3.1 and 2.3.2 several measures of stability were

discussed (e.g. phase and gain margins). In addition, a robust stability margin for a multiplicative perturbation model has been introduced in chapter II by equation 2.24. Equation 2.24 is shown below for convenience.

$$\delta_{sup} = \sup\{\delta \quad : \quad \|\delta W_m T\|_\infty \le 1\} \quad = \|W_m T\|_\infty^{-1}$$

It will be shown in this section that the problem of synthesizing a robust control law is solved by optimizing the stability margin, which in turn reduces to a model matching problem as explained in the previous section. The optimization problem discussed here regards to the special case where the set P_m consists of multiplicative perturbations of a nominal plant P. The method of solution which will be presented was developed by Doyle, Francis and Tannenbaum [5]. A procedure for a set of perturbed plants under additive perturbations is available from Kimura [10].

Let's reiterate the robust stability problem. Given a plant P, member of a set of the form of equation 2.22, and a unity feedback structure, the robust stability problem is to find a compensator C that achieves stability for every plant member P of the set. According to theorem 1, a compensator C achieves stability for every plant in P_m, if and only if it achieves stability for the nominal plant P and satisfies $\|W_2 T\|_\infty < 1 / \delta$, where δ is the stability margin and T is the nominal complementary sensitivity. A compensator C is said to be optimal if it achieves the maximum stability margin δ_{sup} while it is considered sub optimal if it achieves a stability margin $\delta < \delta_{sup}$. Let γ_{opt} be defined by equation 3.14,

$$\gamma_{opt} = \inf_C \|W_2 T\|_\infty \qquad \textbf{(3.14)}$$

where the infimum is taken over all stabilizing compensators. Note that under this definition T_{vz} has been taken to be merely W_2T. It follows that the maximum stability margin is[2]

$$\gamma_{opt} = 1/\delta_{sup}. \qquad \textbf{(3.15)}$$

The procedure to synthesize a compensator that satisfies the robust stability criteria is now explained.

Consider a coprime factorization of the nominal plant such that 3.4 and 3.5 hold. Then by theorem 4 the parametrization of all stabilizing controllers for the nominal plant is expressed by 3.16.

$$C = \frac{X + MQ}{Y - NQ}, \qquad Q \in \varphi. \qquad \textbf{(3.16)}$$

$$T = N(X + MQ) \qquad \textbf{(3.17)}$$

It is readily demonstrated that the complementary sensitivity transfer function T is equal to 3.17 if P and C are substituted by their coprime factor equivalents. Substituting 3.17 into 3.14 yields 3.18. Notice, that the infinity norm term in 3.18 is equivalent to the robust stability test introduced in chapter II. By substitution of $T_1 = W_2NX$ and $T_2 = - W_2NM$ in 3.18 it becomes evident that the formulation of equation 3.18 is nearly equivalent to the model matching problem of equation 3.9.

---

[2] The proof of this statement follows directly from theorem 1 and equations 2.24 and 3.14. For instance, if $\delta < \delta_{sup}$, then there exist a robust stabilizer and therefore from theorem 1, $\|W_2T\|_\infty < 1/\delta$. But from equation 3.14 γ_{opt} is the infimum of $\|W_2T\|_\infty$ over all stabilizing comtrollers. Thus, $\gamma_{opt} = 1/\delta_{sup}$.

$$\gamma_{opt} = \inf_{Q \in \varphi} \| W_2 N (X + MQ) \|_\infty \qquad \textbf{(3.18 } a\textbf{)}$$

$$\text{note that } \| W_2 NX - (-W_2 NM) Q \|_\infty = \| T_1 - T_2 Q \|_\infty \qquad \textbf{(3.18 } b\textbf{)}$$

$$\text{with } T_1 = W_2 NX \text{ and } T_2 = W_2 NM$$

In addition, recall that it is assumed in section 3.2.3 that T_2 has no zeros in the imaginary axis. To avoid conflict with the previous postulation it is assumed that P has no poles or zeros on the jω axis and W_2 has no zeros on the imaginary axis.

The only difference between the model matching problem in 3.9 and the equivalent formulation in 3.18 is that the parameter Q in 3.18 must be proper in contrast to the situation of equation 3.9, where Q is only required to be stable. Therefore, before itemizing a systematic procedure for the design of a robust stabilizer, it is necessary to address the extra requirement that the parameter Q be proper. The solution with this minor impediment is a result of direct application of lemma 2 below. The strategy is to initially ignore the properness requirement of Q and find a new parameter, possibly improper but stable, and denoted Q_{im}. Equation 3.18 *a* is then slightly modified to

$$\gamma_{opt} = \inf_{Q \in \varphi} \| W_2 N (X + MQ_{im}) \|_\infty \qquad \textbf{(3.18 } c\textbf{)}$$

A proper Q is developed by rolling off Q_{im} at high frequency through multiplication of Q_{im} by a filter of the form of 3.19.

$$J(s) = \frac{1}{(s\tau + 1)^\kappa} \qquad \textbf{(3.19)}$$

Lemma 2: *Let $J(s)$ be described by 3.19, where τ is real and κ is an integer. If G is stable and strictly proper, then* $\lim_{\tau \to 0} \|G(1-J)\|_\infty = 0.$

To show that the suggested manipulation does not affect the integrity of the formulation of equation 3.18 we can review the proof of lemma 2. Figure 3.4 illustrates the generalize Bode and Nyquist plots of $J(s)$ for several values of τ and κ.

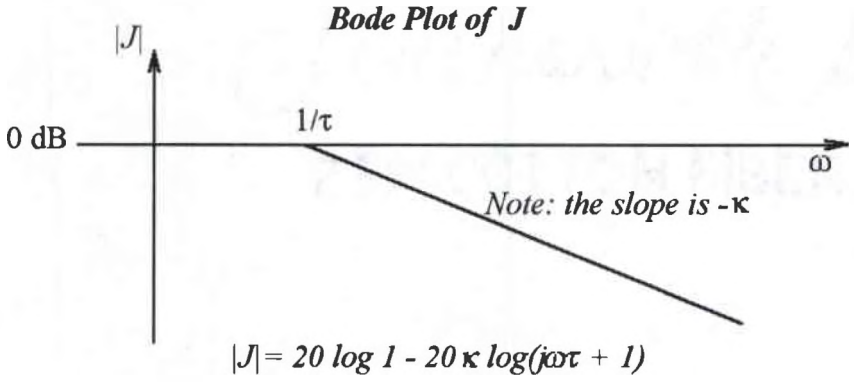

(*a*)

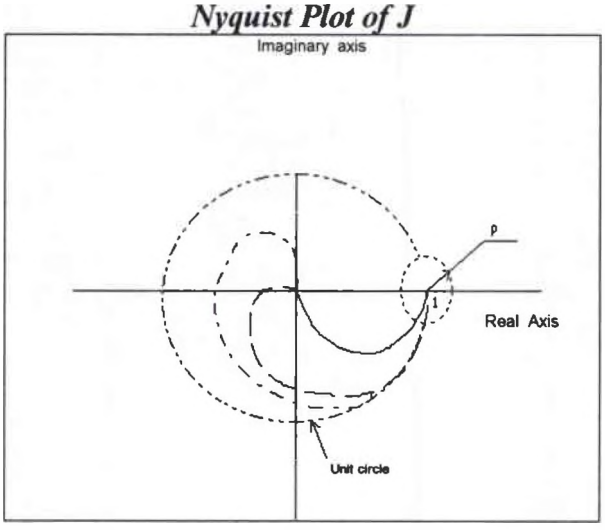

(*b*)

Solid: $\kappa = 1$, Dashed: $\kappa = 2$, Dashed-dot: $\kappa = 3$.

Figure 3.4 (*a*) Bode plot of J (*b*) Nyquist plot of J

Consider figure 3.4. Let ρ be a small positive number and ω_1 be the -3dB frequency of $J(j\omega)$. Notice that if τ is small enough, then the Nyquist plot of J lies in a disk of center 1, radius ρ for frequencies less than ω_1 and in a disk of center 0, radius 1 for frequencies greater than ω_1. This condition is expressed mathematically by equation 3.20.

$$\|G(1-J)\|_\infty = \begin{cases} \max\limits_{\omega \le \omega_1} |G(j\omega)[1-J(j\omega)]| \\ \max\limits_{\omega \ge \omega_1} |G(j\omega)[1-J(j\omega)]| \end{cases} \qquad \textbf{(3.20)}$$

Consider the case when $\omega \le \omega_1$ in 3.20. Since $|1-J|$ is the distance from the point (1,0) in the Nyquist plane to the polar plot of $J(j\omega)$, this distance is bounded by the radius ρ when $\omega \le \omega_1$. Therefore, for $\omega \le \omega_1$, the norm $\|G(1-J)\|_\infty$ is bounded by $\rho\|G\|_\infty$. To illustrate, suppose $\omega_1 = 1/\tau$, then for $\omega \le \omega_1$, $|J| \cong 1$ and the distance $|(1-J)|$ is very small.

Conversely, for the case when $\omega \ge \omega_1$ the lower term in 3.20 can be expressed as in 3.21*a*.

$$\|(1-J)\|_\infty \cdot \max_{\omega \ge \omega_1} |G(j\omega)| \qquad \textbf{(3.21 } \boldsymbol{a}\textbf{)}$$

The infinity norm of $(1-J)$ in this case is bounded by 2 as can be seen in the following equation.

$$\|(1-J)\|_\infty \le \|1\|_\infty + \|J\|_\infty = 2 \qquad \textbf{(3.21 } \boldsymbol{b}\textbf{)}$$

Thus, for the case when $\omega \ge \omega_1$, $\|G(1-J)\|_\infty$ is bounded by the expression shown below.

$$2 \max_{\omega \ge \omega_1} |G(j\omega)| \qquad \textbf{(3.22)}$$

In general, the infinity norm of $\|G(1-J)\|_\infty$ is bounded by the expression in 3.23. Note, that the right hand side of 3.23 can be made arbitrarily small by suitable choice of ρ and ω_1 because, in the limit as ω_1 approaches infinity, G approaches zero. In conclusion, for every small number $\lambda > 0$, if τ is small enough, then $\|G(1-J)\|_\infty \leq \lambda \cong 0$.

$$\textit{For sufficiently small } \tau\text{:}\quad \|G(1-J)\|_\infty \leq \max\left\{\rho\|G\|_\infty, 2\max_{\omega\geq\omega_1}|G(j\omega)|\right\} \quad \textbf{(3.23)}$$

Equation 3.18 c is reorganized in 3.24 after Q_{im} is rolled off by the filter $J(s)$.

$$W_2N(X + MQ_{im}J) \quad \textbf{(3.24)}$$

$$W_2N(X + MQ_{im})J \; + \; W_2NX(1-J) \quad \textbf{(3.25)}$$

Notice that 3.24 can be factored into 3.25. From lemma 2 it is evident that the infinity norm of the right hand term in 3.25 goes to zero as τ approaches zero. The left hand term has infinity norm less than one since the infinity norm of J is one and that of the term $W_2N(X + MQ_{im})$ is less than one by definition. Thus, the postulation of 3.18 has not been affected by the given manipulation.

The H_∞ Design Procedure.

Given the nominal plant P and the uncertainty weighting W_2, the procedure for the design of a robust stabilizer controller is as follows:

i. Select W_2 such that $W_2(p) < 1$ where p are poles of P in RHP.

ii. Form a coprime factorization of P such that $P = \dfrac{N}{M}$, $N, M \in \omega$, and $NX + MY = 1$ (using Euclid's algorithm)

iii. Solve the model matching problem with $T_1 = W_2 NX$ and $T_2 = -W_2 NM$. (using Nevanlinna's algorithm and the procedure outlined in section 3.2.3.)

iv. Denote the solution of the previous step Q_{im} and let $\gamma_{inf} = \gamma_{opt}$ (the minimum model matching error). Then $\delta_{sup} = 1/\gamma_{opt}$.

v. Choose an arbitrary number $\delta \leq \delta_{sup}$. Set $J(s) = \dfrac{1}{(s\tau + 1)^k}$ with k large enough to make $Q_{im}J$ proper and τ small enough that $\|W_2 N(X + MQ)\|_\infty \leq 1/\delta$

vi. Set $Q = Q_{im}J$ and find $C = \dfrac{X + MQ}{Y - NQ}$.

A routine written for the Matlab environment was designed to compute the optimum gamma in step iii, given the uncertainty weighting function and the coprime factorization of P. This program named "gamopt.m" is included in appendix C.

3.3.2 A Simple Example

Consider the following unstable plant: $P(s) = \dfrac{s-1}{(s+1)(s-.5)}$

The procedure for obtaining the robust stabilizer is as follows:

Step i: Determine the uncertainty weight $W_2(s)$. In this case, $W_2(s)$ is arbitrarily selected as, $W_2(s) = \dfrac{(s+.1)}{(s+1)}$

Step ii: Compute the coprime factorization of the plant following Euclid's algorithm and the procedure outlined in appendix B. The results are:

$$N(s) = \frac{s-1}{(s+1)^2} \qquad X(s) = -4.5$$

$$M(s) = \frac{s-.5}{s+1} \qquad Y(s) = \frac{s+7}{s+1}$$

Step iii: Compute T_1 and T_2 and solve the model matching problem to find γ_{opt} and Q_{im}. Solution of the previous step leads into the following results:

$$T_1 = W_2NX = \frac{-4.5(s+.1)(s-1)}{(s+1)^3}$$

$$T_2 = -W_2NM = \frac{-(s-.5)(s+.1)(s-1)}{(s+1)^4}$$

The associated NP problem data and the value of γ_{opt} are found using the Matlab routine in appendix C. The NP problem data involved is:

$$\textit{related NP problem data:} \begin{cases} 1 & 0.5 & [\textit{zeros of } T_2 \textit{ in the RHP}] \\ 0 & 0.4 & [\gamma^{-1}T_1(z_i)] \end{cases}$$

Using the Nevanlinna Pick algorithm outlined in appendix B with the data shown above yields the function, $G(s) = \frac{1-s}{s+1}$. The value of γ_{inf} is obtained from execution of the Matlab routine "gamopt.m" and is found to be $\gamma_{inf} = 1.2$. The solution of the model matching problem, Q, is found to be

$$Q = \frac{T_1 - \gamma_{inf}G(s)}{T_2} = -\frac{1.2(s+1)(s-1.25)}{s+0.1}.$$

Step iv: Since the function Q found in step iii is improper, denote it Q_{im} and set $\gamma_{opt} = \gamma_{inf} = 1.2$. The maximum stability margin $\delta_{sup} = \frac{1}{1.2} = 0.8333$.

Step v: Arbitrarily select $\delta = 0.8$ as the required stability margin.

According to the defined procedure, a roll-off filter J must be selected with τ small enough to make Q_{im} proper and such that $\|W_2N(X+MQ_{inf}J\|_\infty < 1/\delta$ or 1.25.

Let, $$J(s) = \frac{1}{(\tau s+1)}$$

Note that κ in this case is 1 which is the relative degree of Q_{im}. Table 3.1 shows the results of the iterations on τ. From table 3.1 its obvious that $\tau = 0.01$ is the an acceptable time constant.

τ	$\|W_2N(X+MQ_{im}J)\|_\infty$
1	2.1188
0.1	1.4925
0.01	1.2396

Table 3.1 Results of robust stability tests for several τ

Step vi: Set $Q = Q_{inf}J$ to find the parameter that characterizes the set of all robust stabilizing controllers for the given nominal plant and uncertainty weighting. Then,

$$\text{Set } Q(s) = Q_{im}J = \frac{-120\,(s+1)(s-1.25)}{(s+0.1)(s+100)}$$

The resulting controller is found from 3.16 and is equal to:

$$C = \frac{X + MQ}{Y - MQ} = \frac{-(s+1)\,(124.5s^2 + 240.45s + 120)}{(s^3 + 227.1s^2 + 440.7s + 220)}$$

and the design is complete. Figure 3.5 provides the graphical interpretation of the robust stability test for this problem with different values of τ. Notice from figure 3.5 and table 3.1 that this a sub optimal controller since it does not quite achieve the maximum robust stability margin. Recall from step v that we set $\delta = 0.8$. Thus the robust stability test requires that $\|W_2N(X+MQ_{im}J\|_\infty < 1 / \delta$ or 1.25. With τ equal to 1 and 0.1 the infinity norm of the weighted complementary sensitivity (i.e. $\|W_2N(X+MQ_{im}J\|_\infty$) is 2.1188 and 1.4925 respectively. Thus, the requirement that the infinity norm of the weighted complementary sensitivity be less than 1.25 is not met. With τ equal to 0.01, however, the infinity norm of $\|W_2N(X+MQ_{im}J\|_\infty$ is equal to 1.2396 satisfying the robust stability test for this case.

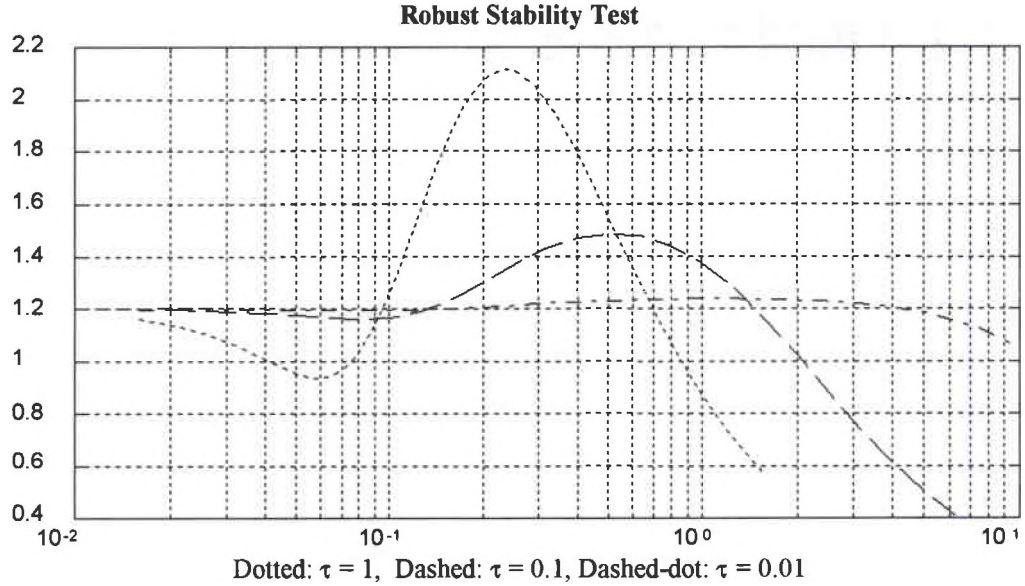

Figure 3.5 Frequency Response of $W_2N(X+MQ_{im}J)$ for the τ of table 3.1

3.4 Optimal and Sub optimal Robust Performance

The solution of the problem 2 statement (i.e. the standard H_∞ control problem as defined in section 3.1.2) is the subject under examination in this section. In this case T_{vz} is chosen with non zero weighting functions W_1 and W_2. The test for the robust performance condition introduced in section 2.4, is formulated in the context of theorem 3, and is repeated below to refresh the readers memory.

$$\left\| |W_1 S| + |W_2 T| \right\|_\infty < 1 \qquad \textbf{(3.26 } a\textbf{)}$$

Recall from the final section of chapter II that a systematic procedure to find a controller which satisfies the condition shown above has not yet been devised. Instead, Doyle, Francis, and Tannenbaum [5] have proposed a method to design robust controllers which comply with the robust performance condition by solving an alternate, related but more conservative problem. This alternate problem requires that the condition expressed in 3.26 below be met. Simple plane geometry shows that if condition 3.26 is met then the robust performance test of theorem 3 holds. A proof of this is provided in appendix A.

$$\left\| |W_1 S|^2 + |W_2 T|^2 \right\|_\infty < 0.5 \qquad \textbf{(3.26 } b\textbf{)}$$

The strategy for finding a controller satisfying the robust performance test is very similar to the procedure for optimizing the robust stability margin. Some adjustments are essential due to the evident differences between the robust stability test and the robust performance test. As in the development of the former section, the scope of the problem treated here is restricted to the case where the set P_m consists of multiplicative

uncertainties of a nominal plant P. The solution of the robust performance problem that will be introduced in this section is based on the work of Doyle [14], and Francis [15], [16]. However, the procedure is outlined in the more recent publication of Doyle, Francis and Tannenbaum [5]. The following compromising assumptions are made throughout the development:

1. P is strictly proper and has no poles or zeros on the imaginary axis.
2. W_1 and W_2 are stable and proper.
3. W_1 and W_2 have no common zeros on the imaginary axis.

3.4.1 Spectral Factorization

Spectral factorization will be used as a tool in the solution process. Given a rational function $F(s)$ with real coefficients, let $\overline{F}(s)$ denote the function $F(-s)$. If such a function F has the property $\overline{F} = F$, then its poles and zeros form a symmetrical pattern in the s-plane with respect to the real and imaginary axis. A function F having this property may be written in terms of its gain, poles and zeros as,

$$F(s) = cF_1(s), \quad where\ F_1(s) = \frac{\prod(z_i - s)(z_i + s)}{\prod(p_i - s)(p_i + s)} \qquad \textbf{(3.27 } \boldsymbol{a}\textbf{)}$$

$$F(s) = c\overline{H}(s)H(s), \quad where\ H(s) = \frac{\prod(z_i + s)}{\prod(p_i + s)} \qquad \textbf{(3.27 } \boldsymbol{b}\textbf{)}$$

Note that $F_1(0) > 0$. Both c and $F_1(0)$ will be greater than zero if and only if $F(0) > 0$. By letting a new function $H(s)$ be composed of the LHP factors of $F_1(s)$ and $\overline{H}(s)$ to be

formed from the factors with RHP poles and zeros of $F_1(s)$, $F(s)$ may be factored into the form given in 3.27 *b*. Define a *spectral factor* $F_{sf}(s)$ of $F(s)$ as in equation 3.28 where $c > 0$.

$$F_{sf}(s) = \sqrt{c}\,\frac{\prod(z_i + s)}{\prod(p_i + s)} \qquad \textbf{(3.28)}$$

The function $F(s)$ may now be factored to get $F = F_{sf}\tilde{F}_{sf}$ with F_{sf}, F_{sf}^{-1} stable. This is called a spectral factorization of F.

Consider the following function as an example: $F(s) = \frac{1}{1 - s^2}$. This function may be factored into $F(s) = \frac{1}{(1-s)}\frac{1}{(1+s)}$, therefore it has a spectral factor $F_{sf}(s) = \frac{1}{1+s}$.

The discussion above may be summarized into a lemma:

> ***Lemma 3:*** *If a real rational function F has the properties,* $\tilde{F} = F$, *no zeros or poles in the imaginary axis, and* $F(0) > 0$, *then it has a spectral factorization.*

3.4.2 Robust Performance Optimization

To synthesize the problem, the coprime factorization of the plant is computed using the procedure outlined earlier in the solution of the robust stability problem. Substitution

of S and T into inequality 3.26 *b* in terms of Q and the coprime factors of P yields inequality 3.29.

$$\left\| |W_1 M(Y - NQ)|^2 + |W_2 N(X + MQ)|^2 \right\|_\infty < 1/2 \qquad \textbf{(3.29)}$$

The problem now, as before, is to manipulate equation 3.29 to fit the formulation of the model matching problem. Defining the following identities,

$$\begin{aligned} R_1 &= W_1 MY & S_1 &= W_2 NX \\ R_2 &= W_1 MN & S_2 &= -W_2 NM \end{aligned} \qquad \textbf{(3.30)}$$

substitution into 3.29 yields,

$$\left\| |R_1 - R_2 Q)|^2 + |S_1 - S_2 Q)|^2 \right\|_\infty < 1/2 \qquad \textbf{(3.31)}$$

The inequality in 3.31 has two square terms in Q. To approximate the model matching formulation, equation 3.31 must now be manipulated so that a single inequality in Q appears. The general formulation of the model matching problem is $\|A - BQ\|_\infty < 1$. Thus, we will start with a term of the form

$$|A - BQ|^2 < 1 \qquad \textbf{(3.32)}$$

and mathematically manipulate the inequality to have the form of equation 3.31. Substituting $A = U_1 U_3^{-1}$ and $B = U_2 U_3^{-1}$ into 3.32 yields

$$\left|U_3^{-1}U_1 - U_3^{-1}U_2Q\right|^2 < 1, \quad \forall\omega \tag{3.33}$$

Continuing the development then equation 3.33 is reorganized as

$$|U_1 - U_2Q|^2 < |U_3|^2 \quad ,\forall\omega \tag{3.34}$$

Substituting the right hand term in 3.34 by the algebraic summation of $\frac{1}{2}$ with an arbitrary variable, as shown in 3.35, leads into the expression in equation 3.36.

$$|U_1 - U_2Q|^2 < \frac{1}{2} - U_4, \quad \forall\omega \tag{3.35}$$

$$|U_1 - U_2Q|^2 + U_4 < \frac{1}{2}, \quad \forall\omega \tag{3.36}$$

So far the general form of the model matching problem may be transformed into the expression in equation 3.37.

$$\left\|U_1 - U_2Q|^2 + U_4\right\|_\infty < \frac{1}{2} \quad ,\forall\omega \tag{3.37}$$

In order to make equation 3.31 be equivalent to equation 3.37 expand and equate the left half term of both 3.31 and 3.37. The result is expressed in equation 3.38 below,

$$(\overline{R}_1 - \overline{R}_2\overline{Q})(R_1 - R_2Q) + (\overline{S}_1 - \overline{S}_2\overline{Q})(S_1 - S_2Q) = (\overline{U}_1 - \overline{U}_2\overline{Q})(U_1 - U_2Q) + U_4 \tag{3.38}$$

By multiplying out factors and collecting terms in 3.38 the following equations result:

$$\overline{R}_2R_2 + \overline{S}_2S_2 = \overline{U}_2U_2, \tag{3.39}$$

$$\overline{R}_2 R_1 + \overline{S}_2 S_1 = \overline{U}_2 U_1, \tag{3.40}$$

$$\overline{R}_1 R_1 + \overline{S}_1 S_1 = \overline{U}_1 U_1 + U_4. \tag{3.41}$$

These equations must hold in order for 3.38 to be true. Using equations 3.39 through 3.41 the terms U_1, U_2, U_3, and U_4 can be determined. So the final model matching problem then, from equation 3.33, is to find Q in φ satisfying:

$$\left\| U_3^{-1} U_1 - U_3^{-1} U_2 Q \right\|_\infty < 1 \tag{3.42}$$

The model matching problem variables T_1 and T_2 are now equal to $U_3^{-1}U_1$ and $U_3^{-1}U_2$, respectively. Recall that since T_1 and T_2 must be elements of the set φ, U_1 and U_2 must also be members of φ. U_3 is taken as the spectral factor of $(1/2 - U_4)$ since the following expression must hold

$$|U_3|^2 = |U_3||\overline{U}_3| = \left(\frac{1}{2} - U_4\right) \tag{3.43}$$

However, U_4 must have the property $U_4 = \overline{U}_4$ and be real rational. Notice, that by letting U_3 be a spectral factor, both T_1 and T_2 are guaranteed to be stable and proper. It is necessary now to develop a procedure to find the functions U_1, U_2, U_3, and U_4.

In order to determine the functions U_1 and U_2 equations 3.39 and 3.40 are used. Note that U_2 could be determined directly from 3.39. U_2 is the spectral factor of the right hand term in 3.39, and therefore it will be stable and proper. Unfortunately, U_1 which has a unique solution from equation 3.40 is not in φ due to the unstable roots of the complemented U_2 term. The alternative is to multiply the term U_2 resulting from equation

3.39 by an all-pass function $V(s)$. Then, solve equation 3.40 for U_1 in terms of $V(s)$. The idea is to make the zeros of $V(s)$ equal to the unstable poles of the solution to 3.40 such that U_1 is in φ. The next example will help clarify these ideas:

Suppose that

$$R_1(s) = \frac{1}{2+s}, \qquad S_1(s) = 0$$
$$R_2(s) = \frac{1}{1+s}, \qquad S_2(s) = 1.$$

Now, from 3.39 and 3.40

$$\overline{U}_2(s)U_2(s) = \frac{(\sqrt{2}-s)(\sqrt{2}+s)}{(1-s)(1+s)},$$
$$\overline{U}_2(s)U_1(s) = \frac{1}{(1-s)(2+s)}.$$

Clearly $$U_2(s) = \frac{\sqrt{2}+s}{1+s}, \text{ and } U_1(s) = \frac{1}{(2+s)(\sqrt{2}-s)}.$$

Thus, according to the procedure let

$$U_2(s) = \frac{\sqrt{2}+s}{1+s}V(s), \text{ then } U_1(s) = \frac{1}{(2+s)(\sqrt{2}-s)}V(s).$$

Now to get U_2 and U_1 in φ let $V(s) = \frac{\sqrt{2}-s}{\sqrt{2}+s}$.

Recall from 3.43 that U3 is the spectral factor of $(1/2 - U_4)$. U_4 is determined directly from 3.41. Following appropriate substitution for R_1 and S_1 equation 3.44 is obtained.

$$U_4 = \frac{W_1\overline{W}_1 W_2\overline{W}_2}{\overline{W}_1 W_1 + \overline{W}_2 W_2} \qquad \textbf{(3.44)}$$

The H_∞ Robust Performance Algorithm:

Given P, W_1, W_2

i. Select W_2 such that $W_2(p) < 1$ and W_1 such that $W_1(z) < 1$. Verify that the cross over frequency of $W_1(j\omega)$ is much smaller than that of $W_2^{-1}(j\omega)$.

ii. Compute U_4 by equation 3.44 and check if $\|U_4\|_\infty < 1/2$. If so, continue. Otherwise the problem is not solvable. (consult [5])

iii. Obtain a coprime factorization of P and compute R_1, R_2, S_1, S_2 from equation 3.30.

iv. Set $F = \overline{R}_2 R_2 + \overline{S}_2 S_2$ and compute its spectral factor F_{sf}.

v. Select an all-pass function $V(s)$ such that $\frac{\overline{R}_2 R_1 + \overline{S}_2 S_1}{\overline{F}_{sf}} V \in \varphi$.

vi. Set $U_1 = \frac{\overline{R}_2 R_1 + \overline{S}_2 S_1}{\overline{F}_{sf}} V, \qquad U_2 = F_{sf} V.$

vii. Compute the spectral factor of $U_3 = 1/2 - U_4$.

viii. Set $T_1 = U_3^{-1} U_1$ and $T_2 = U_3^{-1} U_2$. Compute γ_{opt}. If it is less than 1 continue. Otherwise robust performance problem is not solvable.

ix Solve the model matching problem to find Q. If Q is not proper roll it off at high frequency while keeping gamma optimum less than one.

x. Set $C = \dfrac{X + MQ}{Y - NQ}$.

3.4.3 Sample Problem

Step i: Let the nominal plant be $P(s) = \dfrac{1}{s+1}$ and suppose that the performance and uncertainty weighting functions are:

$$W_1(s) = \frac{a}{s+1}, \quad W_2(s) = \frac{0.02s}{0.01s+1}$$

The term a in $W_1(s)$ is a positive constant which will be used as design variable.

Step ii: U_4 is computed from equation 3.44 and the weighting transfer functions shown above. The resulting U_4 is

$$U_4(s) = -\frac{0.0004a^2s^2}{a^2 - (0.0001a^2 + 0.0004)s^2 + 0.0004s^4}$$

The infinity norm of U_4 i computed for arbitrary values of a. The outcome of the iterations on a are tabulated in table 3.2.

a	$\|U_4\|_\infty$
50	0.444
54	0.476
56	0.491
57	0.500

Table 3.2 Infinity norm of U_4

According to the defined procedure a can take any positive value in the range 0 to 57 since when a equals 57 the infinity norm of U_4 is 0.5. a is arbitrarily set to 57.

Step iii: The coprime factorization of the plant is obtained following the procedure outlined in section 3.2.1. Since the plant is open loop stable the coprime factors are selected as $N = P, M = 1, X = 0, Y = 1$.

From equation 3.30 the following variable transfer functions are determined:

$$R_1(s) = \frac{a}{s+1}, \quad R_2(s) = \frac{a}{(s+1)^2},$$
$$S_1(s) = 0, \quad S_2(s) = \frac{0.02s}{(s+1)(0.01s+1)}$$

Step iv: Setting $F = \overline{R}_2 R_2 + \overline{S}_2 S_2$ yields,

$$F(s) = \frac{a^2 - (0.0001a^2 + 0.0004)s^2 + 0.0004s^4}{(1-s)^2(1+s)^2(1-0.01s)(1+0.01s)}$$

$$\text{with } F_{sf}(s) = \frac{a + bs + 0.02s^2}{(1+s)^2(1+0.01s)}, \quad \text{where } b = (0.0001a^2 + 0.04a + 0.0004)^{1/2}$$

Step v: Set $V(s) = \dfrac{a - bs + 0.02s^2}{a + bs + 0.02s^2}$

Step vi: Setting $U_1 = \dfrac{\overline{R}_2 R_1 + \overline{S}_2 S_1}{\overline{F}_{sf}} V, \qquad U_2 = F_{sf} V$ yields

$$U_1(s) = a^2 \frac{1-0.01s}{(1+s)(a+bs+0.02s^2)}, \quad U_2(s) = \frac{a-bs+0.02s^2}{(1+s)^2(1+0.01s)}$$

Step vii: U_3 is obtained by computing the spectral factor of $U_3 = 1/2 - U_4$. The results are shown below.

$$U_3(s) = \frac{a+cs+0.02s^2}{\sqrt{2}(a+bs+0.02s^2)}, \quad where\ c = (-0.0007a^2 + 0.004a + 0.0004)^{1/2}$$

Step viii: The model matching variables T_1 and T_2 are found in the following manner,

$$T_1(s) = U_3^{-1}(s)U_1(s) = \sqrt{2}a^2 \frac{1-0.01s}{(1+s)(a+cs+0.02s^2)}$$

$$T_2(s) = U_3^{-1}(s)U_2(s) = \sqrt{2} \frac{(a-bs+0.02s^2)(a+bs+0.02s^2)}{(1+s)^2(1+0.01s)(a+cs+0.02s^2)}$$

γ_{opt} is computed using the Matlab routine "gamopt.m" for selected values of a in order to make the robust performance test be satisfied, that is, to make γ_{opt} less than one. The outcome of the iterations is shown in table 3.3.

a	$\gamma_{opt} = \|(U_3)^{-1}U_1+(U_3)^{-1}U_2Q\|_\infty < 1$
36	0.938
37	0.956
38	0.974
39	0.993
40	1.012

Table 3.3 Robust performance test

Step ix: The model matching problem is solved but Q is found not to be proper.

$$Q_{im}(s) = \frac{0.3317s^4 + 55.19s^3 + 2838s^2 + 64215s + 61432}{s^3 + 97.42s^2 + 3978s + 62585}$$

This Q_{im} must be rolled off. Since the relative degree of the Q_{im} is 1, set

$$Q(s) = Q_{im}(s)\frac{1}{s\tau + 1}.$$

It is determined after several iterations on τ that a value of $\tau = 0.0009$ yields $\|T_1 - T_2Q\|_\infty = 0.999$.

Step x: By setting

$$C = \frac{X + MQ}{Y - NQ} = \frac{(0.3317s^4 + 55.19s^3 + 2838s^2 + 64215s + 61432)(s + 1)}{0.999s^5 + 99.05s^4 + 4117.02s^3 + 67773.8s^2 + 64908s + 1153}$$

the controller transfer function is found and the design is terminated.

CHAPTER IV
A CASE STUDY: THE INVERTED PENDULUM

In this chapter a controller will be designed for the inverted pendulum control problem using the H_∞ technique discussed in the previous chapter. A simulation of the control system will be performed with a program written for the Matlab simulation environment. The objective of this case study is to provide a comprehensive example of the SISO H_∞ design procedure presented in chapter III and the related considerations and ideas introduced in chapter II.

4.1 System Modeling

4.1.1 The Inverted Pendulum Positioning System

There are some classical control problems that feedback control designers and particularly theoreticians have long sought use as case studies to test the features and effectiveness of control techniques under research. A classical problem which has gained reputation in the control theory context because it is often adopted for such purposes is the inverted pendulum positioning system, sometimes referred to as a beam balancer. The inverted pendulum system consists of a cart which has a stick mounted on a bearing at its top surface. See figure 4.1 for an illustration and table 4.1 for a description of the system variables.

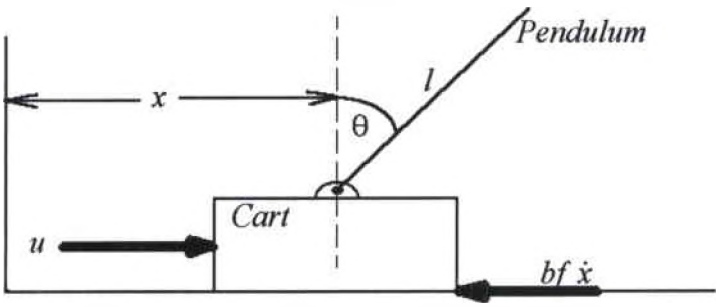

Figure 4.1 Inverted Pendulum Positioning System

The inverted pendulum control problem is to maintain the beam balanced about an equilibrium position, typically the upright position or vertical. This system is naturally unstable, for the beam will most definitely fall in the absence of an external driving force that counteracts the effects of gravity.

Moment of inertia of the pendulum = J	Mass of the cart = M
Horizontal position of the cart = x	Mass of the pendulum = m
Dynamic Friction = bf	Actuator force = u
Acceleration of gravity = g	Angular displacement of the pendulum = θ

Table 4.1 Definition of variables

Under control action, an external driving force is applied to the cart to force it to move in either a forward or backward direction counteracting the gravitational pull and stabilizing the pendulum. Note that the problem naturally implies a regulator control

structure since there is no reference signal commanding the beam to position in a particular angular location. Instead, the system continuously measures its current angular position and instructs the cart to react in a fashion that will maintain the beam vertical. Figure 4.2 illustrates the basic regulator structure which provides the context for this H_∞ design. This figure clearly identifies the input to the system as a command force $u(t)$. The output signal, however, may be any of the system's related variables depending on the control problem of interest of to the designer. The H_∞ control techniques introduced in chapter III apply exclusively to the single input-single output case. The inverted pendulum problem, on the other hand, has a single input/multi-output structure. Nevertheless, this case study will focus on the control of a single output variable, $\theta(s)$, the angular deviation of the beam from a vertical reference position, in order to illustrate the SISO H_∞ control techniques of chapter III.

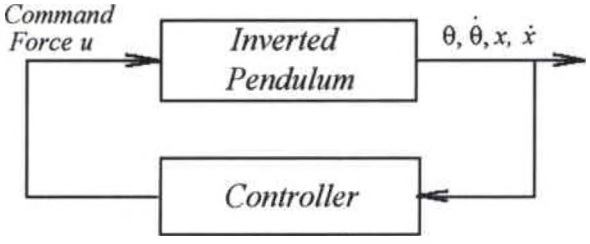

Figure 4.2 Basic regulator structure

The fact that the system is open loop unstable makes it an appealing system for the study of the robust stabilization ideas discussed in the earlier chapters. In order to restrict the problem complexity and concentrate on the robustness features of the design, the motion of the cart will be restrained to one axis. Dynamic friction will be asserted as a source of model perturbation.

4.1.2 Model Development

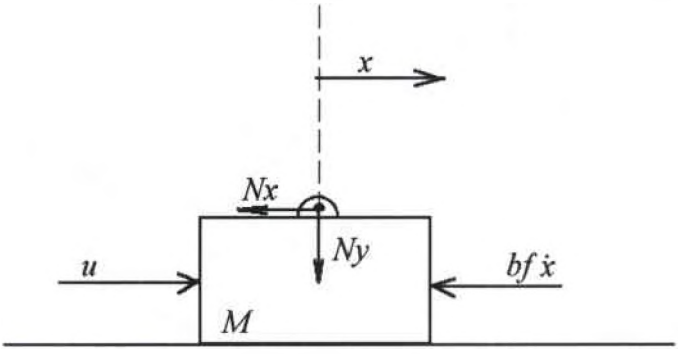

Figure 4.3 Force diagram of the cart

In figure 4.1 it is assumed that the cart is driven by some actuator that exerts a horizontal force $u(t)$ at time t. The laws of physics are applied to the system to derive mathematical equations that model the dynamics of motion of the system. First, the free body diagram of the cart is examined as shown in figure 4.3. This figure reveals that the forces acting on the cart are the actuator force, the friction force, and the vertical and horizontal reaction forces on the hinge. Application of Newton's second law of motion leads to the summation of all the forces in the horizontal axis yielding equation 4.1.

$$\begin{aligned} \sum \bar{F}_x &= M\ddot{x} \\ M\ddot{x} &= u - bf\dot{x} - N_x \\ M\ddot{x} + bf\dot{x} &= u - N_x \end{aligned} \qquad \textbf{(4.1)}$$

Similarly, a free body diagram of the pendulum, illustrated in figure 4.4, indicates that forces affecting the motion of the pendulum are a component of the centripetal and the centrifugal accelerations, the reaction forces on the hinge, and the gravitational pull.

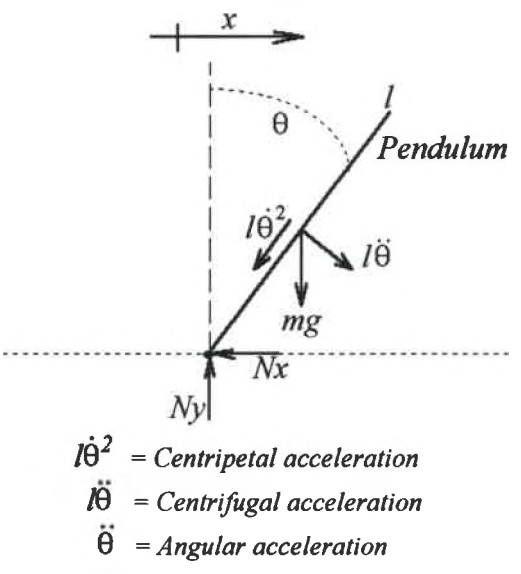

Figure 4.4 Force diagram of the pendulum

The equations of motion of the pendulum are derived by summing the forces in the horizontal axis and by summing the torques about the center of mass of the pendulum. In addition, the summation of the forces in the direction perpendicular to the pendulum will be used in the derivation of the model. The results are given by equations 4.2, 4.3, and 4.4 respectively.

$$\begin{aligned} \sum F_x &= m\ddot{x} \\ m\ddot{x} &= N_x - ml\dot{\theta}^2 sin\theta - ml\ddot{\theta}cos\theta \\ m\ddot{x} &+ ml\dot{\theta}^2 sin\theta - ml\ddot{\theta}cos\theta = N_x \end{aligned} \tag{4.2}$$

$$\begin{aligned} \sum T &= J\ddot{\theta} \\ J\ddot{\theta} &= N_y lsin\theta - N_x lcos\theta \end{aligned} \tag{4.3}$$

$$N_x lcos\theta - N_y lsin\theta + mglsin\theta = ml\ddot{x}cos\theta + ml^2\ddot{\theta} \tag{4.4}$$

By combining equation 4.1 and 4.2 equation 4.5 is derived. Then, solving for $N_x l\cos\theta - N_y l\sin\theta$ in equation 4.4 and substituting into the right hand side of 4.3 yields equation 4.6. The following set of nonlinear equations completely describe the dynamics of the pendulum.

$$J\ddot{\theta} = -ml(\ddot{x}\cos\theta + l\ddot{\theta} - g\sin\theta) \qquad \textbf{(4.5)}$$

$$u = (M+m)\ddot{x} + bf\dot{x} + ml(\dot{\theta}^2\sin\theta - \ddot{\theta}\cos\theta) \qquad \textbf{(4.6)}$$

The principal objective of the inverted pendulum problem is to stabilize the beam about the upright position. The angular deviation of the pendulum will be measured from this position and a value of zero radians will be assigned to this angular location. Thus, the operating point of the system corresponds to an angular location of zero radians. Having defined the operating point, the next step is to linearize the equations of motion of the pendulum about the given operating point. The procedure used is standard and is drawn from Dorf [3]. First, manipulate 4.5 to the form:

$$\ddot{\theta} = -l'\ddot{x}\cos\theta + l'g\sin\theta, \qquad \text{where } l' = \frac{ml}{J+ml^2}. \qquad \textbf{(4.7)}$$

Let $\theta_o = 0$ rads be the equilibrium point. To linearize equation 4.7 about θ apply Taylor's series expansion taking only the first order terms. The results are presented below with the linearized equivalent of 4.5 being 4.10.

$$\ddot{\theta} = -l'\ddot{x}\cos\theta_o - \left.\frac{d\,l'\ddot{x}\cos\theta}{d\theta}\right|_{\theta=\theta_o} \cdot(\theta-\theta_o) + l'g\sin\theta_o + \left.\frac{d\,l'g\sin\theta}{d\theta}\right|_{\theta=\theta_o} \cdot(\theta-\theta_o) \qquad \textbf{(4.8)}$$

$$\begin{aligned}\ddot{\theta} &= -l'\ddot{x}\cos\theta_o + l'\ddot{x}\sin\theta_o \bullet \theta + l'g\sin\theta_o + l'g\cos\theta_o \bullet \theta \\ \ddot{\theta} &= -l'\ddot{x} + l'g\theta\end{aligned} \qquad \textbf{(4.9)}$$

Thus,

$$\left(J + ml^2\right)\ddot{\theta} = mlg\theta - ml\ddot{x} \qquad \textbf{(4.10)}$$

Similarly, the linearized equivalent of 4.6 is given by equation 4.11.

$$u = (M+m)\ddot{x} + bf\dot{x} + ml\ddot{\theta} \qquad \textbf{(4.11)}$$

Hence, the linearized set of equations that model the dynamics of the inverted pendulum are given by 4.10 and 4.11.

To gain a better understanding of the system and facilitate the analysis and simulation, the equations of motion of the system will be posed in a vector matrix format. That is, a state space representation of the system will be developed. Recall that dynamic friction will be asserted as perturbation of the system model. Thus, two state space models as described by 4.12 will be obtained. The first equation, 4.12*a* denotes the perturbed model, that is, the model with friction, and the second one 4.12*b* denotes the nominal model[1].

$$\dot{\boldsymbol{\lambda}}(t) = A_p\boldsymbol{\lambda}(t) + B_p z(t) \qquad \textbf{(4.12 } \boldsymbol{a}\textbf{)}$$

$$\dot{\boldsymbol{\lambda}}(t) = A_n\boldsymbol{\lambda}(t) + B_n z(t) \qquad \boldsymbol{\lambda}(0) = \boldsymbol{\lambda}_o \qquad \textbf{(4.12 } \boldsymbol{b}\textbf{)}$$

---

[1]Here $\boldsymbol{\lambda}$ is the state vector and z is the vector of input signals. Notice that in this case z is composed of a single input signal: the horizontal actuator's force $u(t)$.

$$\begin{bmatrix} \lambda_1(t) \\ \lambda_2(t) \\ \lambda_3(t) \\ \lambda_4(t) \end{bmatrix} = \begin{bmatrix} x(t) \\ \dot{x}(t) \\ \theta(t) \\ \dot{\theta}(t) \end{bmatrix} \qquad \textbf{(4.13)}$$

The dynamics of the system then are described by the state variables: the cart's position and velocity, $x(t)$ and $\dot{x}(t)$, and the pendulum's angular position and velocity, $\theta(t)$ and $\dot{\theta}(t)$. These define the state vector as expressed in 4.13. The perturbed plant model is derived by substitution of the corresponding state variables into the equations of motion 4.10 and 4.11. Solving for the state derivatives yields,

$$\dot{\lambda}_1(t) = \lambda_2(t) \qquad \textbf{(4.14 } a\textbf{)}$$

$$\dot{\lambda}_2(t) = a \cdot \lambda_2(t) + d \cdot \lambda_3(t) + e \cdot u(t) \qquad \textbf{(4.14 } b\textbf{)}$$

$$\dot{\lambda}_3(t) = \lambda_4(t) \qquad \textbf{(4.14 } c\textbf{)}$$

$$\dot{\lambda}_4(t) = b \cdot \lambda_2(t) + c \cdot \lambda_3(t) + f \cdot u(t) \qquad \textbf{(4.14 } d\textbf{)}$$

The set of equations expressed in 4.14 define the perturbed model plant matrix A_p which is given by 4.15.

$$A_p = \begin{bmatrix} 0 & 1 & 0 & 0 \\ 0 & a & d & 0 \\ 0 & 0 & 0 & 1 \\ 0 & b & c & 0 \end{bmatrix}, \qquad \textbf{(4.15)}$$

where a, b, c, and d are defined by 4.16 and bf denotes the coefficient of friction.

$$a = -bf\left[\frac{1}{M+m} + \frac{l'ml}{(M+m)[(M+m)-l'ml]}\right] \qquad \textbf{(4.16 } a\textbf{)}$$

$$b = bf\left[\frac{l'}{(M+m)-l'ml}\right] \qquad \textbf{(4.16 } b\textbf{)}$$

$$c = \frac{(M+m)l'g}{(M+m)-l'ml} \qquad \textbf{(4.16 } c\textbf{)}$$

$$d = \frac{l'mlg}{(M+m)-l'ml} \qquad \textbf{(4.16 } d\textbf{)}$$

Similarly, the perturbed system's input matrix B_p corresponds to

$$B_p = \begin{bmatrix} 0 \\ e \\ 0 \\ f \end{bmatrix}, \qquad \textbf{(4.17)}$$

where e and f are given by

$$e = \frac{1}{M+m} + \frac{l'ml}{(M+m)[(M+m)-l'ml]} \qquad \textbf{(4.18 } a\textbf{)}$$

$$f = \frac{-l'}{(M+m)-l'ml} \qquad \textbf{(4.18 } b\textbf{)}$$

The nominal model of the inverted pendulum is readily developed by equating the friction coefficient bf to zero. It is evident from 4.16 that the a and b terms become zero under this assignment. However, the remaining terms are unaltered and are therefore

identical to the corresponding parameters of the perturbed model. The nominal plant matrix A_n becomes:

$$A_n = \begin{bmatrix} 0 & 1 & 0 & 0 \\ 0 & 0 & d & 0 \\ 0 & 0 & 0 & 1 \\ 0 & 0 & c & 0 \end{bmatrix}, \qquad \textbf{(4.19)}$$

and the nominal system input matrix B_n is identical to the perturbed system input matrix B_p.

$$B_n = [B_p] \qquad \textbf{(4.20)}$$

The state space model of 4.12 and the four element state vector of 4.13 can be partitioned into subsystems by defining a new two element state vector as shown in 4.21 and 4.22. Note that each component of the new state vector in 4.22 is composed of a two element vector itself.

$$\begin{aligned} &\textit{Cart's subsystem} && \dot{\boldsymbol{\lambda}}_c(t) = A_{11}\boldsymbol{\lambda}_c(t) + A_{12}\boldsymbol{\lambda}_p(t) + B_{11}z(t) \\ &\textit{Pendulum's subsystem} && \dot{\boldsymbol{\lambda}}_p(t) = A_{21}\boldsymbol{\lambda}_c(t) + A_{22}\boldsymbol{\lambda}_p(t) + B_{21}z(t) \end{aligned} \qquad \textbf{(4.21)}$$

$$\textit{Where } A = \begin{bmatrix} A_{11} & A_{12} \\ A_{21} & A_{22} \end{bmatrix}, \; B = \begin{bmatrix} B_{11} \\ B_{12} \end{bmatrix}, \; \boldsymbol{\lambda} = \begin{bmatrix} \lambda_c \\ \lambda_p \end{bmatrix} \; \textit{and} \; \boldsymbol{\lambda}_c = \begin{bmatrix} x \\ \dot{x} \end{bmatrix}, \; \boldsymbol{\lambda}_p = \begin{bmatrix} \theta \\ \dot{\theta} \end{bmatrix} \qquad \textbf{(4.22)}$$

It is worth noting that the cart subsystem in 4.21 may not be considered a decoupled system. For both the nominal and the perturbed plant terms *b* and/or *d* in the system matrix couple the subsystem together. Note however that if $M >> m$, or alternatively, as

m approaches zero, the term *d* becomes very small, until the point where the nominal cart subsystem can be considered decoupled. This argument is obvious, since the larger the mass of the cart as compared to the mass of the stick, the less effect the stick will have on the motion of the system. The system's physical parameters will be selected to reflect this condition. The pendulum subsystem in 4.21 on the other hand, may be considered decoupled for the nominal plant since the submatrix $A_{21} = 0$.

The models developed above will be used mainly for simulation purposes. It was mentioned in the previous section that the design technique presented in the preceding chapter has been developed for SISO systems represented by the transfer function models. Thus, in order to carry out the design procedure as outlined in chapter III, a transfer function model will be computed next. According to the theory of linear system analysis the transfer function matrix of a system in state space may be determined from equation 4.23 [1], [2] as.

$$H(s) = C(sI - A)^{-1}B \qquad \textbf{(4.23)}$$

where A, B, and C are the matrices of the state space model.

The system's output matrix *C* must be determined before *H*(*s*) can be developed. By careful selection of *C*, the desired output signal may be obtained as a linear combination of all possible states of the system as defined in 4.13. In this particular case, the system objective is to control the angular position. Therefore, the state $\lambda_3 = \theta$ is the corresponding output signal of interest and the *C* matrix is accordingly selected as:

$$C = \begin{bmatrix} 0 & 0 & 1 & 0 \end{bmatrix} \qquad \textbf{(4.24)}$$

The transfer function of the perturbed plant model then is expressed as ,

$$H_p(s) = \frac{ebs + f(s-a)s}{s^4 - as^3 - cs^2 - (bd-ac)s} \qquad \textbf{(4.25)}$$

For the nominal transfer function model of the system, $bf = 0$ forces substitution of $a = b = 0$ in 4.25 to obtain 4.26.

$$H_n(s) = \frac{fs^2}{s^4 - cs^2} \qquad \textbf{(4.26)}$$

Note that whether the transfer functions above model the perturbed or the nominal case, they both relate the input signal of the system (i.e. the actuator force) to the output signal of the system (i.e. the angular displacement of the pendulum).

Before engaging in the design procedure, the physical parameters of the system will be selected. The actual parameter values for this study have been obtained from Hoffman [16]. Hoffman presented a state variable feedback solution with optimal estimation to the stabilization problem of the inverted pendulum. Table 4.2 presents a list of these parameters and table 4.3 displays the corresponding values of the coefficients of 4.14.

Mass of the cart = 1 Kg
Mass of the pendulum = 0.15 Kg
Length of the pendulum = 1 m
Gravitational acceleration = 9.81 m/s^2
Moment of Inertia = 0.2 Kg-m^2

Table 4.2 System parameters for the inverted pendulum

a = -0.9211*bf
b = 0.3947*bf
c = 4.4532
d = -0.5809
e = 0.9211
f = -0.3947

Table 4.3 Coefficients of equation 4.14

In addition, it will be assumed that the coefficient of dynamic friction has been found to vary between two extremas. Therefore, the coefficient of friction will be arbitrarily modeled by a set of the form $bf \in [bf_{min}, bf_{max}]\ Kg/s$. With the parameters given in table 4.3 the numerical values of the coefficients of the transfer function models of the system are computed. The resulting values are displayed in the transfer functions of equations 4.27 and 4.28.

$$H_p(s) = \frac{\theta_p(s)}{u_p(s)} = \frac{-0.3947\ s}{s^3 + 0.9211 \cdot bf\, s^2 - 4.4532\ s - 3.8724 \cdot bf} \qquad \textbf{(4.27)}$$

$$H_n(s) = \frac{\theta_n(s)}{u_n(s)} = \frac{-0.3947}{s^2 - 4.4532} \qquad \textbf{(4.28)}$$

Note that 4.27 is left in terms of the coefficient of friction. Furthermore, both perturbed and nominal models have an unstable pole at $s = 2.1$, thus, confirming the aforementioned instability of the system. It is worth reiterating that the robust design technique will be employed in this case study to account for unmodeled dynamic effects introduced by

friction . For the inverted pendulum problem, it is evident by comparizon of 4.27 with 4.28 that the presence of friction in the system perturbs the second order model of 4.28 into the higher order model of 4.27 through the addition of both a pole and a zero. Figure 4.5 shows the frequency response of the nominal model and the perturbed model with coefficients of friction of 1 and 10 *Kg/s*. This figure reveals that the addition of friction perturbs the low frequency components of the nominal model. The larger the value of *bf* the more severe the perturbation and the larger the range of frequencies affected. In the final analysis, *bf* will be restricted to the set $bf \in [0.5, 2]$ with a nominal value of one.

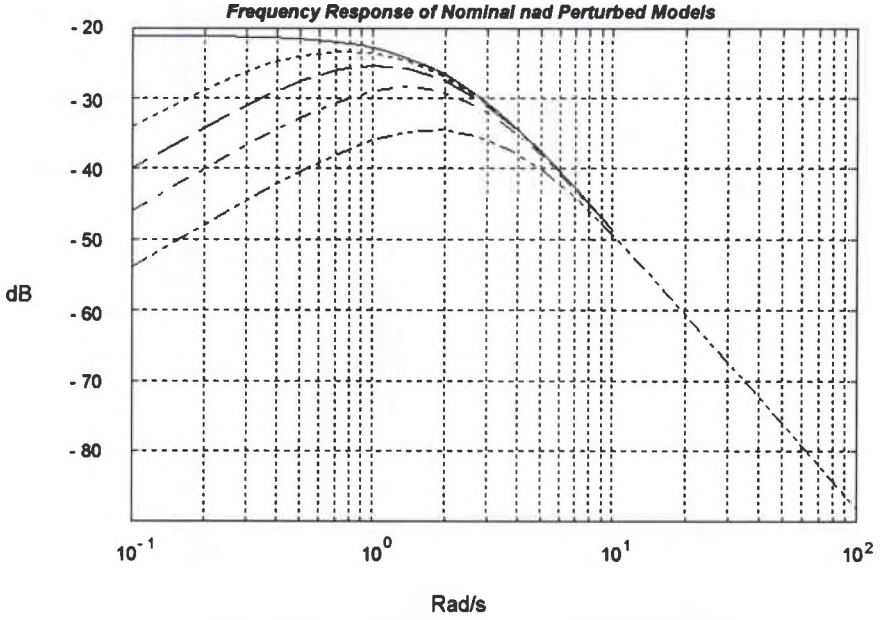

Solid: bf = 0, Dotted: bf = 0.5, Dashed: bf =1,
Dashed-dot: bf =2, Dashed-dot-dot: bf =3

Figure 4.5 Frequency response of $H_n(j\omega)$ and $H_p(j\omega)$

4.2 H_∞ Controller Design

The control structure which will be utilized to stabilize the inverted pendulum is the regulator structure introduced in the previous section and shown in figure 4.2. Since the control objective for this problem is one of robust stabilization, the design algorithm that will be use is the one outlined in section 3.3, "Optimal and Sub optimal Robust Stabilization". This algorithm is repeated below.

The H_∞ Robust Stability Algorithm

Given the nominal plant P and the uncertainty weighting W_2, the procedure for the design of a robust stabilizer controller is as follows:

i. Select W_2 such that $W_2(p) < 1$ where p are poles of P in RHP.

ii. Form a coprime factorization of P such that $P = \frac{N}{M}$, $N, M \in \varphi$, and $NX + MY = 1$

iii. Solve the model matching problem with $T_1 = W_2 NX$ and $T_2 = -W_2 NM$.

iv. Denote the solution of the previous step Q_{im} and let $\gamma_{inf} = \gamma_{opt}$ (the minimum model matching error). Then $\delta_{sup} = 1/\gamma_{opt}$.

v. Choose an arbitrary number $\delta \leq \delta_{sup}$. Set $J(s) = \frac{1}{(s\tau + 1)^k}$ with k large enough to make $Q_{im}J$ proper and τ small enough that $\|W_2 N(X + MQ)\|_\infty \leq 1/\delta$

vi. Set $Q = Q_{im}J$ and find $C = \frac{X + MQ}{Y - NQ}$.

The H_∞ Robust Stability Solution

Step i: Using transfer functions of equations 4.27 and 4.28 the first step in the design procedure can be taken. That is, to find the uncertainty profile transfer function W_2.

$$|W_2(j\omega)| \geq \left|\frac{H_p(j\omega)}{H_n(j\omega)} - 1\right|, \qquad \forall\omega. \qquad \textbf{(4.29)}$$

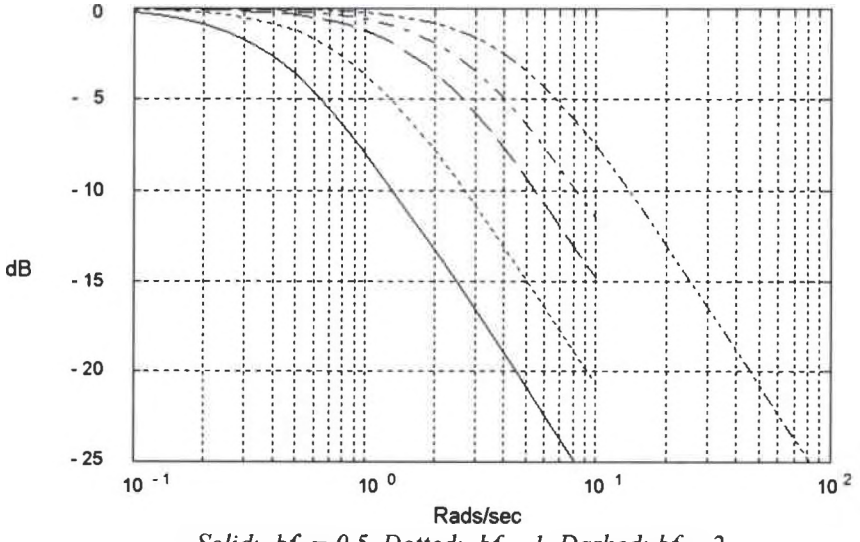

Solid: bf = 0.5, Dotted: bf = 1, Dashed: bf = 2, Dashed-dot: bf = 3, Dashed-dot-dot: bf = 5

Figure 4.6 Magnitude response of $\left|\frac{H_p(j\omega)}{H_n(j\omega)} - 1\right|$

A multiplicative perturbation model will be pursued. It follows from equation 2.14 that in order for the inequality in 4.29 to be satisfied, the weighting transfer function W_2 must have a magnitude response greater or equal to the curves shown in figure 4.6 for the corresponding coefficients of friction. After several design iterations it was empirically determined that better results are obtained by allowing the magnitude of the uncertainty

weighting transfer function to increase with frequency. An explanation for this statement conclusion will be given latter when the computation of the parameters of the H_∞ control solution is discussed. However, according to the restriction of $W_2(s)$ that preceded from analysis of section 2.3.4, the magnitude of the weighting transfer function must be less than one at the RHP pole of the plant. As a result, W_2 will be allowed to increase with frequency after 10 rad/s, but will be maintained below 1 in the vicinity of 2 rad/s, the RHP pole of the plant. Equation 4.30 defines the mathematical expression for the uncertainty profile transfer function selected. Figure 4.7 illustrates the magnitude response of the Bode plot of $W_2(j\omega)$.

$$W_2(s) = 0.024\frac{(s+10)^2}{(s+2)} \qquad \textbf{(4.30)}$$

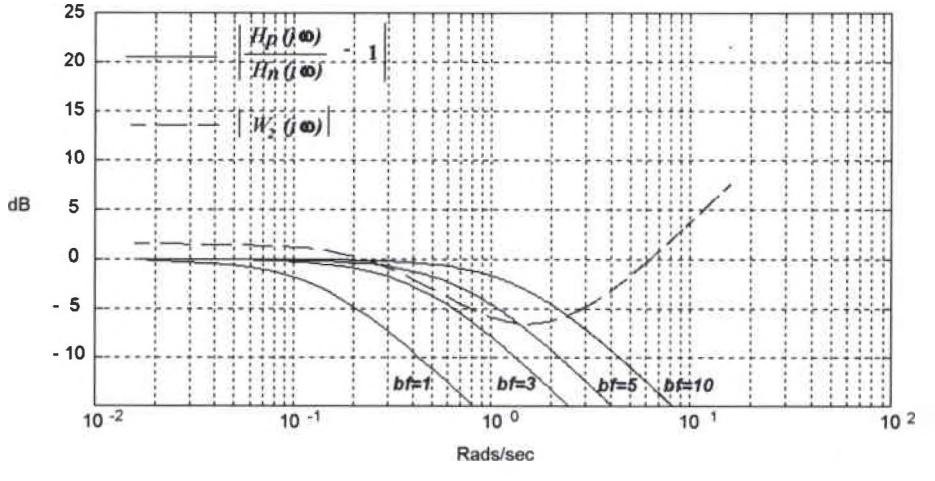

Figure 4.7 Frequency response of uncertainty weights

Consider figure 4.7. It is evident that as *bf* increases the robust stabilization problem becomes more difficult to solve. This is a consequence of the fact that W_2 must be less

than one at 2.1 rads/sec, but for increasing *bf* the requirement of 4.29 forces W_2 to be close to one at this frequency. In addition, it is clear from the graph that the defined weighting transfer function W_2 in this case will yield a robust stabilizer only for the plant perturbed by a coefficient of friction of three or less. For larger magnitudes of *bf* the characterization of W_2 becomes more difficult.

Step ii: A coprime factorization of the nominal plant is now sought. According to the procedure outlined at the beginning of this section, let $G(s)$ be the nominal plant transfer function found in 4.28. That is,

$$G(s) = H_n(s) = \frac{\theta_n(s)}{u_n(s)} = \frac{-0.3947}{s^2 - 4.4532} \qquad \textbf{(4.31)}$$

and substitute $s = \frac{1-\lambda}{\lambda}$ into 4.31 to get 4.32.

$$G(s) = \frac{0.3947\,\lambda^2}{3.4532\lambda^2 + 2\lambda - 1} \qquad \textbf{(4.32)}$$

Using Euclid's algorithm with the polynomials of λ expressed by equation 4.33 as inputs, yields the functions $x(\lambda)$, and $y(\lambda)$ in 4.34.

$$\begin{aligned} n(\lambda) &= 0.3947\,\lambda^2 \\ m(\lambda) &= 3.4532\lambda^2 + 2\lambda - 1 \end{aligned} \qquad \textbf{(4.33)}$$

$$\begin{aligned} x(\lambda) &= 17.5\lambda + 18.883 \\ y(\lambda) &= -2\lambda - 1 \end{aligned} \qquad \textbf{(4.34)}$$

$x(\lambda)$ and $y(\lambda)$ satisfy the requirement that $nx + my = 1$. The coprime factors are obtained by substituting the inverse transformation $\lambda = 1/(s+1)$ into 4.33 and 4.34 and are expressed by equations 4.35 and 4.36 respectively. Notice that all four transfer functions are members of the set φ as expected. Equally important is the fact that the condition $NX + MY = 1$ holds.

$$N(s) = \frac{0.3947}{(s+1)^2}, \qquad M(s) = \frac{-(s^2 - 4.4532)}{(s+1)^2} \tag{4.35}$$

$$X(s) = \frac{18.88(s+1.92)}{s+1}, \qquad Y(s) = \frac{-(s+3)}{s+1} \tag{4.36}$$

Step iii: The algorithm now dictates that the model matching problem variables T_1 and T_2 be computed. The calculations are included below:

$$T_1(s) = W_2NX = 181\times 10^{-3}\frac{(s+1.92)(s+10)^2}{(s+1)^3(s+2)} \tag{4.37}$$

$$T_2(s) = -W_2NM = 9.473\times 10^{-3}\frac{(s^2 - 4.4532)(s+10)^2}{(s+1)^4(s+2)} \tag{4.38}$$

The solution of the model matching problem is computed for T_1 and T_2 given above.

Step iv: The minimum model matching error γ_{opt}, is computed through execution of the MATLAB routine "gamopt.m" included in appendix C and is found to be 0.868. Recall from section 3.3.1 that the inverse of γ_{opt} is the maximum robust stability margin. Thus,

for the given weighting transfer function, the maximum obtainable robust stability margin is 1.152. Contrary to the classical gain and phase margins, the robust stability margin has no direct relationship to the performance of the closed loop control system. It does, however, provide a measure of the tolerance of the system to the perturbations in question. The larger the robust stability margin is, the smaller the infinity norm of W_2T . Consequently, the stability of the closed system is less affected by perturbations.

Note that the transfer function T_2 in 4.38 has only one zero in the RHP at the same location as the unstable pole of the inverted pendulum system. The solution of model matching problem (i.e the parameter Q) in the particular case when T_2 has only one RHP zero is obtained from equation 3.11 with γ_{opt} as found above and $G(s) = 1$ (the proof is in appendix B). Equation 4.39 illustrates this fact.

$$Q_{im} = \frac{T_1 - \gamma_{opt}}{T_2} \qquad \textbf{(4.39)}$$

It is interesting to note that all of the coprime factors in 4.35 and 4.36 except $X(s)$ have relative degrees[2] of zero. $X(s)$, on the other hand, is strictly proper with a relative degree of 2. It was mentioned earlier that better results were obtained by allowing the magnitude of W_2 to increase with frequency. This implies that W_2 be improper. Had W_2 been chosen strictly proper of relative degree 1, or proper of relative degree 0, the parameter Q would have been improper of relative degree 1 or 2 respectively. Thus, the filter $J(s)$ mentioned in the procedure in section 3.3.1 would have to be used to roll off

[2] The relative degree of a rational transfer function is equal to the difference:
{ | order of denominator - order of numerator | }.

the resulting improper Q at high frequency to enforce $JQ(s)$ to be proper. It was empirically determined, after some iterations, that the higher the order of the filter $J(s)$ the more difficult it became to obtain optimal or close to optimal stability margins. In fact, it is noted that nearly optimal solutions could be achieved the lower the order of the filter $J(s)$. By letting W_2 be improper and of relative degree 2, the same as $X(s)$, proper Q's could be obtained directly without the need for a roll off filter. Furthermore, selection of an improper W_2 of relative degree 1 would require $J(s)$ to be only of first order. It appears that the requirement for the filter $J(s)$ and the restrictions on its form can be significantly impacted by the selection of $W_2(s)$. Thus, several solutions to the model matching problem can be developed for the same robust stability problem.

In this case, W2 is selected to be improper and of relative degree 1. Thus, the model matching solution corresponding to the given T_1 and T_2 (equations 4.37 and 4.38) yields an improper Q of relative degree 1 which is expressed below in equation 4.40.

$$Q_{im}(s) = -90.26\frac{(s+1)(s+1.92)\left[(s+2.5)^2+1.8^2\right]}{(s+10)^2(s+2.1)} \qquad \textbf{(4.40)}$$

Step v: A proper Q is now obtained by rolling off Q_{im} with the filter $J(s)$ shown in 4.41. The resulting proper Q is given by 4.42. The filter $J(s)$ has been successfully selected such that the subsequent robust stabilizer is optimal.

$$J = \frac{1}{(1\times 10^{-3}s+1)} \qquad \textbf{(4.41)}$$

Step vi:

$$Q = Q_{im}(s)J(s) = -90.26\frac{(s+1)(s+1.92)\left[(s+2.5)^2+1.8^2\right]}{(s+10)^2(s+2.1)(1\times10^{-3}s+1)} \qquad \textbf{(4.42)}$$

The corresponding controller/compensator is found directly by substitution of Q, X, Y, M, N into equation 3.16. The mathematical expression of this controller is given by equations 4.43.

$$C(s) = 90.28\frac{s^5+7.11s^4+19.6s^3+26.1s^2+16.86s-4.23}{-0.001s^5-1.025s^4+10.306s^3+36.65s^2+37.65s+11.18}, \qquad \textbf{(4.43 } \boldsymbol{a}\textbf{)}$$

or in polar form:

$$C(s) = -90276.88\frac{(s+2.1)(s+2)(s+.78)\left[(s+1.1)^2+0.215^2\right]}{(s+0.519)(s-12.89)(s+1035.033)\left[(s+1.22)^2+0.34^2\right]} \qquad \textbf{(4.43 } \boldsymbol{b}\textbf{)}$$

This is a rather complex and unusually high ordered compensator compared to the usual phase lead/lag compensators achieved by more classical SISO frequency domain methods. The controller itself is unstable since its transfer function has a pole in the RHP at $s = 12.89$. Nevertheless, the close loop transfer function of the system is stable. The closed loop transfer function is given by 4.44.

$$T = \frac{PC}{1+PC} = \frac{35632.29(s+0.785)(s+2)[(s+1.1)^2+0.215^2]}{(s+10)^2(s+1000)(s+0.633)[(s+1.18)^2+0.32^2]} \qquad \textbf{(4.44)}$$

Since this transfer function is analytic in the RHP the inverted pendulum system will be stabilized under feedback action with the compensator given by equation 4.43. The fact that the controller is unstable has no significant implications in this particular problem since the open loop plant itself is unstable.

Figure 4.8 illustrates the robust stability test for this controller. Notice that the value of γ achieved is 0.86. Therefore, the controller may be consider optimal under the definition expressed by equation 3.1. The controller design is now completed.

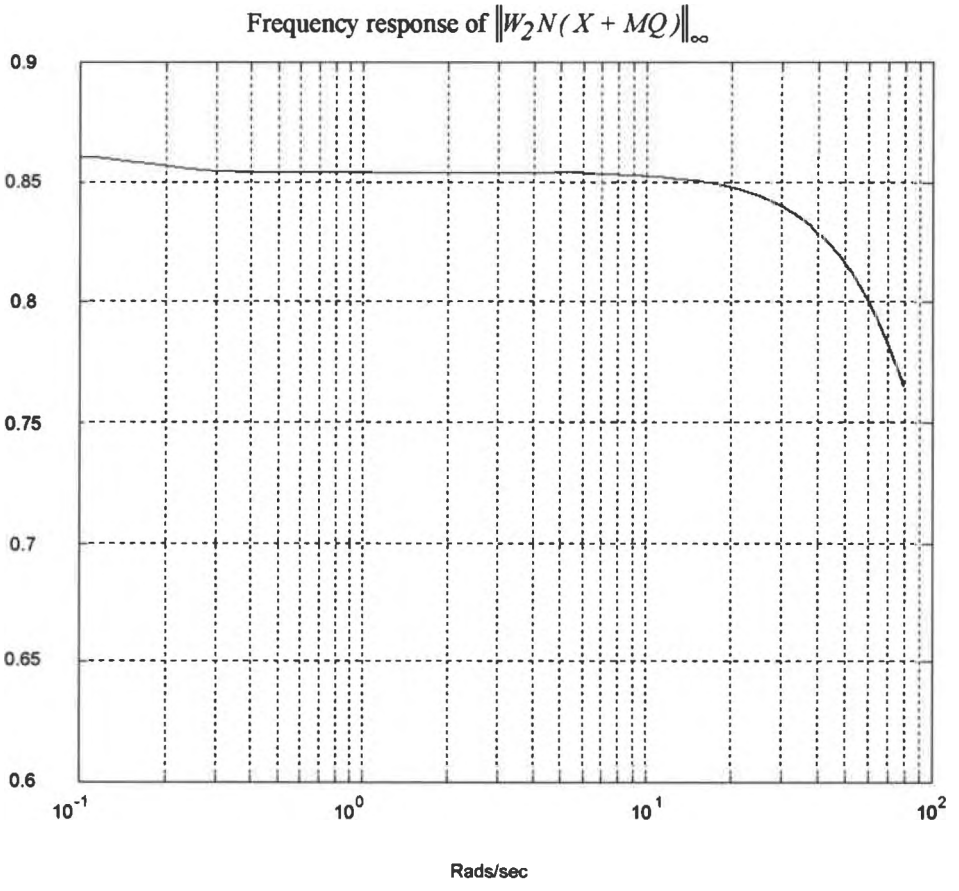

Solid: Graph of W_2T for controller in equation 4.43

Figure 4.8 Robust stability test

4.3 SIMULATION AND RESULTS

The robust stability test shown in figure 4.8 indicates that the system can be balanced and stabilized by the feedback controllers of equations 4.43. In this section the simulations of the inverted pendulum positioning system will be discussed for the controller designed in section 4.2. The objective of the simulation is to investigate the behavior of the system under the stipulated control action. The results of the simulation will demonstrate that the system performs satisfactorily in the presence of plant perturbations.

In order to simulate the inverted pendulum feedback system response, separate state space models will be used, one for the plant and one for the controller of equation 4.43. This approach was taken in order to maintain the integrity of the state variables of the plant since the plant models discussed in sections 4.1 are of a lower order than the controller designed in section 4.2. An illustration of the configuration used for simulation is given in figure 4.9. Recall that the state variables of the inverted pendulum system were defined in 4.13. These variables are the cart's position and velocity, and the pendulum's angular position and velocity. If the controller and the plant are integrated into a single block structure, a new undefined state vector will be inherently formed by the new integrated model whose states are not easily traced back to the plant's states. Thus, cascading the controller with the plant, but maintaining their simulations separate, provides a mechanism which maintains the state vector of the plant intact. The simulation is accomplished by a computer program written in MATLAB. The name of the program is "simulate.m" and a copy has been included in appendix C. This program implements a recursive solution of the discretized versions of the state space models that describe the behavior of the system in figure 4.9 for a specified interval of time.

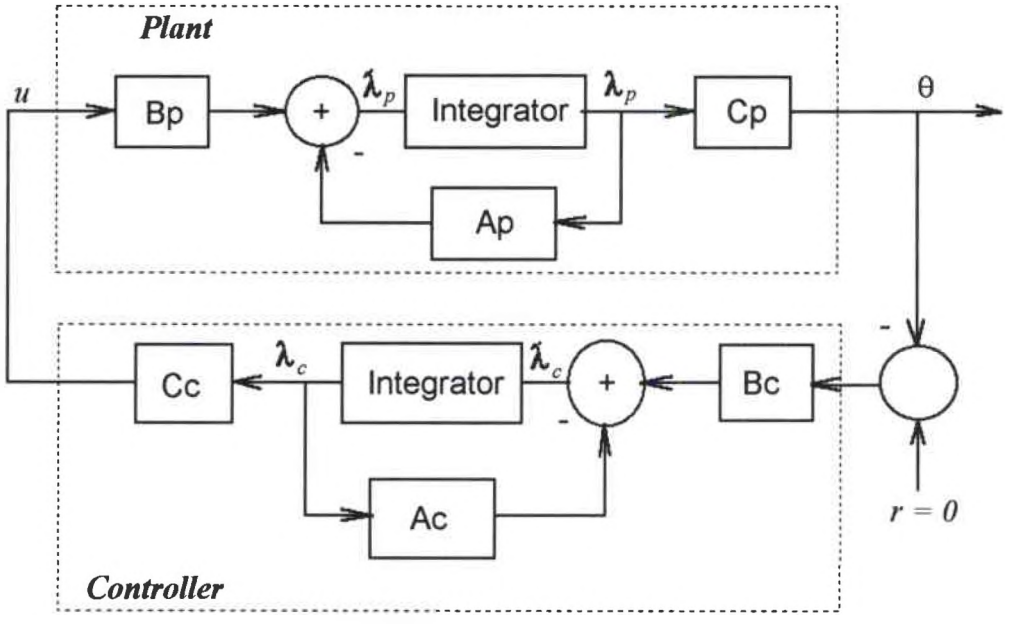

Figure 4.9 Feedback system in state space form

The simulation will be performed for two sets of plants. These plants will be denoted: (i) *the nominal reduced state plant a*nd (ii) *the perturbed full state plant*. The nominal reduced state plant is the state space equivalent of the nominal system used for design[3]. The controller will be tested first with this model since this was the model used for design. Notice that the nominal reduced state plant is only a second order system while the controller is of higher order as was previously mentioned. The system matrices of the nominal reduced state model are shown below.

$$A_{22} = \begin{bmatrix} 0 & 4.4532 \\ 1 & 0 \end{bmatrix}, \quad B_{12} = \begin{bmatrix} 1 \\ 0 \end{bmatrix}$$

$$C = [0 \quad -0.3947], \qquad D = [0] \tag{4.45}$$

[3]The state space equivalent of the system described by the transfer function expressed by equation 4.31.

The perturbed full state plant was derived in section 4.1.2. and was expressed in section 4.1 by equations 4.15 and 4.18. The system matrices for this model are also included here and are detailed in 4.46. The remainder of the simulations will be done with the perturbed full state plant to test the performance of the controller under perturbed conditions.

$$A=\begin{bmatrix} 0 & 1 & 0 & 0 \\ 0 & -0.9211*bf & -.5809 & 0 \\ 0 & 0 & 0 & 1 \\ 0 & 0.3947*bf & 4.4532 & 0 \end{bmatrix}, \quad B=\begin{bmatrix} 0 \\ 0.9211 \\ 0 \\ -0.3947 \end{bmatrix}$$

$$C=[0 \;\; 0 \;\; 1 \;\; 0], \qquad D=[0] \tag{4.46}$$

The simulations are grouped into seven distinct cases. Each case contains particular initial conditions and coefficients of friction. These cases are tabulated in table 4.4.

	Initial	**Conditions**	
Case	**Angular Position** *(rad)*	**Angular Velocity** *(rad/s)*	**Coefficient of Friction** *bf* **(kg/s)**
I	0.5	0.1	0
II	1	0.1	0
III	0.5	0.1	1
IV	1	0.1	1
V	0.5	0.1	2
VI	1	0.1	2
VII	0.5	0.1	5

The cart's initial position and velocity equal 0 for all cases

Table 4.4 Simulation Cases

Consider the inverted pendulum in figure 4.1 with the initial conditions for case I and case II in table 4.4. The result of the simulation for case I is illustrated in figure 4.10 and 4.11, and that for case II in figure 4.12. Both cases I and II in table 4.4 have been simulated with the nominal reduced state plant.

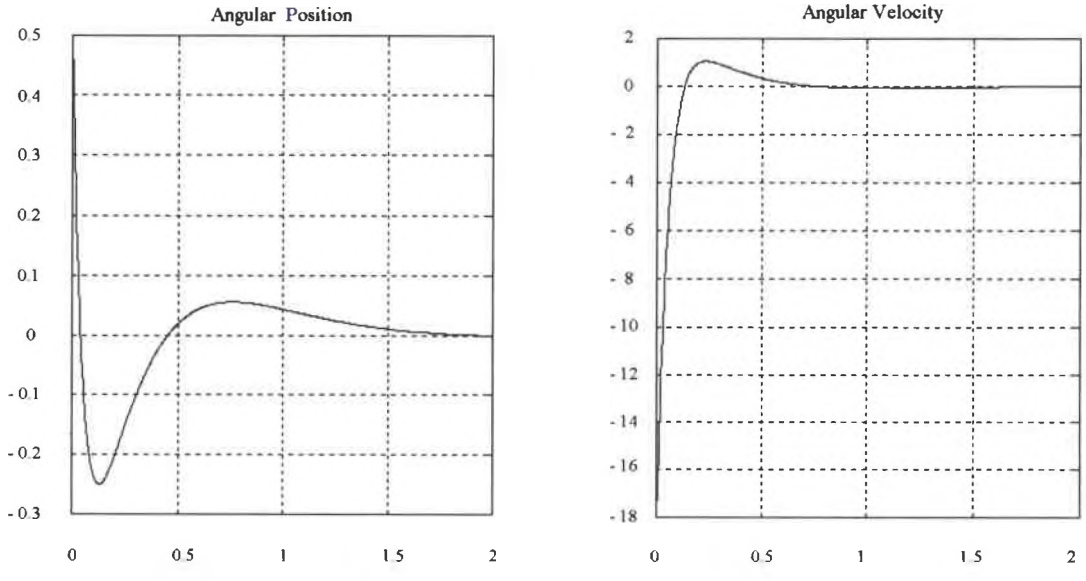

Nominal Reduced State Model
Figure 4.10 Simulation case I

In case I the pendulum's initial angular position has been set to 0.5 rad which is approximately 28.6 degrees and the pendulum's initial angular velocity has been set to 0.1 rads/sec. These seem to be reasonable initial conditions and the system is expected to balance the pendulum with little trouble. The left figure in 4.10 shows the angular displacement of the pendulum. The response reveals that the pendulum's angular position is indeed stabilized about the 0 radian operating point in shortly less than two seconds. In general, the response of the pendulum's angular position is slightly

underdamped, but quite swift. The speed of the response is the combined effect of the two closed loop poles at $s = -10$ and the slower poles at $s = -0.633$ and the complex poles at $s = -1.18 \pm j0.32$. The pole at $s = -1000$ is extremely fast and its contribution to the system's response is overshadowed by the more dominant and slower poles. In addition, the angular velocity of the pendulum is somewhat underdamped, however, it does reach a rather large overshoot which should be of concern had the system been expected to perform in an actual physical setup.

Since the response of the angular velocity cannot be resolved for times in the interval [0, 0.15] seconds, the response has been repeated for this time interval and it is shown in figure 4.11.

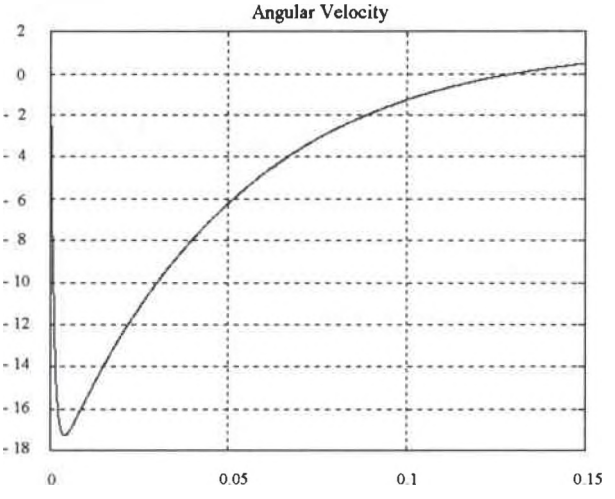

Nominal Reduced State Model

Figure 4.11 Zoom of angular velocity response (case I)

The pendulum's angular velocity starts at 0.1 rads/sec and rapidly increases to roughly -17 rads/sec in about 0.01 seconds. At this instant of time the pendulum passes by the equilibrium point with a rather large angular velocity. The pendulum continues to rotate in

this direction until it reaches - 0.25 rads or roughly -14.5 degrees. At this moment the angular velocity of the pendulum momentarily becomes 0 radians/sec as the pendulum begins to travel in the opposite direction. The pendulum passes by the equilibrium point once again at 0.45 seconds but with a much slower velocity than the first time. This behavior continues until the beam is finally positioned at 0 radians in about 2 seconds.

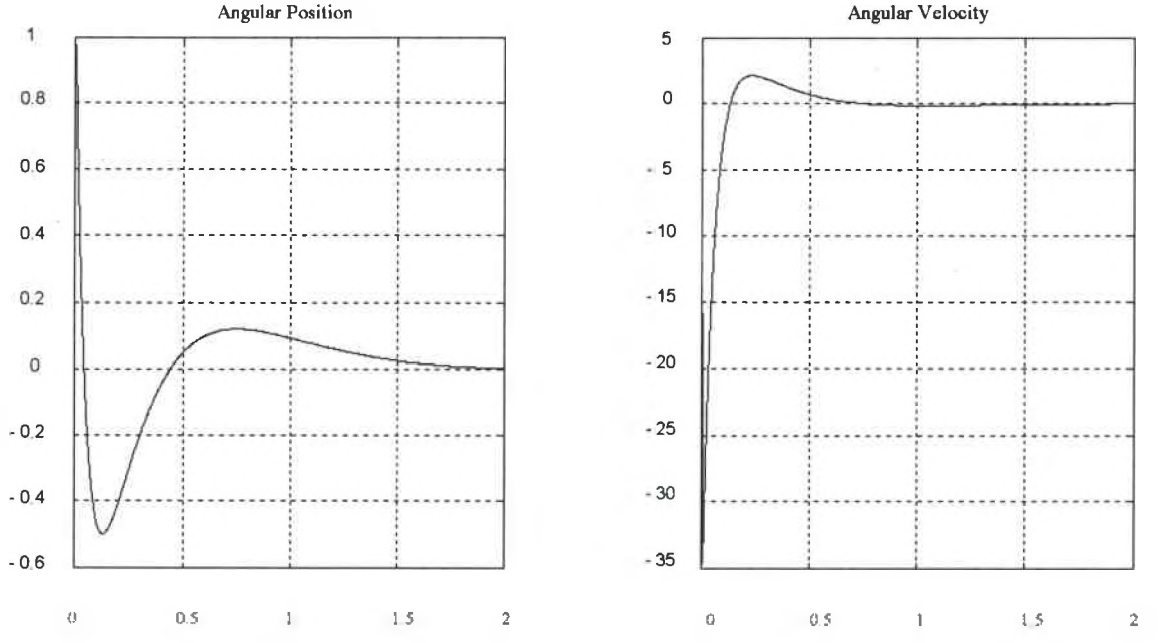

Nominal Reduced State Model
Figure 4.12: Simulation case II

The outcome of the simulation for the second case is shown in figure 4.12. In this case the pendulum's initial angular position has been set to 1 radian which is approximately 57.3 degrees and the pendulum's initial angular velocity has been set to 0.1 rads/sec. The inverted pendulum system has been conceptually structured to operate within the angular range [$\pi/2$,-$\pi/2$] radians. In this case the pendulum is being initially positioned at more than half the angular distance away from the equilibrium position. Thus, in this respect

this case portrays a somewhat worst scenario than the first case. Nevertheless, the controller is successful once again in regulating the pendulum to its equilibrium point in a stable fashion. The dynamics of the system are very similar to case I with the difference that the magnitudes of the response of the system are proportionally increased. This is expected since the plant model in this case is linear.

Consider again the pendulum system of figure 4.1 and the initial conditions for cases III and IV in table 4.4. Both of these cases have been simulated with the perturbed full state model with a corresponding coefficient of friction of 1 Kg/s. Recall from section 4.1 that the variation in the coefficient of friction of the system was restricted to the range [0.5,2] with a nominal value of $bf = 1$. Thus, cases III and IV test the performance of the system perturbed by the nominal value of dynamic friction bf as defined in section 4.1.

Figures 4.13 and 4.14 illustrate the results of the simulation for the third and fourth cases respectively. A first glance at these figures reveals the success of the controller in balancing the beam for both scenarios. The dynamics of the pendulum's angular displacement and velocity are very similar to the nominal cases. This similarity in the behavior of these variables suggests that the earlier assumption that the pendulum subsystem is naturally decoupled is sound. There are no major differences in the behavior of the angular position and velocity between cases I, II and III, IV except that the settling time in the latter cases is marginally increased. Additional insight into the behavior of the whole system is gained due to the available information about the cart's position and velocity. From figure 4.13 it is evident that the cart's position increases rather rapidly until the pendulum reverses its direction and then decreases to settle around 0.9 meters. The fact that the position does not return to zero may be attributed to the possible interaction between the system variables. Although, the physical parameters of the system were

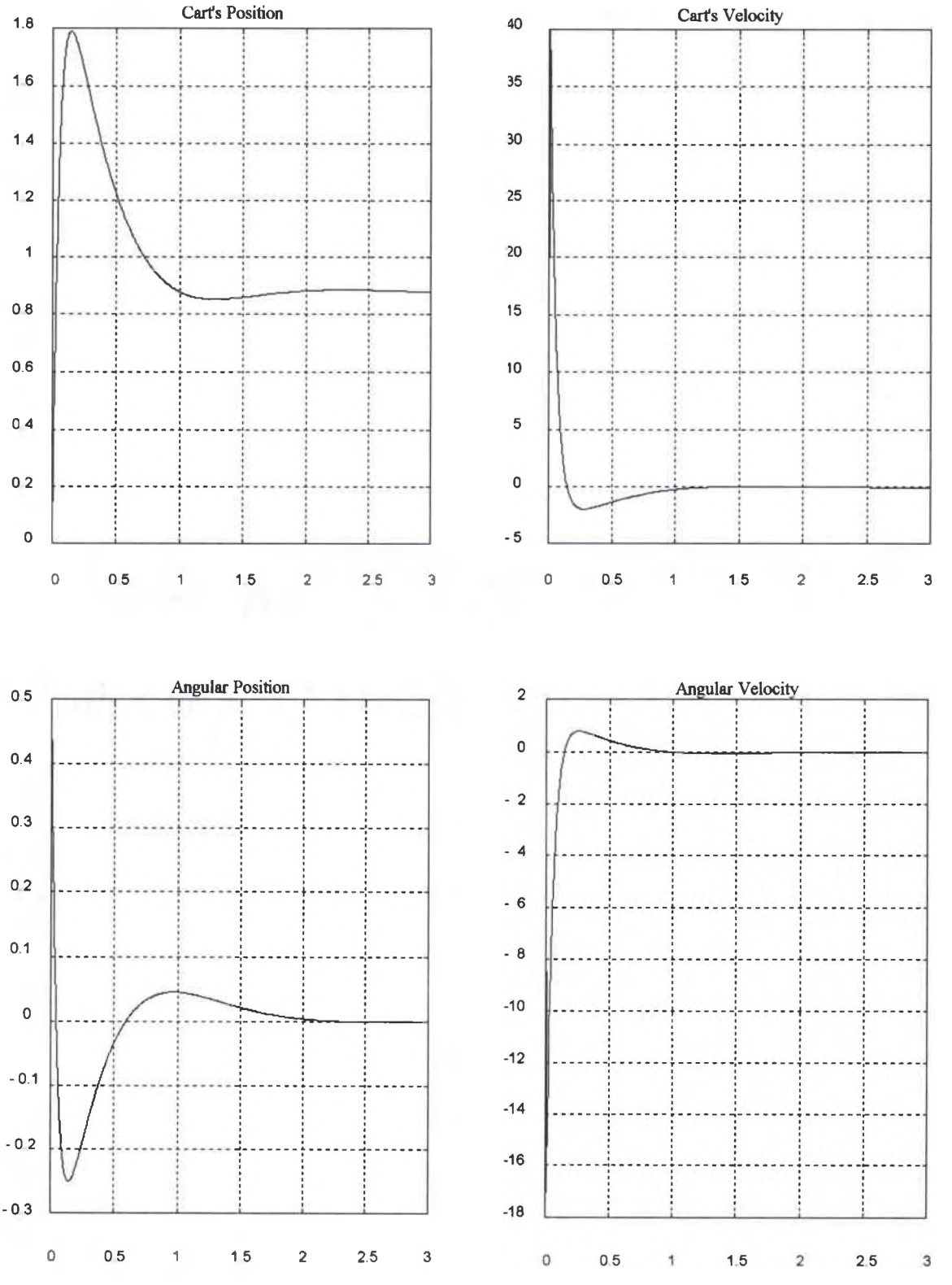

Perturbed Full State Model

Figure 4.13 Simulation case III

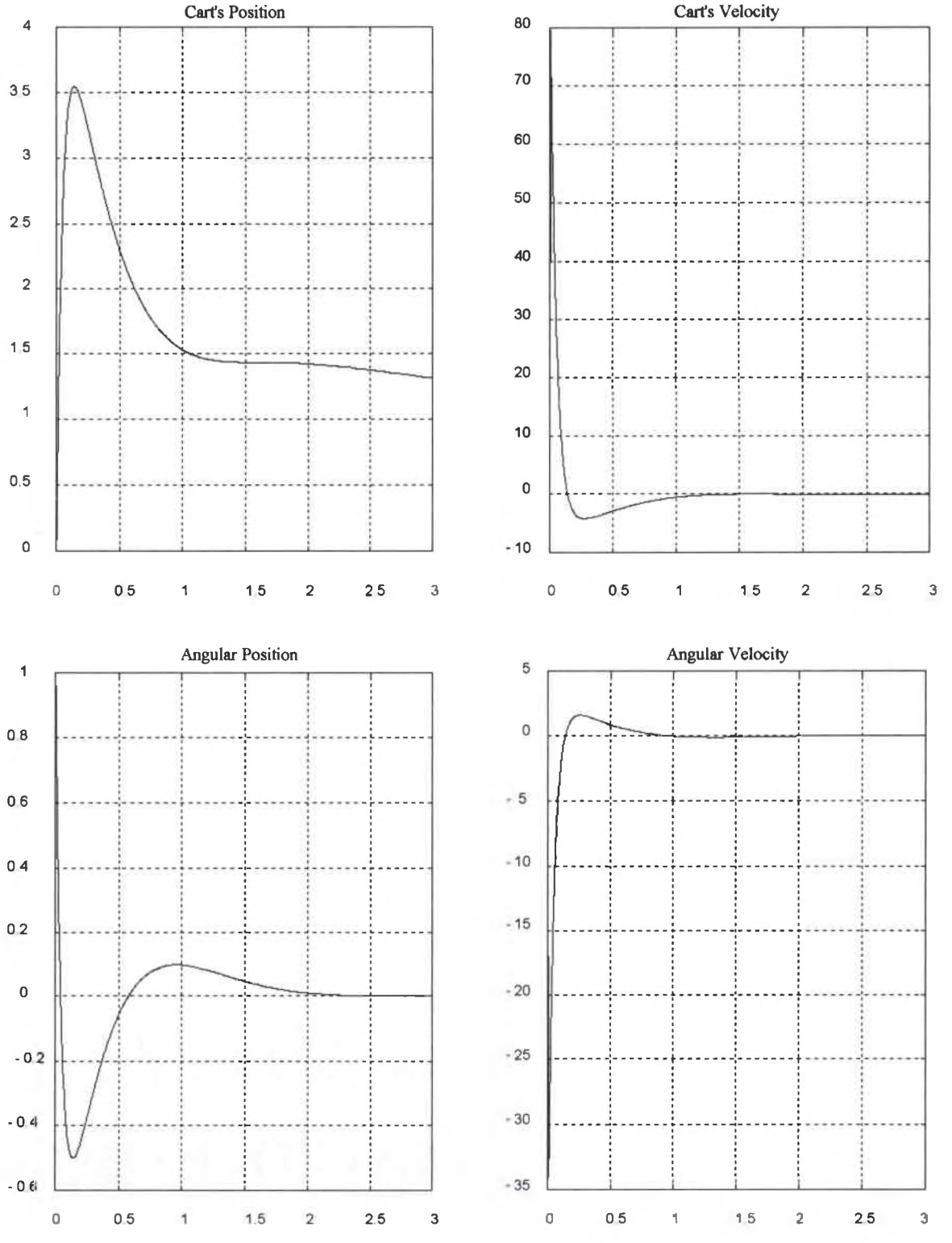

Perturbed Full State Model

Figure 4.14 Simulation case IV

selected to reduce the effects of coupling between the system variables, the cart submatrix A_{12} is not quite equal to zero. Therefore, the position of the cart is somewhat coupled to the pendulum's state variables. In addition, it is observed that as the initial angular position of the pendulum is strectched the cart's final position is increased. In case IV it appears as if the cart's position continues to decrease slowly and as if the cart's velocity is zero after 3 seconds, when in fact, it is small but not identically zero. The velocity of the cart actually decays in an oscillatory manner within a very small dynamic range. This makes the cart to slowly oscillate until it eventually settles. The details are not included due to the significant amount of time required to run a simulation of only a few seconds for this plant. Again, the only significant differences between case III and IV are the magnitudes of the responses.

Consider now the next two cases in table 4.4: cases V and VI. These cases represent the system under extreme perturbation, since the value of the dynamic friction term is at the allowable maximum. Figures 4.15 and 4.16 display the results of the simulation. Again, the pendulum is suitably regulated for both cases, however, the settling time has increased compared to the previous cases. The beam reaches equilibrium at about 2.5 seconds.

An interesting observation is that the settling time has increased with increasing coefficient of friction. It appears that the significant differences between the nominal cases and the perturbed cases occur as the pendulum angle slows approaching equilibrium. Perhaps this effect may be attributed to the fact that the presence of friction in the system primarily affects the low frequency components of the plant. Nevertheless, the general dynamics of the system are not significantly affected.

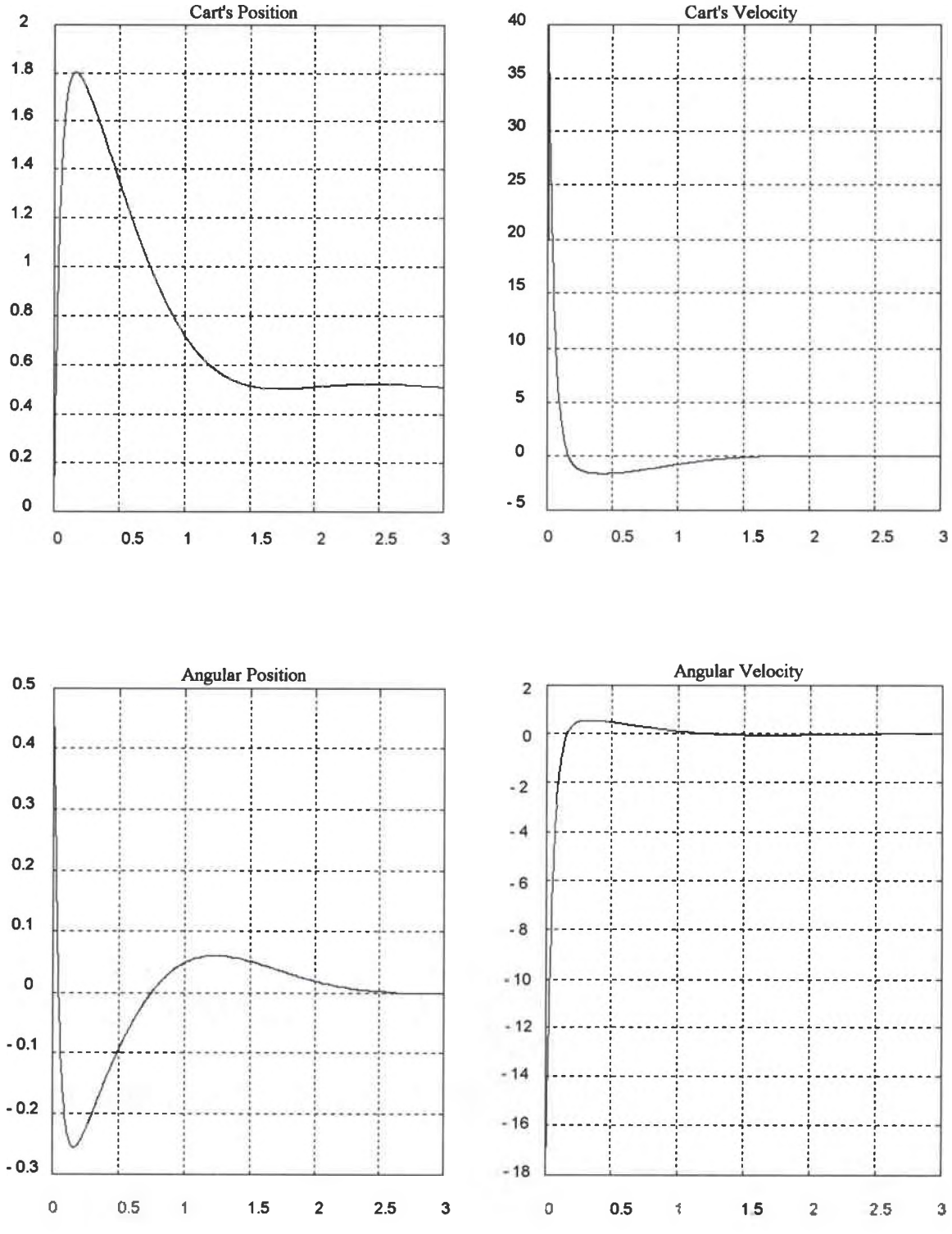

Perturbed Full State Model

Figure 4.15 Simulation case V

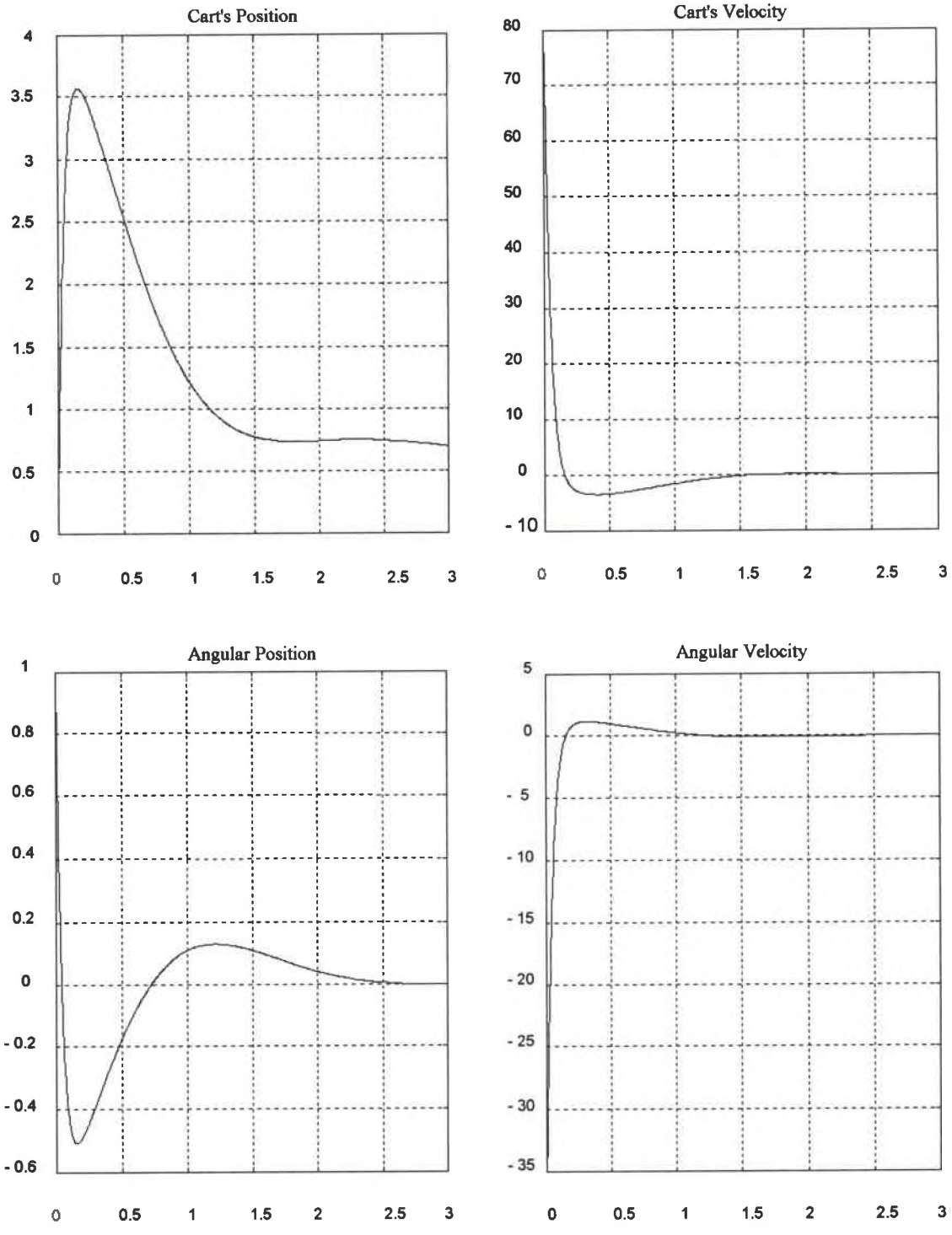

Perturbed Full State Model

Figure 4.16 Simulation case VI

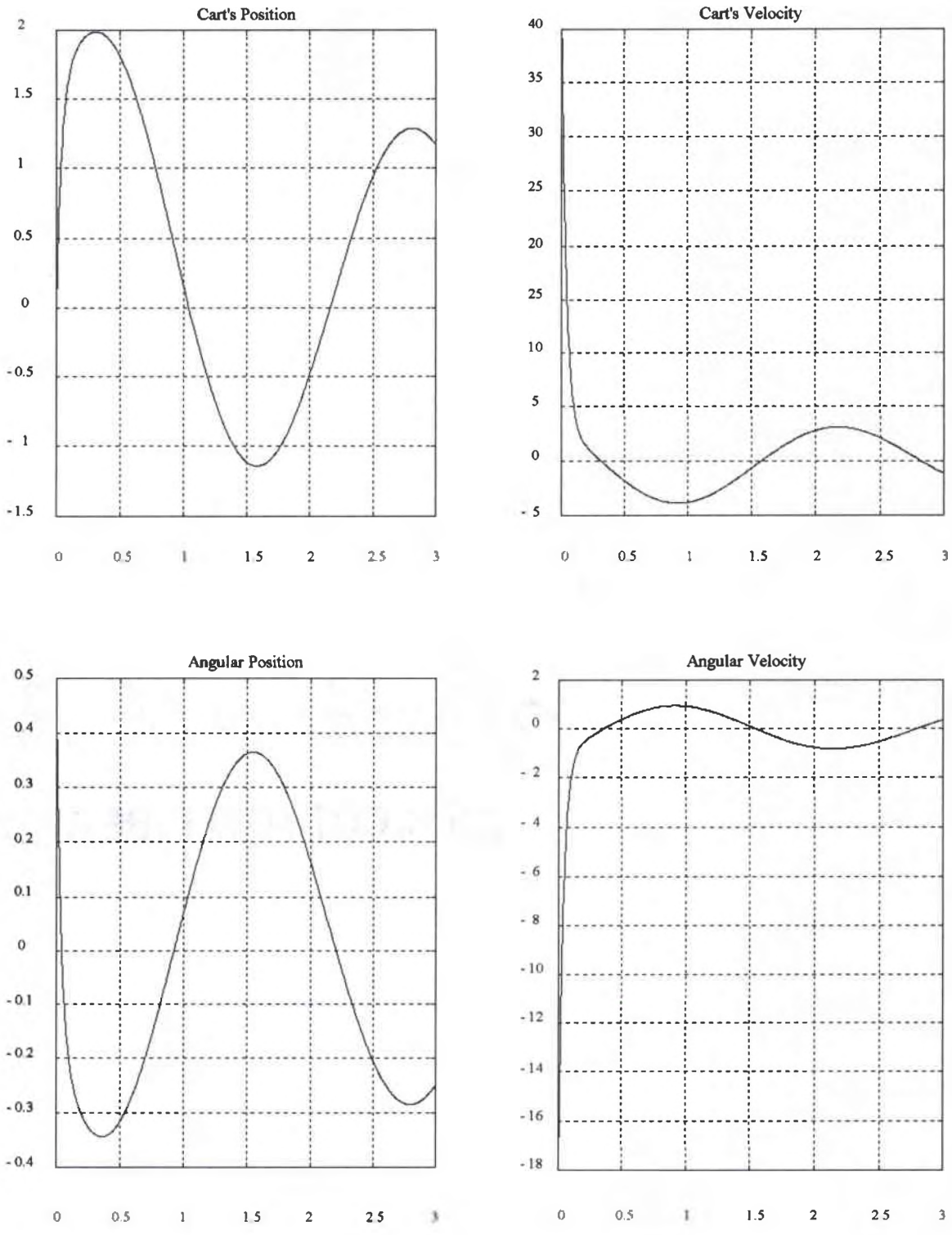

Perturbed Full State Model

Figure 4.17 Simulation case VII

Although large overshoots of the cart's velocity and the pendulum's angular velocity might be of concern if this system was to implemented physically, the control objective of the system has been achieved for both nominal and perturbed conditions. Since the specifications of the inverted pendulum system have been accomplished by the controller designed in section 4.2 and the procedure has been succesfully illustrated, the case study serves its purpose thus far. Nonetheless, it would interesting to see how the system behaves as the coefficient of friction is increased. Consider case VII where the coefficient of friction is equal to 5 Kg/second. Figure 4.17 illustrates the result of this simulation. Significant changes have occurred in the dynamics of the plant by the introduction of this rather large coefficient of friction. It was asserted previously (section 4.2) that the plant was guaranteed to be stable for perturbed plants with friction coefficients up to 3 kg/sec. This characteristic is not guaranteed, although it may be the case for higher values of *bf*. Note in this case that the magnitude of the angle appears to be decreasing, but the response is characterized by significant oscillations. This suggests that the system is close to the stability boundary. It could be expected that the system will be driven into instability by higher coefficients of friction. Thus the system is robustly stable with respect to parameter uncertainty albeit in a restricted sense.

It was argued in earlier chapters that most modern control design techniques do not address the issue of uncertainty and perturbations in the model of the plant and throughout the design process. One of the most common modern design techniques used in recent years is the state variable feedback approach. It proves interesting to pursue a simple SVF controller for the inverted pendulum in order to test its effectiveness in dealing with the perturbations introduced by the dynamic friction in the system. Consider a state variable feedback solution to the inverted pendulum system. Figure 4.18 illustrates the

structure of the state feedback controller where K is the state feedback gain matrix, and A, B, C are the state space system's matrices. Hoffman [16] designed such a controller using the nominal model presented in section 4.1 and expressed by equations 4.20 *a* and *b*. The solution that Hoffman [16] presented yields four closed loop poles at the point (-1,0) in the s-plane. Hoffman's work was involved with the investigation of optimal estimation and Kalman filtering. His desicion to place the closed loop poles at (-1,0) was merely for investigative purposes, to study the stabilization of the inverted pendulum in the presence of measurement noise and the estimation problem. Nevertheless, his results will be replicated here.

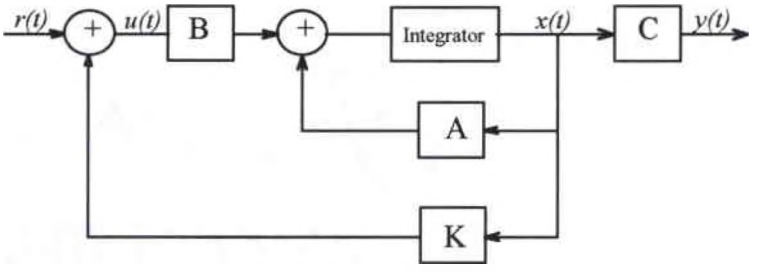

Figure 4.18 State variable feedback Structure

In order to compare the performance of the controller designed in section 4.2 with the state variable feedback solution of Hoffman, the system will be simulated with the initial conditions of case I in table 4.4. In addition, the inverted pendulum will be tested for both the nominal and the perturbed models with several coefficients of friction. The effect of additional closed loop pole locations will be investigated. The state variable feedback simulations performed on the nominal model are tabulated in table 4.5. The objective of these simulations is two fold. Firstly, to examine the general performance of the state variable feedback solution, and secondly, to study the response of the system as the closed loop poles are moved farther away from the jω-axis.

Poles at	Gain Matrix	Figure #
(-1,0)	K= -1*[0.26 1.033 27.082 12.54]	4.19
(-3,0)	K= -1*[20.14 27.11 192.6 93.4]	4.20
(-5,0)	K= -1* [157.8 126.96 755.4 346.7]	4.21
(-7,0)	K= -1*[610.2 350.1 2174.2 887.6]	4.22

bf = 0 Kg/s (Nominal Plant)

Table 4.5 State Variable Feedback Simulations

Figure 4.19 below illustrates the results of the simulation for the a case with coefficient of friction equal to zero, that is the nominal plant, and the poles located on the real axis at *s=-1*.

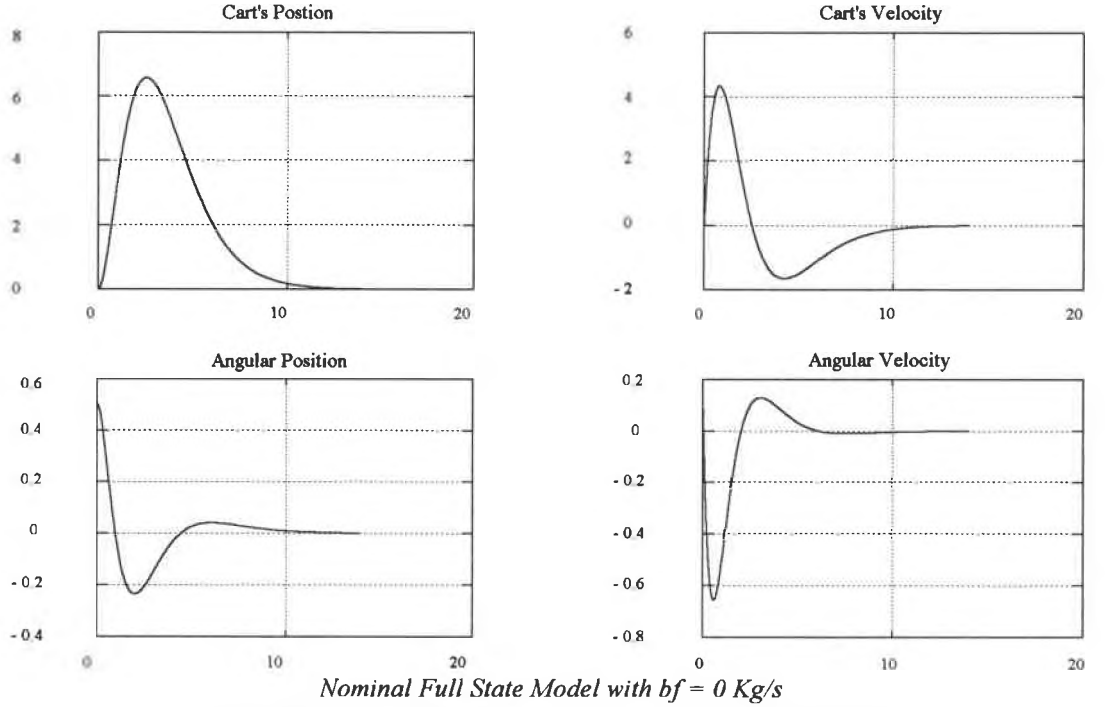

Nominal Full State Model with bf = 0 Kg/s

Figure 4.19 *State Variable Feedback Solution (nominal Plant)*

The performance of the system is satisfactory since the pendulum is indeed balanced. The overall dynamics of the system, however, is slower than for the H_∞ controller cases since the closed loop poles are so close to the jω-axis. The beam reaches the equilibrium position in roughly 13 seconds. The overshoots of the cart's and the pendulum's angular velocity are more reasonable when compared to the H_∞ cases.

Figures 4.20 to 4.22 display the results of the simulation for nominal systems with closed loop (c. l.) poles located at points *s* = *-3*, *-5* and *-7* on the real axis respectively. As the c. l. poles move away from the imaginary axis, the system settling time improves significantly, as expected. In fact, for the last two cases in table 4.5 the system's dynamic response is comparable to the H_∞ cases with respesct to the settling time. The overshoot of all the responses, however, are significantly increased as the closed loop poles are placed farther away from the jω-axis.

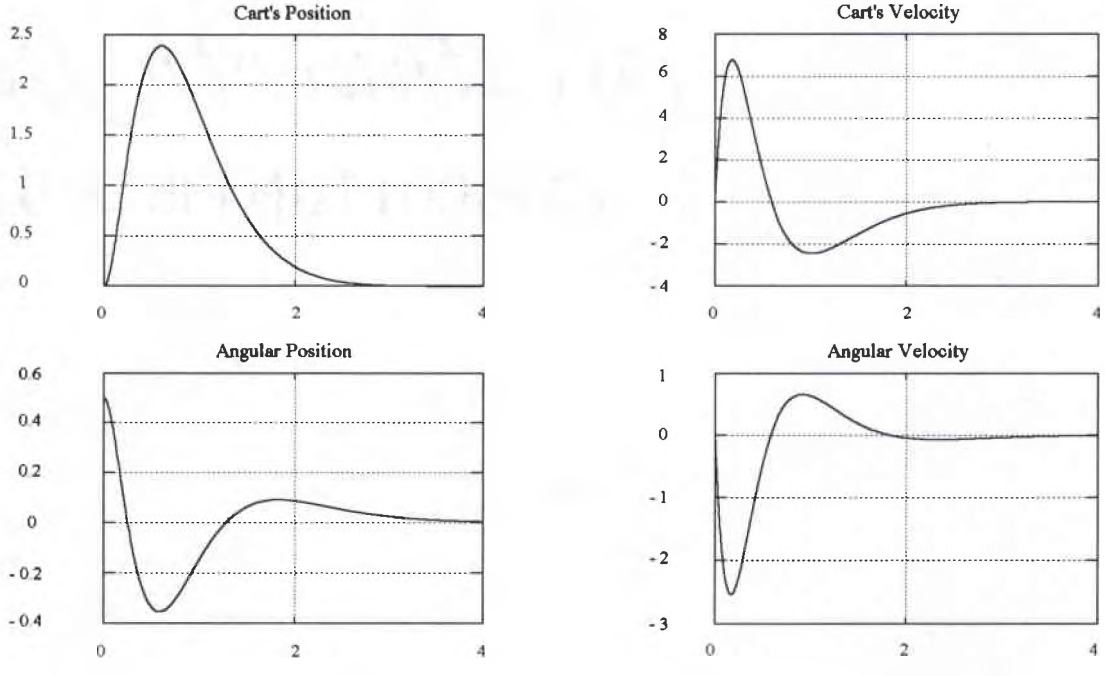

Nominal Full State Model with bf = 0 Kg/s

Figure 4.20 *State Variable Feedback Solution (Nominal Plant)*

In particular, figures 4.21 and 4.22 reveal that as the response becomes faster as a consequence of placing the c.l. poles farther away from the origin, the overshoot of the angular position response approaches the physical angular boundary. Recall that the inverted pendulum system is conceptually confined to a physical angular range of [90, -90] degrees or approximately [1.57, -1.57] rads. For the case when the c. l. poles are placed at $s = -5$ (figure 4.21) the pendulum starts at $s = 0.5$ rads and quickly overshoots to - 0.6 rads. Furthermore, when the c. l. poles are located at $s = -7$ (figure 4.22) the pendulum starts at 0.5 rads and quickly overshoots to -1 rads. It can be expected then that the overshoot of the angular position response will exceed the confined physical angular range for faster pole locations, and therefore, forcing the system to collapse during the regulating process. The danger that the system in figure 4.22 may collapse is heighten by the fact that the design has been done using a linear model, but the system is intrinsically nonlinear.

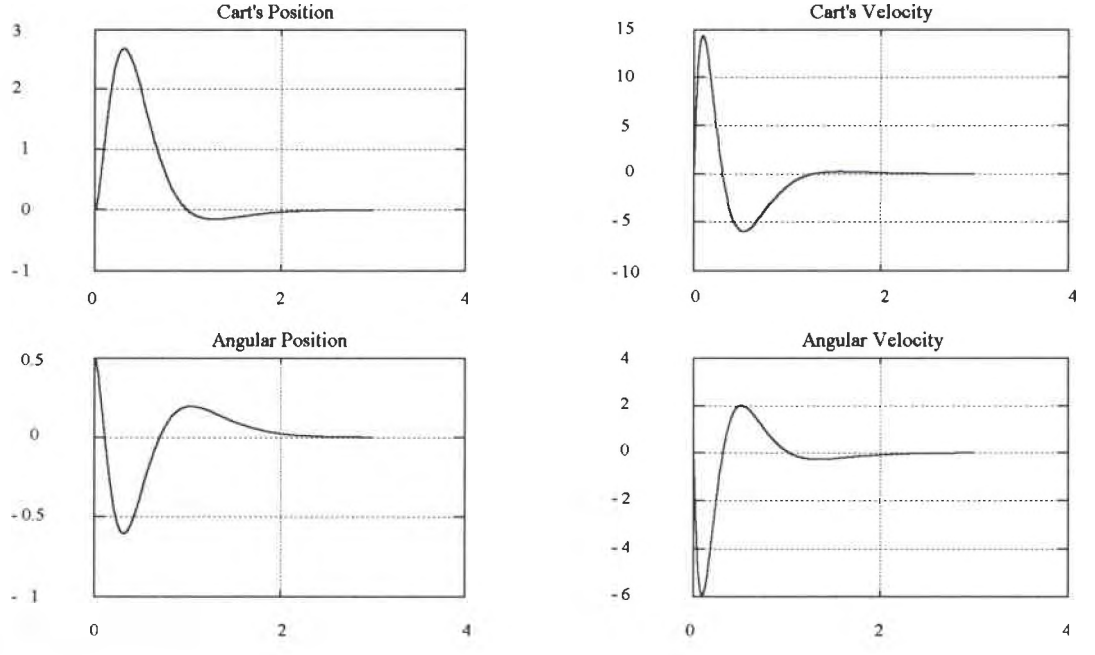

Nominal Full State Model with bf = 0 Kg/s

Figure 4.21 *State Variable Feedback Solution (Nominal Plant)*

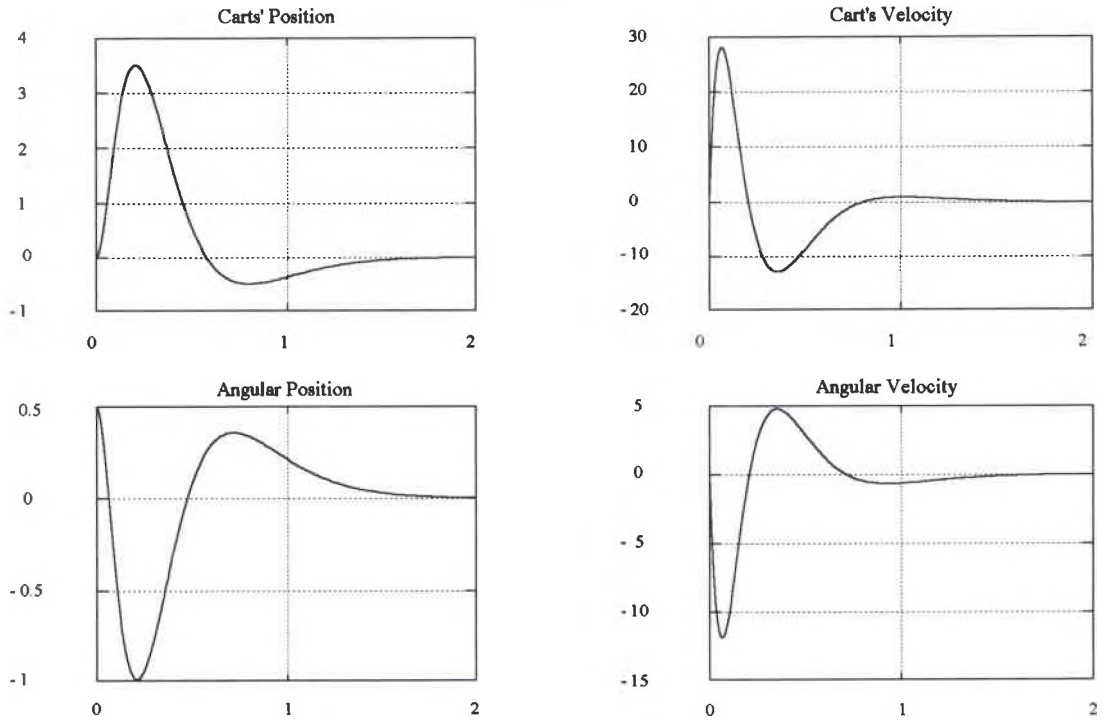

Nominal Full State Model with bf = 0 Kg/s

Figure 4.22 *State Variable Feedback Solution (Nominal Plant)*

Thus, in a real physical implementation of the system the pendulum could very likely collapse in this situation. Also, note the rather large overshoots of the cart's velocity and the angular velocity of the pendulum. These reach values very similar to the H_∞ simulations. As a consequence, to obtain comparable dynamics to the H_∞ solution, the SVF solution requires that the closed loop poles be placed in the conservative range $s < -5$, yet the system is put at a greater risk of collapsing.

The simulations performed on the perturbed model are grouped in table 4.6. The same values of coefficients of friction used for the H_∞ simulations have used in these cases to assess the sensitivity of the system to a single parameter variation. The closed loop poles have been placed in three different locations to determine the stability robustness of the system with respect to system dynamics.

Closed Loop Poles at	*bf*	Figure #
(-1,0)	1	4.23
(-1,0)	2	4.24
(-1,0)	5	4.25
(-2,0)	1	4.26
(-2,0)	2	4.27
(-2,0)	5	4.28
(-3,0)	1	4.29
(-3,0)	2	4.30
(-3,0)	5	4.31

Table 4.6 State Variable Feedback Simulations *(Perturbed Plant)*

Figure 4.23 reveals the behavior that every control systems engineer fears of a control system which lacks the ability to account for expected unmodeled dynamics. The system in figure 4.23 is closed loop unstable and has no chance to recuperate from the addition of friction. In fact, after taking a closer look at the results it is evident that all of the systems which had their closed loop poles located at the point (-1,0) are closed loop unstable for the three coefficients of friction used (see figures 4.23, 4.24, 4.25). As the coefficient of friction increases the systems oscillatory behavior is severely aggravated. This behavior was also observed in the H_∞ simulations. Most of the variables display significant oscillatory behavior and there magnitudes became unbounded.

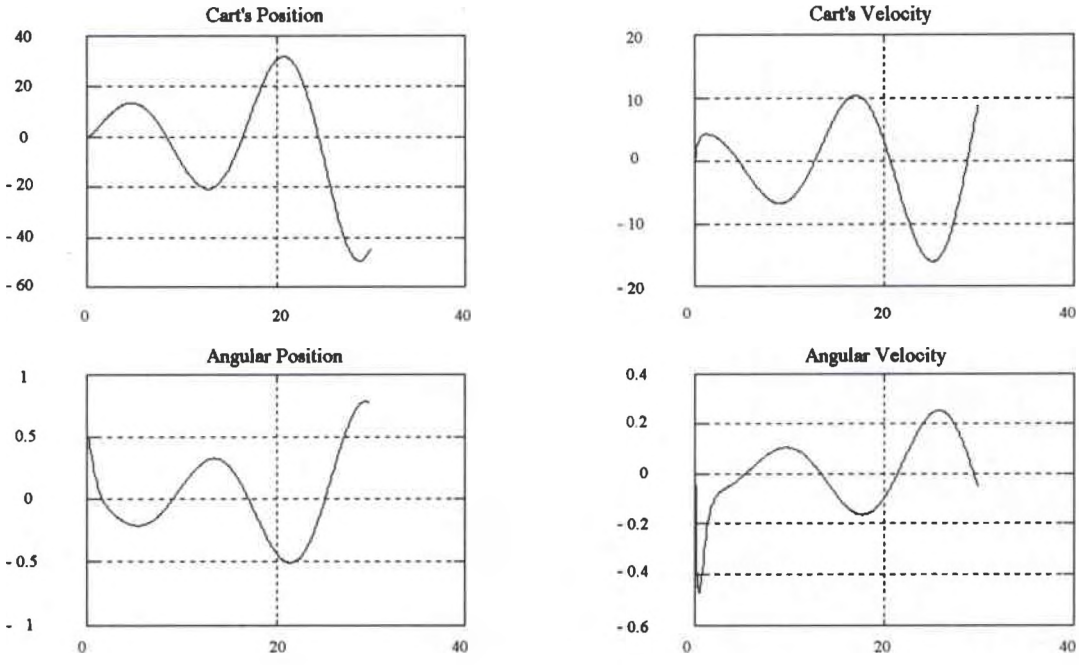

Perturbed Full State Model With bf = 1 Kg/s, poles at (-1,0)
Figure 4.23 State Space Feedback Solution *(Perturbed Plant)*

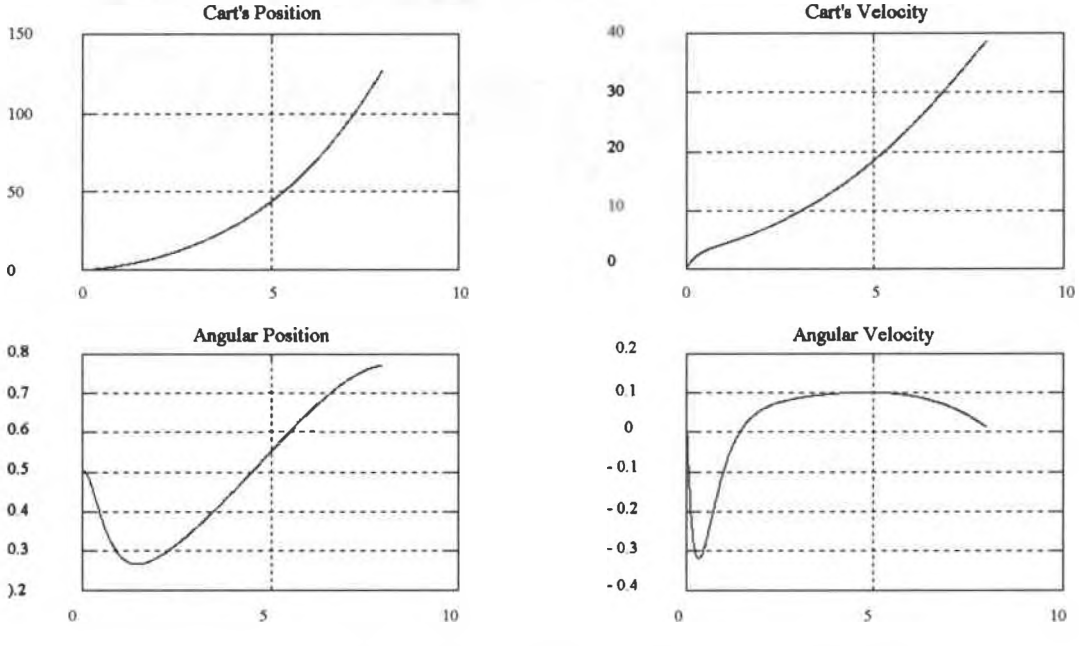

Perturbed Full State Model With bf = 2 Kg/s, poles at (-1, 0)
Figure 4.24 State Space Feedback Solution *(Perturbed Plant)*

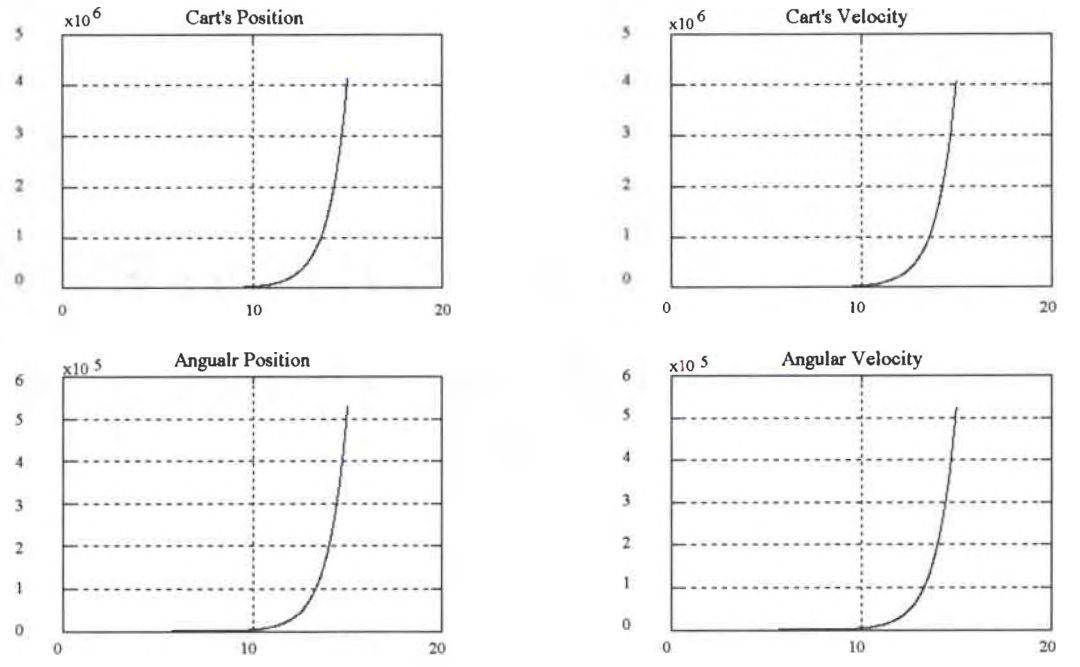

Perturbed Full State Model With bf = 5 Kg/s, poles at (-1,0)
Figure 4.25 State Space Feedback Solution *(Perturbed Plant)*

These results illustrate the kind of situation which may occur as a result of neglecting the uncertainties and perturbations inherent in the models throughout the design process.

When the closed loop poles where placed at the point (-2, 0) the results were completely opposite to the case with poles at (-1, 0). The responses for these cases are shown in figures 4.26, 4.27, and 4.28. The perturbed inverted pendulum system is now closed loop stable for coefficients of friction equal to 1, 2 and 5. The response is in general slower than the response for the H_∞ case, but this is expected since the poles are so close to the imaginary axis. The trend observed in the preceding simulations holds in these cases also. Namely, the system approaches marginal stability for increasing values of the coefficient of friction. Actually, it was determined experimentally that the closed loop

system is unstable for the range $bf > 5.75$. Consequently, in terms of stability robustness this particular design achieves roughly the same margin of robustness to variations in the coefficient of friction as the H_∞ solution.

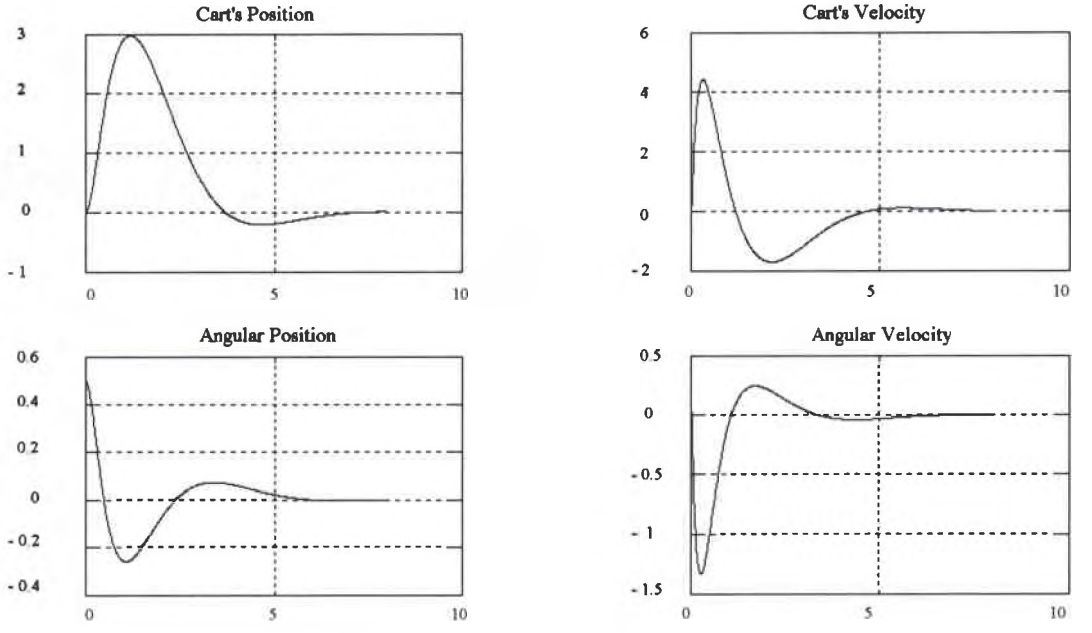

Perturbed Full State Model With bf = 1 Kg/s, poles at (-2,0)
Figure 4.26 State Space Feedback Solution *(Perturbed Plant)*

Figures 4.29, 4.30, and 4.31 illustrate the responses for the inverted pendulum system with closed loop poles a s = -3. Examination of the responses in figures further confirms our previous discussion that increasing coefficient of friction severely increases the oscillations in the responses. In this case the inverted pendulum is unstable for the range, $bf > 17$.

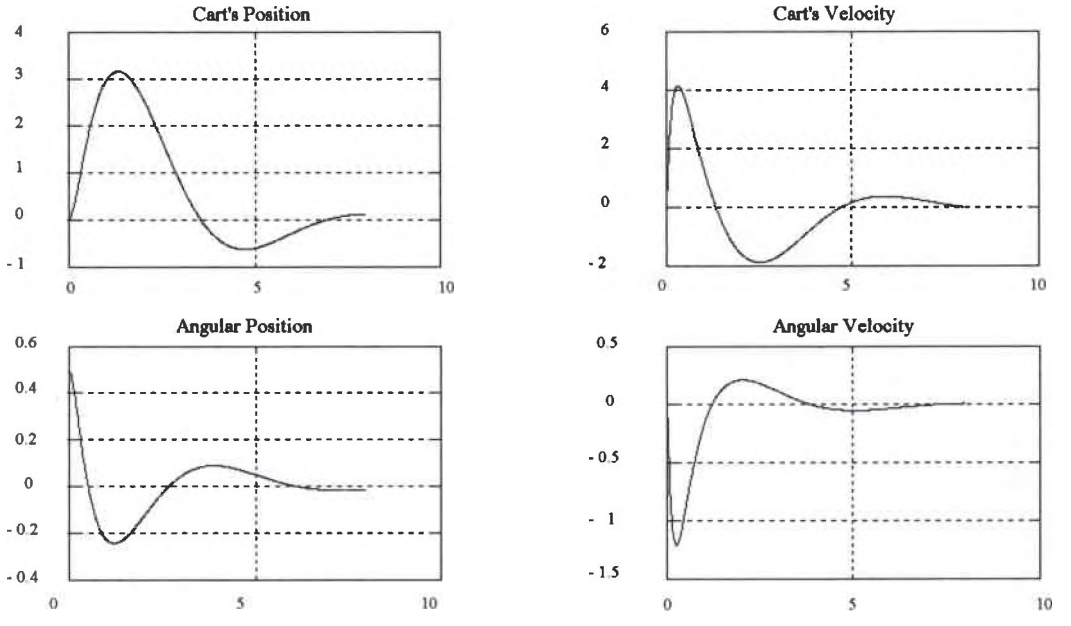

Perturbed Full State Model With bf = 2 Kg/s, poles at (-2,0)
Figure 4.27 State Space Feedback Solution *(Perturbed Plant)*

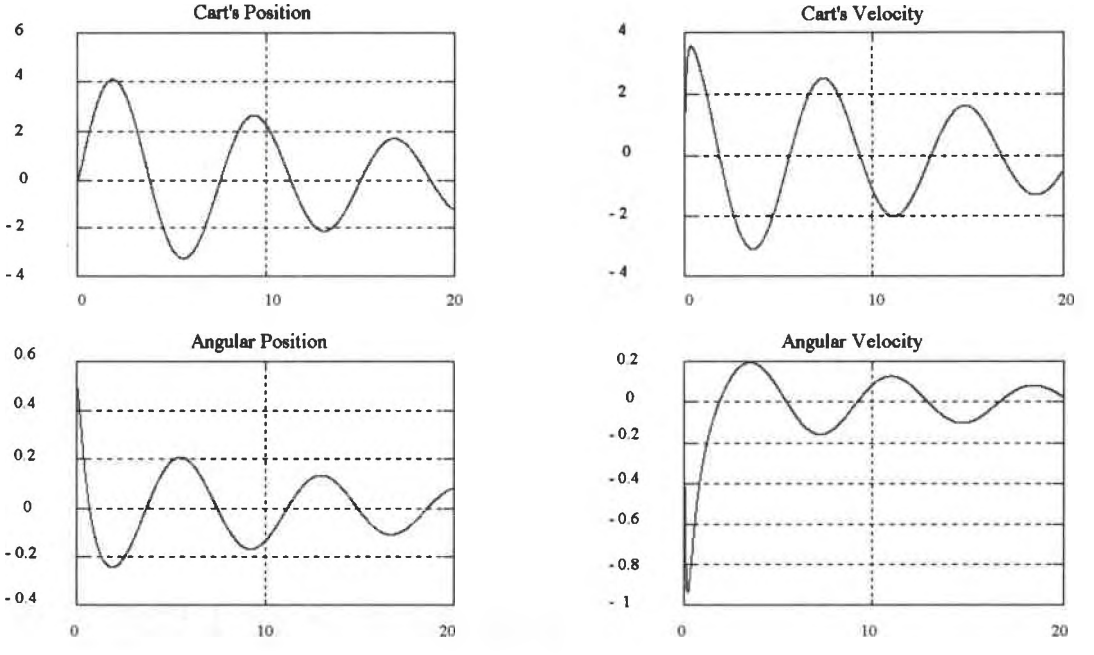

Perturbed Full State Model With bf = 5 Kg/s, poles at (-2,0)
Figure 4.28 State Space Feedback Solution *(Perturbed Plant)*

After analyzing the overall results, it is obvious that there is a trend in the behavior of the c. l. system with respect to both pole location and the value of coefficient of friction. It may be argued that for this particular problem the tolerance of the closed loop system to variations in the coefficient of friction improves as the c. l. poles move away from the jω-axis. There is an evident trade off, however, between the achievable dynamics and the robustness of the system to variations in the coefficient of friction. Recall that the farther the poles are placed away from the origin of the s-plane the more acute the response and the higher the risk that the pendulum's angular response overshoot the allowed angular range. Thus, in order to achieve both good robustness and acceptable performance the poles of the closed loop system must be placed in the closed range [-5, -3] in the s-plane.

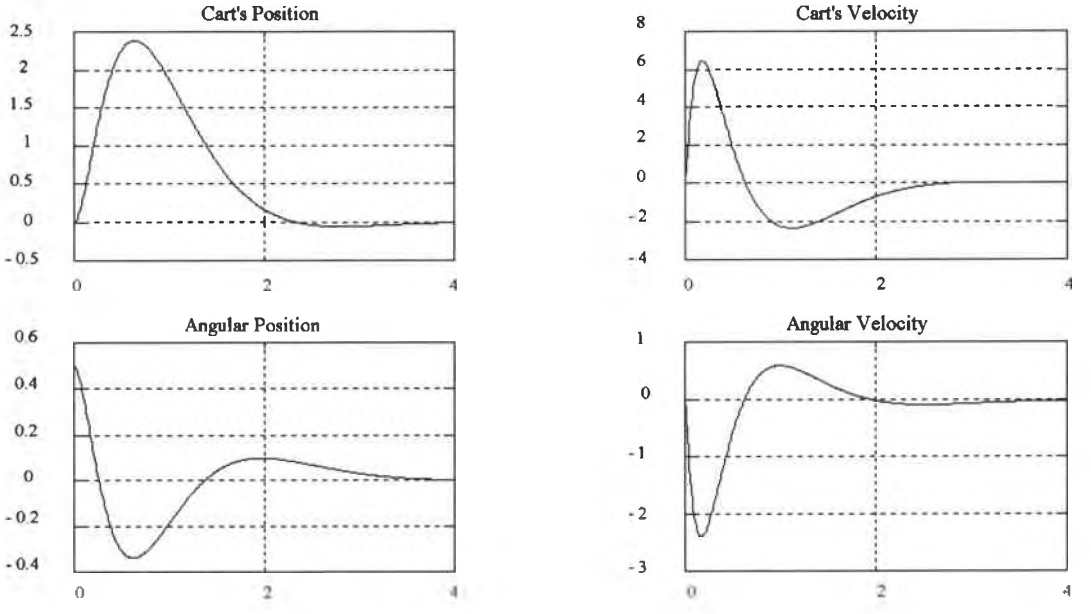

Perturbed Full State Model With bf = 1 Kg/s, poles at (-3,0)
Figure 4.29 State Space Feedback Solution *(Perturbed Plant)*

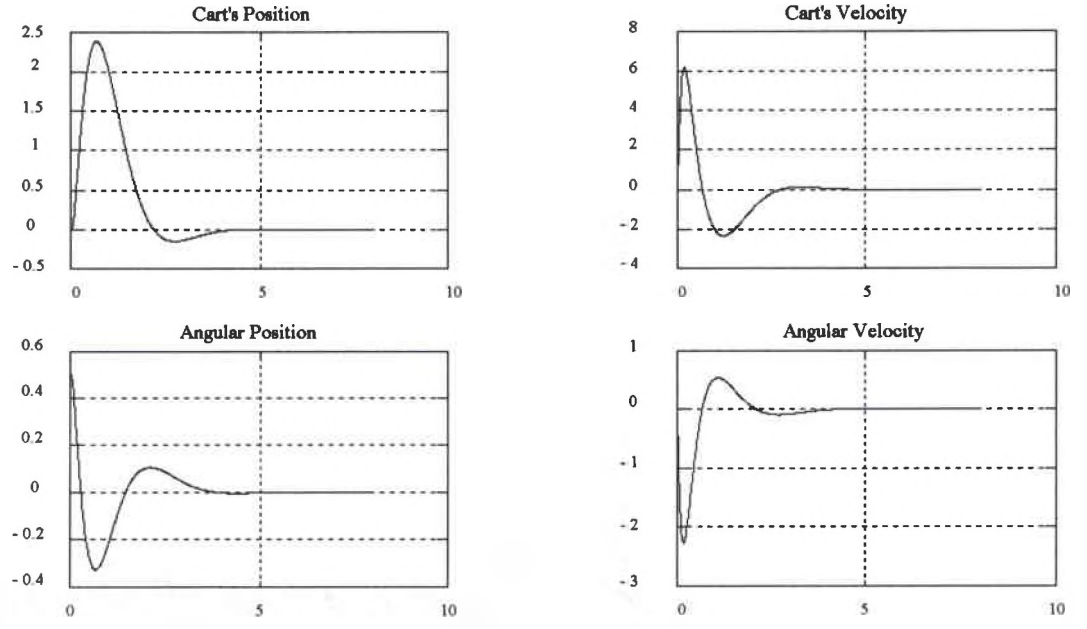

Perturbed Full State Model With bf = 2 Kg/s, poles at (-3,0)
Figure 4.30 State Space Feedback Solution *(Perturbed Plant)*

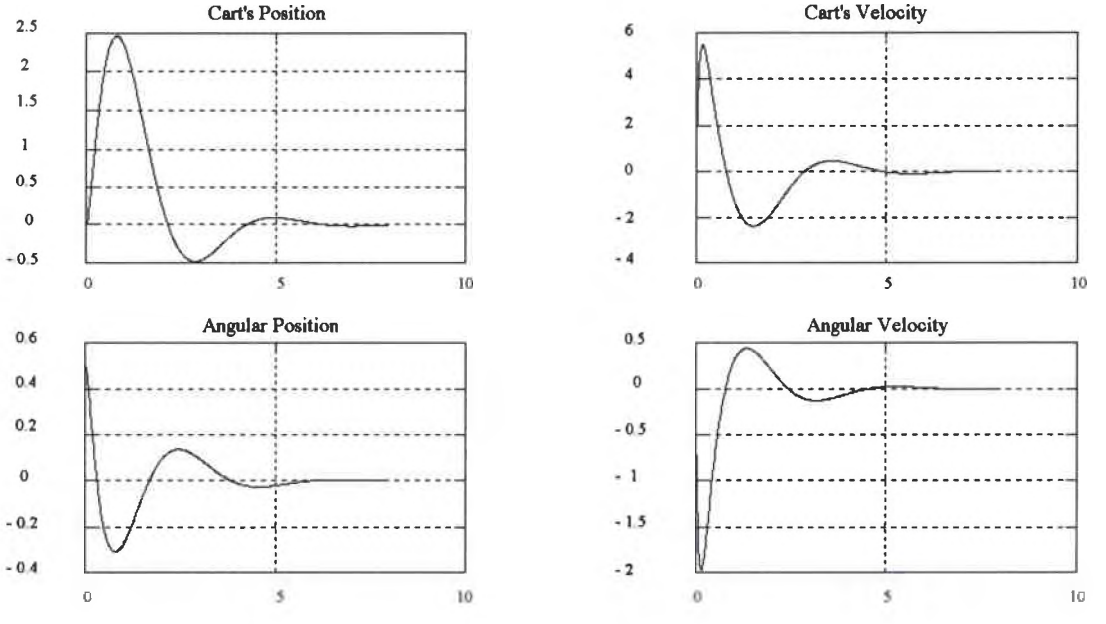

Perturbed Full State Model With bf = 5 Kg/s, poles at (-3,0)
Figure 4.31 State Space Feedback Solution *(Perturbed Plant)*

It would have been interesting to pursue a more conventional phase lead/lag SISO design for comparison purposes. Also, it would be enticing to redesign the control system for the inverted pendulum with a MIMO H_∞ approach. Nevertheless, it has been demonstrated that in the process of designing controllers, plant perturbation is not to be taken lightly. Had Hoffman's design been physically implemented, a nominal value of coefficient of friction would have had catastrophic effects in the regulation of the pendulum, as figures 4.23, 4.24, and 4.25 revealed.

Comparative Assessment:

It is difficult to pin point either control solution as superior. In fact, it is not evident in the available literature that there is a definite answer to the question of superiority. In this particular case study, both solutions were able to accomplished the desired task, although, each had favorable features of its own. Certainly, the SISO H_∞ control solution to the inverted pendulum problem successfully met its design criteria, yielding a satisfactory response for the nominal inverted pendulum model while providing the system with stability robustness to variation of the coefficient of friction for the specified parameter range. The H_∞ controller allowed for a fast response without jeopardizing the stability of the system. On the other hand, the SVF control solution achieves higher tolerance to variation in the coefficient of friction when the c. l. poles are placed in the range $-5 < s < -3$. Thus, the data gathered appears to indicate that the SVF solution yields better stability robustness to parameter changes. This poses an intriguing question. Can the results observed in this case study be extended to the general case, or are these observations particular to the inverted pendulum problem?

CHAPTER V
CONCLUSION

5.1 Concluding Remarks

The goal of this work was to investigate a design technique which would account for model uncertainties in the design procedure. In achieving this goal several objectives have been met. These objectives are enumerated below:

i. A new approach to the control problem analysis and synthesis has been reported.

ii. A method for representation of plant model uncertainties and perturbations was discussed.

iii. An alternate way to formulate the performance specification and a technique for treatment of plant perturbations and disturbances in the design process has been demonstrated.

iv. An algorithm for designing controllers achieving robust stability and robust performance for plants with RHP poles and zeros has been presented.

v. A comparative assessment of the H_∞ control method was pursued.

In order to achieve the above objectives some preliminary topics and definitions were treated in the introduction. For example, the differences between real systems and mathematical models of systems, as well as the definitions of signal and system norms were discussed in chapter I. A formulation for the performance specification in terms of the infinity norm of the weighted sensitivity transfer function was presented. Several

representations of unstructured uncertainty in linear models were discussed followed by a comparison between the classical and the modern measures of robust stability. The robust stability and performance conditions were analyzed and tests were presented to determine if a system complies with these conditions. Some related design constraints were also discussed. It was shown that the values of the uncertainty and performance weighting functions must be restricted within a certain range at the unstable poles and RHP zeros of the nominal model in order for the system to be robustly stabilizable and to achieve robust performance. It was demonstrated that either the robust stability or the robust performance control problem can be formulated into the standard or optimum H_∞ control problem. An outline was developed for a systematic procedure to design H_∞ controllers based on the solution of the Nevanlinna Pick theory and the model mathching problem and some simple examples were constructed to illustrate these procedures. A comprehensive example was developed using the inverted pendulum position system as a case study to illustrate the SISO H_∞ design procedure as well as the related concepts of robustness. A controller was devised that achieved robust stability in the presence of dynamic friction as source of model perturbation. Finally a comparative assessment of the performance of the H_∞ controller was pursued by comparing its behavior to a more familiar state variable feedback solution.

Most design techniques lack the ability to incorporate the effects of uncertainty and model perturbations in the design process. Rather the controllers are first designed to satisfy particular performance specifications and the system's robustness is subsequently determined through simulation or experimentation. This is the case with the state variable feedback solution that was developed in chapter IV. In contrast, the SISO H_∞ design technique introduced here achieves a control system which takes into account such perturbations as part of the design process. The results of chapter four were both

satisfactory and revealing. These results left unanswered the question of whether the robustness feature of the SVF solution to the inverted pendulum of chapter IV is particular to this problem or if it can be generalized to all problems. It is evident that any attempt to provide an answer to this question with a somewhat scientific basis would require at least additional testing of both methods with a spectrum of possible control problems. Nevertheless, the fact remains that SVF solutions as such are not concerned with the robustness features of the control system while H_∞ solutions do. The pole placement approach of SVF controllers focuses on achieving a specified dynamic performance for the nominal plant and therefore can not guarantee robustness in the face of uncertainty and model perturbations. The H_∞ control techniques, on the other hand, take into consideration the issues of robustness and uncertainty and actively integrate these issues into the design process providing a guaranteed level of robustness for a specified set of perturbed plants.

5.2 Future Developments

A continuation of the work accomplished in this thesis requires further illustration of the robust performance problem and the corresponding SISO H_∞ design procedure introduced in chapter III. In order to provide a logical development, it would be interesting to apply the H_∞ control method to the inverted pendulum counter problem. That is, the controlled positioning of the beam of a crane. Figure 5.1 provides a graphical illustration of the problem. The problem requires the design a servo mechanism with certain robust performance characteristics which could accurately place the beam of a crane in any desired position.

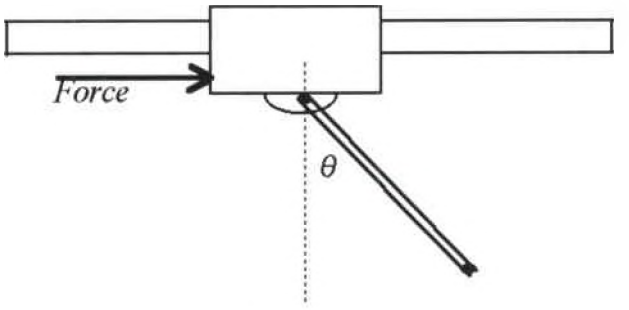

Figure 5.1 Crane positioning system

The typical undergraduate feedback control theory course concentrates on the study of SISO design methods. These usually include root locus and frequency domain methods for obtaining phase lead/lag type compensators. State variable feedback control and certainly MIMO control in general are rarely addressed in the context of undergraduate control courses. The characterization of robustness and robust design discussed in this paper are of significant relevance in the design of practical control systems. It is only reasonable therefore that undergraduate control students are exposed to control theories which have practical and realistic value. The design algorithms presented in this thesis address the issue of system robustness in the context of SISO feedback control structures which makes them attractive for undergraduate academic purposes. However, these design algorithms may be somewhat complex for undergraduate level courses. Although, it was included in the original plans, the efforts of this thesis were concentrated on the analysis and synthesis of robustness in control theory and not on the pedagogical aspects of it. Therefore, the development of design methodologies of robust control which are adequate for undergraduate study are left open for future work. The systematic features of this SISO H_∞ design process however and the aid of digital computers heightens its academic and practical value.

Most practical control problems have multiple inputs and/or multiple outputs to be controlled. It is difficult to find real life problems which require a single variable to be controlled. Thus, a possible next step in this investigation is to expand the results of the analysis of systems for robust design into the multi-input/multi-output scene. Although MIMO H_∞ control techniques have been developed in recent years, it is my opinion that these revolutionary control theories should be learned in the context of single input/single output control structures.

APPENDIX A

A.1 Proof of Equation 2.28

Fix a frequency and let $x = |W_1 S|$ and $y = |W_m T|$. The region in the xy plane where $x + y < 1$ is the triangle as illustrated in the figure below:

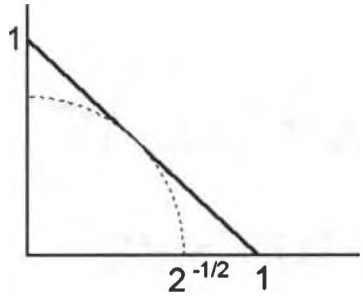

Imagine a circle with center zero and radius $1/\sqrt{2}$ is super imposed on the triangle. It follows that if the condition $x^2 + y^2 < 1/2$ is satisfied then the condition $x + y < 1$ will also be satisfied. It is evident form the figure shown above that the first condition is somewhat more conservative since those solution which comply with the first condition are a subset of the much larger set of solutions which comply with the second condition. Consequently, a sufficient condition for $\| |W_1 S| + |W_m T| \|_\infty < 1$, is that

$$\| |W_1 S|^2 + |W_m T|^2 \|_\infty < 1/2$$

A.2 Proof of Theorem 4

Theorem 4: *Let $P = N/M$ be a coprime factorization over φ, where P may or may not be stable. Let X and Y be two functions in φ such that $NX + MY = 1$. Then the set of all controllers C for which the feedback system is stable equals:*

$$\left\{C = \frac{X + MQ}{Y - NQ} : \quad Q \in \varphi\right\}.$$

In chapter I it was argued that the feedback system is internally stable if all nine transfer function of 1.17 are stable. Let $P=N/M$ and $C=N_C/M_C$ be a coprime factorization over φ and substitute into 1.17. The result is

$$\begin{bmatrix} e_r \\ e_d \\ e_n \end{bmatrix} = \frac{1}{NN_C + MM_C} \begin{bmatrix} MM_C & -NM_C & -MM_C \\ MN_C & MM_C & -MN_C \\ NN_C & NM_C & MM_C \end{bmatrix} \cdot \begin{bmatrix} r \\ d \\ n \end{bmatrix}$$

Sufficiency is now evident. The feedback system will be stable if and only if

$$(NN_C + MM_C)^{-1} \in \varphi$$

Now suppose that Q belongs to φ and $C = \dfrac{X + MQ}{Y - NQ}$.

To show that the feedback system is stable, define

$$N_C = X + MQ, \qquad M_C = Y - NQ$$

Now since $NX + MY = I$ it follows that

$$X = N_C - MQ \; ; \; Y = M_C + NQ$$
$$N(N_C - MQ) + M(M_C + NQ) = I$$
$$NN_C + MM_C = I$$

Therefore, $C=N_C/M_C$ is a coprime factorization and the feedback system is stable.

APPENDIX B

B.1 Euclid's Algorithm

The input to Euclid's algorithm are two polynomials n, m such that the degree of n is greater than that of m. If the degree of n is not greater than the degree of m, then interchange n and m.

PROCEDURE:

i. Divide m into n to get quotient q_1 and remainder r_1:

$$n = mq_1 + r_1, \qquad : degree\ r_1 < degree\ m.$$

ii. Divide r_1 into m to get quotient q_2 and remainder r_2:

$$m = r_1 q_2 + r_2, \qquad : degree\ r_2 < degree\ r_1.$$

iii. Divide r_2 into r_1 to get quotient q_3 and remainder r_3:

$$r_1 = r_2 q_3 + r_3, \qquad : degree\ r_3 < degree\ r_2.$$

iv. Continue until the remainder r_k is a non zero constant.

Now the equations used to obtain polynomials x and y such that $nx + my = 1$, depend on the order of the polynomials n and m. For example for the first order case we have $n = mq_1 + r_1$.

Consequently $r_1 = n - mq_1$ and Therefore, we have:

$$1 = \frac{n}{r_1} - \frac{mq_1}{r_1}$$

So let $$x = \frac{1}{r_1}, \quad and \quad y = -\frac{q_1}{r_1}.$$

For the second order case:

$$n = mq_1 + r_1$$
$$m = r_1 q_2 + r_2$$

In matrix form:

$$\begin{bmatrix} 1 & 0 \\ q_2 & 1 \end{bmatrix} \begin{bmatrix} r_1 \\ r_2 \end{bmatrix} = \begin{bmatrix} 1 & -q_1 \\ 0 & 1 \end{bmatrix} \begin{bmatrix} n \\ m \end{bmatrix}$$

solving for r_2 yields: $r_2 = -q_2 n + (1 + q_1 q_2) m$. So select x and y to be:

$$x = -\frac{q_2}{r_2}, \quad and \quad y = \frac{1 + q_1 q_2}{r_2}$$

The pattern becomes obvious now. Simply solve the simultaneous set of equations for r_k, and properly select x and y.

For the third order case:

$$x = \frac{1 + q_2 q_3}{r_3}, \quad and \quad y = \frac{\left[-q_3 - q_1(1 + q_2 q_3)\right]}{r_3}$$

For the fourth order case:

$$x = \frac{-q_2 - q_4(1+q_2q_3)}{r_4}, \quad and \quad y = \frac{q_1(q_2 + q_4(1+q_2q_3)) + (1+q_3q_4)}{r_4}.$$

B.2 Nevanlinna's Algorithm

Nevanlinna's algorithm is a procedure to construct a solution to the NP interpolation problem, if such a solution exists (i.e. to find G in φ such that $\|G\|_\infty \leq 1$ and $G(\alpha_i)=\beta_i, \forall i$). The procedure introduced in this appendix has been drawn directly from Doyle, Francis and Tannenbaum [5]. The steps have been developed inductively: First, the case with a single NP problem data point; then the case with n data points.

Define a *Mobius function* and its inverse:

$$M_b(z) = \frac{z-b}{1-z\bar{b}}, \quad M_b^{-1}(z) = \frac{z+b}{1+z\bar{b}} \quad where |b| < 1$$

The Mobius function has the following properties:

1. M_b has a zero at z = b and a pole at $z = 1/\bar{b}$. Thus M_b is analytic in the open unit circle $|z| < 1$.
2. The magnitude of M_b equals 1 on the unit circle.
3. M_b maps the unit circle onto the unit circle.
4. The inverse map is a Mobius function too since $M_b^{-1} = M_{-b}$.

Also define the all-pass function $A_a(s) = \frac{s-a}{s+a}, \quad Re\, a > 0.$

Now for the single data point (α_1, β_1) there are to possibilities:

Case 1 $|\beta_1| = 1$. The unique solution is $G(s) = \beta_1$. This is evident from the maximum modulus theorem and the discussion in chapter III.

Case 2 $|\beta_1| < 1$. There are an infinite number of solutions. The set of all solutions is parametrized by the following equation where $G_1(s)$ is stable, proper, and has infinity norm less than or equal to one:

$$\left\{G:\ G(s) = M_{-\beta_1}\left[G_1(s)A_{\alpha_1}(s)\right],\ G_1 \in \textit{stable and proper},\ \|G_1\|_\infty \le 1\right\}$$

Note that G interpolates β_1 at α_1:

$$G(\alpha_1) = M_{-\beta_1}\left[G_1(\alpha_1)A_{\alpha_1}(\alpha_1)\right] = M_{-\beta_1}(0) = \beta_1$$

Also, G is made of the composition of two functions

$$s \mapsto G_1(s)A_{\alpha_1}(s)$$
$$z \mapsto M_{-\beta_1}(z)$$

The first one is analytic in the closed RHP and maps into the closed unit circle since $\|G_1\|_\infty \le 1$. The second is analytic in the open unit circle and maps it back into the unit circle. Therefore, G is analytic in the RHP, proper, and $\|G\|_\infty \le 1$. Notice that if G_1 is an all-pass function so is G. G_1 is typically selected to be equal to one or an all-pass function.

Consider the case with n data points and assume the problem to be solvable. Again, there are two possibilities:

Case 1 $|\beta_1| = 1$. Since the problem is solvable, it most be that $G(s) = \beta_1$ by the maximum modulus theorem. Hence $\beta_1 = \cdots = \beta_n$.

Case 2 $|\beta_1| < 1$. Pose a new problem, labeled the NP' problem, with n-1 data points.

$$\begin{matrix} \alpha_2 \cdots \alpha_n \\ \beta_2 \cdots \beta_n \end{matrix} \qquad where\ \beta_i' = M_{\beta_1}(\beta_i) / A_{\alpha_1}(\alpha_i)$$

Now the set of all solutions to the NP problem is given by the formula

$$G(s) = M_{\beta_1}\left[G_1(s) A_{\alpha_1}(s)\right],$$

where G_1 ranges over all solutions of the NP' problem. Note, that n functions G_{n-i}, with $i = 1, \ldots, n$ must be found for n problem data points where the function G_{n-i} is the solution to the n-i NP sub-problem. It follows by induction that the NP problem always has an all-pass function solution.

In the application of the NP theory to the model matching problem it often turns out that the data has conjugate symmetry. In this case the solution may be expressed as $G(s) = G_R(s) + jG_I(s)$, where G_R and G_I are both real rational. It follows that G_R is also a solution to the NP problem.

B.3 Solution of Model Matching Problem With a Single Zero of T_2 in RHP

Suppose that T_2 has only one zero α_1 in RHP. Then, according to the procedure in chapter III the NP problem must be solved with data:

$$\alpha_1$$
$$\gamma_{opt}^{-1}\beta_1,$$

where β_1 is given by $T_1(\alpha_1)$. Also,

$$\gamma_{opt} = \sqrt{A^{-1/2}BA^{-1/2}} = \sqrt{B/A}$$

$$\text{where } A = \frac{1}{\alpha_1 + \bar{\alpha}_1} \quad \text{and} \quad B = \frac{\beta_1\bar{\beta}_1}{\alpha_1 + \bar{\alpha}_1}$$

However,

$$B/A = \beta_1\bar{\beta}_1 = |\beta_1|^2$$
$$\therefore \ \gamma_{opt} = \sqrt{|\beta_1|^2} = \beta_1$$

Thus, the NP problem data above becomes: α_1, 1

From appendix B.2 the NP problem solution for this data is $G(s) = 1$. Therefore, the solution to the model matching problem is:

$$Q = \frac{T_1 - \gamma_{opt}G}{T_2} = \frac{T_1 - \gamma_{opt}(1)}{T_2} = \frac{T_1 - T_1(\alpha_1)}{T_2}$$

APPENDIX C

C.1 Matlab program "simulate.m"

```
echo off
%%%%%%%%%%%%%%%%%%%%%%%%%%%%%%%%%%%%%%%%%%%%%%%%%%%%%%
%
%    This program Simulates the initial conditions response of the full order
%    nominal or perturbed inverted pendulum system under feedback control.
%
%%%%%%%%%%%%%%%%%%%%%%%%%%%%%%%%%%%%%%%%%%%%%%%%%%%%%%
%
Ts=.0001;                              % Sampling Period
Tf=3;                                  % Final Simulation Time
Samples=Tf/Ts;                         % Number of Samples Required
%
%%%%%%%%%%%%%%%%%%%%%%%%%%%%%%%%%%%%%%%%%%%%%%%%%%%%%%
%
%                        PLANT PARAMETERS
%
%%%%%%%%%%%%%%%%%%%%%%%%%%%%%%%%%%%%%%%%%%%%%%%%%%%%%
%
%
bf = 1;                                 % Coefficient of Friction
%
Ap=[0  1  0  0; 0  -0.9211*bf  -.581  0; 0  0  0  1; 0  0.3947*bf  4.4532  0];
Bp=[0;  .9211;  0;  -.3947];
Cp=[0  0  1  0];
Dp=[0];
[Apd,Bpd]=c2d(Ap,Bp,Ts);               %  ZOH transformation of the plant analog
model to
%                                      %  a discrete equivalent model
%%%%%%%%%%%%%%%%%%%%%%%%%%%%%%%%%%%%%%%%%%%%%%%%%%%%%%
%
%                        CONTROLLER PARAMETERS
%
%%%%%%%%%%%%%%%%%%%%%%%%%%%%%%%%%%%%%%%%%%%%%%%%%%%%%
```

```
numc4=[90.277 642.15 1767.832 2354.867 1522.2 382.03];    % Numerator of
%                                                          % the Controller
%                                                          % Transfer
%                                                          % Function
denc4=[-.001 -1.025 10.306 36.65 37.65 11.184];   % Denominator of Controller
%                                                  % Transfer Function
[Ac,Bc,Cc,Dc]=tf2ss(numc4,denc4);          % Transformation of Controller Transfer
%                                          % Function model to State Space Model
%
[Acd,Bcd]=c2d(Ac,Bc,Ts);                   % ZOH transformation of the controller
%                                          % analog model to a discrete
%                                          % equivalent model
%
%%%%%%%%%%%%%%%%%%%%%%%%%%%%%%%%%%%%%%%%%%%%%%%%%%%%%%%%%%%%%%%%%%%%%%%%
%
%                          INITIALIZATION OF ARRAYS
%
%%%%%%%%%%%%%%%%%%%%%%%%%%%%%%%%%%%%%%%%%%%%%%%%%%%%%%%%%%%%%%%%%%%%%%%%
%
Xp=zeros(4,Samples);                       % Plant system state vector
Xp(:,1)=[10;0;1;.1];                       % Initial conditions
Xc=zeros(5,Samples);                       % Controller system state vector
Yp(:,1)=Cp*Xp(:,1);                        % Plant output vector
U=zeros(1,Samples);                        % Controller system output vector (Plant
control
%                                          % input)
Uc=zeros(1,Samples);                       % Controller system input vector
%
%%%%%%%%%%%%%%%%%%%%%%%%%%%%%%%%%%%%%%%%%%%%%%%%%%%%%%%%%%%%%%%%%%%%%%%%
%
%                          SIMULATION ITERATIONS
%
%%%%%%%%%%%%%%%%%%%%%%%%%%%%%%%%%%%%%%%%%%%%%%%%%%%%%%%%%%%%%%%%%%%%%%%%
%
for k=1:Samples,
   td(k)=Ts*(k-1);
   Uc(:,k)=0-Yp(:,k);
   Xc(:,k+1) = Acd*Xc(:,k) + Bcd*Uc(:,k);
   U(:,k) = Cc*Xc(:,k) + Dc*Uc(:,k);
   Xp(:,k+1) = Apd*Xp(:,k) + Bpd*U(:,k);
   Yp(:,k+1) = Cp*Xp(:,k);
end
%
```

```
%%%%%%%%%%%%%%%%%%%%%%%%%%%%%%%%%%%%%%%%%%%%%%%%
%
%                          PLOTING  ROUTINES
%
%%%%%%%%%%%%%%%%%%%%%%%%%%%%%%%%%%%%%%%%%%%%%%%%
%
%
subplot(221)
plot(td,Xp(1,1:Samples))
title('Perturbed Full State Plant')
subplot(222)
plot(td,Xp(2,1:Samples))
title('Perturbed Full State Plant')
subplot(223)
plot(td,Xp(3,1:Samples))
title('Perturbed Full State Plant')
subplot(224)
plot(td,Xp(4,1:Samples))
title('Perturbed Full State Plant')
pause
end
```

C.2 Matlab program "gamopt.m"

```
echo off
%%%%%%%%%%%%%%%%%%%%%%%%%%%%%%%%%%%%%%%%%%%%%%%%
%
%    Execution of this function returns the optimum gamma (γopt) and the corresponding
%    Nevanlinna's problem data given W2, X,Y,N, and M.
%
%%%%%%%%%%%%%%%%%%%%%%%%%%%%%%%%%%%%%%%%%%%%%%%%
%
function [gammaopt,c,b]=gamopts(W2)         % W2 must be a 2 by 1 vector
%                                           % with the numerator of W2 being
%                                           % the first element and the denomi-
%                                           % tor being the second element
% c is a vector containing the RHP zeros of T2
% b is a vector containing the model matching  problem Beta data set
%
N=[0  0  0.3947;1  2  1];
M=[-1  0  4.4532;1  2  1];
X=[18.88  37.3824;1  1];
```

```
Y=[-1  -3;1  1];
%
%%%%%%%%%%%%%%%%%%%%%%%%%%%%%%%%%%%%%%%%%%%%%%%%%%%%%%%%%%%%%%%%%%%%%%%%%%%%%%%%%%%%%
%
%                                    COMPUTING T1 AND T2
%
%%%%%%%%%%%%%%%%%%%%%%%%%%%%%%%%%%%%%%%%%%%%%%%%%%%%%%%%%%%%%%%%%%%%%%%%%%%%%%%%%%%%%
%
%
t1=polmult(polmult(W2,N),X);
t2=polmult(polmult(-W2,M),N);
%
%%%%%%%%%%%%%%%%%%%%%%%%%%%%%%%%%%%%%%%%%%%%%%%%%%%%%%%%%%%%%%%%%%%%%%%%%%%%%%%%%%%%%
%
%                COMPUTINIG THE ZEROS OF T2 IN Re(s>0)
%
%%%%%%%%%%%%%%%%%%%%%%%%%%%%%%%%%%%%%%%%%%%%%%%%%%%%%%%%%%%%%%%%%%%%%%%%%%%%%%%%%%%%%
%
zerost2=roots(t2(1,:));
[mm,nn]=size(zerost2);
n=0;
for k = 1:mm,
  if zerost2(k)>0,
    n=n+1;
    c(n)=zerost2(k);
  end
end
%
%%%%%%%%%%%%%%%%%%%%%%%%%%%%%%%%%%%%%%%%%%%%%%%%%%%%%%%%%%%%%%%%%%%%%%%%%%%%%%%%%%%%%
%
%                EVALUATING T1 AT THE ZEROS OF T2 IN Re(s>0)
%
%%%%%%%%%%%%%%%%%%%%%%%%%%%%%%%%%%%%%%%%%%%%%%%%%%%%%%%%%%%%%%%%%%%%%%%%%%%%%%%%%%%%%
%
for m=1:n,
  val=evalratf(c(m),t1);
  bb(m)=val;
end
%
%
%
%
%
```

```
%%%%%%%%%%%%%%%%%%%%%%%%%%%%%%%%%%%%%%%%%%%%%%%%%%%%%
%
%                     COMPUTING MATRICES B and D
%
%%%%%%%%%%%%%%%%%%%%%%%%%%%%%%%%%%%%%%%%%%%%%%%%%%%%%
%
for f=1:n,
 for g=1:n,
  v=1/(c(g)+conj(c(f)));
  B(g,f)=v;
  D(g,f)=v*(bb(g)*conj(bb(f)));
 end
end
%
%%%%%%%%%%%%%%%%%%%%%%%%%%%%%%%%%%%%%%%%%%%%%%%%%%%%%
%
%          COMPUTING GAMMAOPT AND THE PICK MATRIX
%
%%%%%%%%%%%%%%%%%%%%%%%%%%%%%%%%%%%%%%%%%%%%%%%%%%%%%
%
AA=B^.5;
Ap=AA\eye(n);
J=Ap*D*Ap;
V=eig(J);
gammaopt=sqrt(max(V));
for k = 1:n,
   b(k)=bb(k)/gammaopt;
end
pick=B-(D/gammaopt^2);
U=eig(pick);
end
```

C.3 Matlab program "polmult.m"

```
%%%%%%%%%%%%%%%%%%%%%%%%%%%%%%%%%%%%%%%%%%%%%%%%%%%%%
%
% Execution of this function returns the product of two transfer functions V and U,
% where V and U are 2 by 1 vectors having the numerator as the (1,1) element
% and the denominator as the (1,2) element
%
%%%%%%%%%%%%%%%%%%%%%%%%%%%%%%%%%%%%%%%%%%%%%%%%%%%%%
%
```

```
function W=polmult(V,U)
[n,m]=size(V);
[a,b]=size(U);
if((n ~= 2)&(m ~= 1)&(a ~= 2)&(b ~= 1)), error('Incorrect input vectors'); end
num=conv(V(1,:),U(1,:));
den=conv(V(2,:),U(2,:));
W=[num;den];
end
```

C.4 Matlab program "evalratf.m"

```
%%%%%%%%%%%%%%%%%%%%%%%%%%%%%%%%%%%%%%%%%%%%%%%%%%%%%%%%%%%%%%%%%%%%%%%%
%
%  Execution of this function returns the value of the function V evaluated at the point
%  So.  The function V is a 2 by 1 vector where the (1,1) element is the numerator of V
%  and the element (2,1) is the denominator of V.
%
%%%%%%%%%%%%%%%%%%%%%%%%%%%%%%%%%%%%%%%%%%%%%%%%%%%%%%%%%%%%%%%%%%%%%%%%
%
function val=evalratf(So,V)
if (nargin >2),
  error('Too many arguments');
elseif (nargin<2),
  error('Too few arguments')
end
for e=1:2,
   num(e) = evalpol2(So,V(e,:));
end
val = num(1)/num(2);
```

C.5 Matlab program "evalpol2.m"

```
%%%%%%%%%%%%%%%%%%%%%%%%%%%%%%%%%%%%%%%%%%%%%%%%%%%%%%%%%%%%%%%%%%%%%%%%
%
%  Execution of this function returns the value of the polynomial V evaluated at the point
%  So. V is a 1 by 1 vector whose elements are the coefficients of the polynomial in
%  decending order.
%
%%%%%%%%%%%%%%%%%%%%%%%%%%%%%%%%%%%%%%%%%%%%%%%%%%%%%%%%%%%%%%%%%%%%%%%%
%
function val=evalpol2(So,V)
if (nargin >2),
```

```
  error('Too many arguments');
elseif (nargin<2),
  error('Too few arguments')
end
[m,n]=size(V);
sum=0;
limit = n;
for k = 1:limit,
   val1=V(1,k)*So^(n-1);
   sum=sum+val1;
   n=n-1;
end
val = sum;
```

BIBLIOGRAPHY

1. Franklin, G.F., Powell, J.D., & Workman, M.L., Digital Control of Dynamic Systems., Addison-Wesley Publishing Company, Second Edition, 1990.
2. Franklin, G.F., Powell, J.D., & Emami-Naemi, A., Feedback Control of Dynamic Systems, Addison-Wesley Publishing Company, 1988.
3. Dorf, R.C., Modern Control Systems, Addison-Wesley Publishing Company, Fifth Edition, 1989.
4. Chiang, R.Y., Safonov, M.G., Robust Control Toolbox, The Mathworks Inc., 1992.
5. Doyle, J.C., Francis, B.A., & Tannenbaum, A.R., Feedback Control Theory, Macmillan Publishing Company, 1992.
6. Doyle, J.C., & Stein, G., "Multivariable Feedback Design: Concepts for a Classical/Modern Synthesis," IEEE Transactions on Automatic Control, Vol AC-26 (1), 1981.
7. Morari, M., & Doyle, J.C., "A Unifying Framework for Control System Design Under Uncertainty and Its Implications for Chemical Process Control,"
8. Zames, G., & Francis, B.A., "Feedback, Minimax Sensitivity, and Optimal Robustness," IEEE Transactions on Automatic Control, Vol AC- 28 (5), 1983.
9. Francis, B.A., & Zames, G., "On H^{∞} Optimal Sensitivity Theory for SISO Feedback Systems," IEEE Transactions on Automatic Control, Vol AC-29 (1), 1984.
10. Kimura, H., "Robust Stabilizability for a Class of Transfer Functions," IEEE Transaction on Automatic Control, Vol AC-29 (9), 1984.

11. Zames, G., "On the Input-Output Satibility of Time-Varying Nonlinear Feedback Systems Part I: Conditions Derived Using Concepts of Loop Gain, Conicity and Positivity," IEEE Transaction on Automatic Control, Vol AC-11 (2), 1966.

12. Youla, D.C., Jabr, H.A., and Bongiorno, J.J., "Modern Weiner-Hopf Desing of Optimal Controllers, part I," IEEE Transactions on Automatic Control., Vol AC-21, 1967.

13. Walsh, J.L.,"Interpolation and Approximation by Rational Functions in the Complex Domain," Providence, RI: AMS Colloq. Pub., 1935.

14. Doyle, J.C., "Synthesis of Robust Controllers and Filters," Proceedings 22nd IEEE Conference on Decision and Control, 1983.

15. Francis, B.A., "A course in H Control Theory," Lecture Notes in Control and Information Sciences," Vol 88, Springer-Verlag, New York.

16. Hoffman, C.A., "Inverted Pendulum Analysis and Simulation," Theses publication by the University of Dayton, 1990.